USING EDDY COVARIANCE AND OVER-LAKE MEASUREMENTS FROM TWO PRAIRIE RESERVOIRS TO INFORM FUTURE EVAPORATION ESTIMATES

A Thesis Submitted to the
College of Graduate and Postdoctoral Studies
In Partial Fulfillment of the Requirements
For the Degree of Master of Science
In the Department of Civil, Geological and Environmental Engineering
University of Saskatchewan
Saskatoon

By
Jennifer Baergen Attema

Permission to Use

In presenting this thesis as partial fulfillment of the requirements for a Postgraduate degree from the University of Saskatchewan, the author agrees that the Libraries of this University may make it freely available for inspection. The author further agree that permission for copying of this thesis in any manner, in whole or in part, for scholarly purposes may be granted by the professor who supervised this thesis work or, in their absence, by the Head of the Department or the Dean of the College in which this thesis work was done. It is understood that any copying, publication, or use of this thesis or parts thereof for financial gain shall not be allowed without written permission. It is also understood that due recognition shall be given to the author and to the University of Saskatchewan in any scholarly use which may be made of any material in this thesis.

Requests for permission to copy or to make other uses of materials in this thesis in whole or part should be addressed to:

Head of the Department of Civil, Geological and Environmental Engineering
University of Saskatchewan
3B48 Engineering Building, 57 Campus Drive
Saskatoon, Saskatchewan S7N 5A9 Canada

OR

Dean of the College of Graduate and Postdoctoral Studies
University of Saskatchewan
116 Thorvaldson Building, 110 Science Place
Saskatoon, Saskatchewan S7N 5C9 Canada

Reference in this thesis to any specific commercial products, process, or service by trade name, trademark, manufacturer, or otherwise, does not constitute or imply its endorsement, recommendation, or favoring by the University of Saskatchewan. The views and opinions of the author expressed herein do not state or reflect those of the University of Saskatchewan and shall not be used for advertising or product endorsement purposes.

Abstract

Improved evaporation estimates are required to aid water management decisions. Current estimates are limited by the availability of driving meteorological data; estimates are routinely made using land-based data to model over-lake conditions. Collecting evaporation measurements and over-lake meteorological data to validate models in existing use is the first step toward improving future evaporation estimates.

This study presents the first direct open-water evaporation measurements for the southern Prairie Provinces using the eddy covariance technique. Instrumentation for evaporation and meteorological measurements were mounted on moored buoys near the centre of Val Marie and Shellmouth Reservoirs during the 2016 and 2017 open-water seasons (May to October). Relationships between the measured evaporation and potential controls were examined. In addition, four common estimation approaches were evaluated using a combination of land-based and over-lake inputs at various time steps.

Daily evaporation at Val Marie Reservoir averaged 3.0 mm/d during the spring and fall of 2016 and 4.0 mm/d during the full 2017 open water season. Conditions at Shellmouth suggest fluxes of similar magnitude, but evaporation data could not be confidently presented due to technical errors with equipment. Short-term evaporation at Val Marie Reservoir was aerodynamically driven with a minor seasonal influence from heat storage.

Bulk Transfer methods using over-lake data performed best of four methods evaluated at Val Marie and were used to estimate missing evaporation at Shellmouth. More work is required to improve models of land-lake relationships and determine the best procedure for future data limited situations. It is hoped that the dataset created during this study will provide ample opportunity for future work toward improving evaporation estimates.

Acknowledgements

First, I would like to thank my supervisor, Dr. Warren Helgason for providing me with the opportunity to pursue this research. His knowledge, patience and constant encouragement throughout the entire process was invaluable. I am grateful to my committee members, Dr. Jim Kells and Dr. Chris Spence, for their helpful suggestions and genuine interest in the project. Thank you also to the Prairie Provinces Water Board for contributing funding for this research. I would like to acknowledge all those who provided technical support during the data collection phase, particularly Bruce Johnson, Jay Bauer, Newell Hedstrom, Steve Auger, and Braden Magnowski. Last, but certainly not least, thank you to all my family and friends for their continued support throughout this journey. I could not have done this without you.

Table of Contents

List of Tables

List of Figures

1 Introduction

Evaporation from water bodies is an important, but poorly quantified, component of the water balance in many watersheds. Improved evaporation estimates are needed, particularly in arid regions where climate change is impacting limited water resources, to help water managers properly allocate the remaining water resources while fulfilling local water licenses, in-stream flow needs, and interprovincial water management agreements.

Current methods of estimating evaporation are limited by the availability of driving meteorological data. Local, over-lake measurements of meteorological variables are extremely rare, and are practically inaccessible to organizations responsible for making water management decisions. As a result, nearby land-based weather stations are the most common source of model inputs. This can be problematic since the different heat transfer and retention properties of land and water surfaces often create different overlying atmospheric conditions. Another significant challenge is to quantify heat storage in lakes and capture its effect on evaporation. Collecting sub-daily over-lake meteorology and lake temperature profile data is necessary to better understand meteorological controls on evaporation at lakes and reservoirs.

Direct evaporation measurements are also required to improve and validate current evaporation estimation methods. To the best of the author's knowledge, direct measurements of open water evaporation on the Canadian Prairies did not exist prior to this study. However, direct measurements can be made, given adequate resources, using the eddy covariance technique. Evaluating and improving current estimation techniques can only begin when evaporation measurements are combined with measurements of potential meteorological controls to create a reference dataset for prairie reservoir evaporation.

The main purpose of this research is to use direct measurements to develop an improved understanding of the controls governing evaporation from prairie reservoirs and explore how these controls may determine the applicability of common equations for future evaporation estimates. This is achieved through the following specific objectives:

1) collect high-frequency eddy covariance evaporation measurements and meteorological data at two prairie reservoirs during the open water season using instrumentation mounted on moored buoys and nearby land stations;
2) determine the main controls on open water evaporation at the reservoirs by examining relationships between meteorological variables and evaporation; and
3) evaluate the performance of several common evaporation estimation methods using measured and calculated variables from moored buoy and land stations.

2 Literature Review

This chapter summarizes relevant background information found in the literature, highlighting the need for direct evaporation measurements and over-lake meteorological data in the southern Prairie Provinces to improve future evaporation estimates. This is done by (1) discussing the importance of quantifying evaporation, (2) explaining the limitations of practical estimation approaches, (3) establishing the credibility of the eddy covariance method for obtaining direct evaporation measurements, and (4) summarizing recent observations of evaporation controls around the world in order to select the most appropriate potential controls to examine.

2.1 Importance of Quantifying Evaporation

Evaporation is a significant source of water loss from lakes and reservoirs in arid regions throughout the world. Quantified evaporation losses from reservoirs can be higher than industrial demand (Martínez Alvarez et al., 2008) and municipal water use (Wurbs & Ayala, 2014). It is estimated that 40% of the total water storage capacity in Australia is lost annually from open reservoirs (Helfer et al., 2012). At Lake Diefenbaker, Saskatchewan's largest reservoir (225 km long, max depth 66 m, 9.4 km^3 storage volume), over 10% of the total water storage capacity is lost to evaporation during dry years (North et al., 2015). Natural systems also lose a significant amount of water via evaporation. An isotope mass-balance study of 50 Alberta lakes found on average 72% of the natural water losses were due to evaporation, with surface and groundwater outflows making up the remaining 28% (Gibson et al., 2016).

Future evaporation from lakes and reservoirs is likely to increase from the combination of increasing population demand and climate change. Some researchers have recommended increasing reservoir size, number and regulation to combat both demand and climate change (Ehsani et al., 2017), but this could itself contribute to additional evaporation because reservoir creation increases the total surface area of a watershed that is susceptible to evaporation

(Strachan et al., 2016). Estimates of net water loss (net evaporation and unrecoverable seepage losses) from reservoir creation for hydro-generation alone range from 1.5 – 38.9 m^3 freshwater per GJ electricity (Grubert, 2016; Scherer & Pfister, 2016; Zhao & Liu, 2015) and is already increasing (Apergis et al., 2016). While engineered solutions to reduce evaporation have been developed, most methods are not be considered economically viable due to high implementation and/or maintenance costs (Assouline et al., 2011; Han et al., 2019; Jiang et al., 2015; Martínez Alvarez et al., 2009; Youssef & Khodzinskaya, 2019).

Quantifying evaporation not only highlights the urgency of finding management solutions but also informs current practices. Evaporation rates are a key component of water allocation decisions, interprovincial water agreements, basic hydrological models and complex climate change predictions (Liu et al., 2014). Improving evaporation estimates will have widespread impacts across many practical applications and research disciplines.

2.2 Limits of Practical Estimation Approaches

Practical estimation approaches are most often limited by data availability. In the attempts to create equations that rely on readily available land station data, assumptions about the relationship between land and water surface conditions must be made. Sometimes this can be accurately predicted by using local empirical coefficients, but this can restrict the use of the resulting equation to nearly identical sites. An overview of the various practical estimation approaches used for open water evaporation and their specific advantages and limitations is presented in this section.

2.2.1 Water Balances

Lake Water Balance

One way to conceptualize and quantify open water evaporation is through a water balance. A water balance treats the lake or reservoir as a control volume and attempts to quantify all the incoming and outgoing source water. A general water balance expressed in terms of the change in storage is:

$$\Delta S = P - E + SW_{in} - SW_{out} + GW_{in} - GW_{out} \text{ , ……} \quad (2.1)$$

where ΔS is the net change in storage, P is precipitation, E is evaporation, $SW_{in} - SW_{out}$ is net surface water flow, $GW_{in} - GW_{out}$ is net groundwater flow (Figure 2.1). However, it is often impractical to isolate and measure each component. In fact, evaporation estimation equations are sometimes used to solve for another unknown variable such as net groundwater flow (Hood et al., 2006).

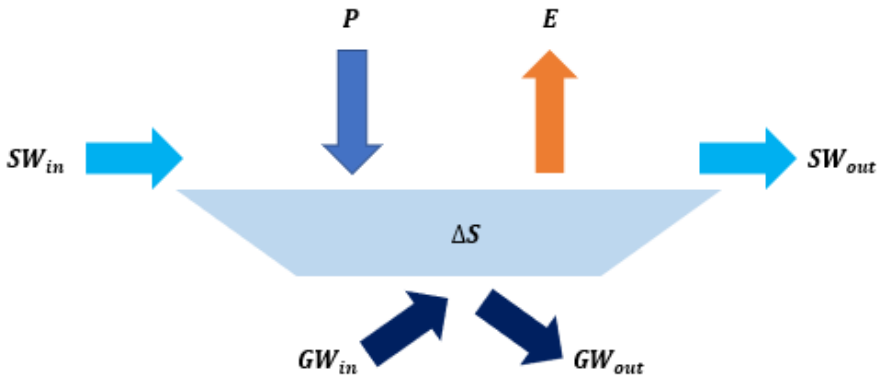

Figure 2.1 – Water balance conceptual diagram

Pan Evaporation

A simple application of the water balance approach is the evaporation pan. This approach uses a small circular pan partially filled with water as a small-scale model of a nearby water body. The water level and rainfall are measured, and additional water is added regularly to maintain a consistent water level. The depth of water that must be added to maintain this water level is the assumed net evaporation loss. Land-based evaporation pans have been used to estimate lake evaporation rates for decades, but local coefficients are required for transferring raw measurements from the small pan to the larger water body area (Kohler et al., 1955).

Floating pans are sometimes preferred because of the reduced need for pan coefficients (Liu et al., 2016). By mounting the pans on a raft or floating them directly in the water, land effects are eliminated; however, the properties of the pan and wave action can disturb these measurements and frequent maintenance is still required (Liu et al., 2016; McMahon et al., 2013).

2.2.2 Energy Balances

Lake Energy Balance

An energy balance can also be used to determine evaporation by calculating the energy available for the transfer of latent heat from the water surface to the air:

$$\lambda E = R_n - H - Q_b + A_w - \frac{\Delta Q_s}{dt}, \quad \text{(2.2)}$$

where λE is the latent heat flux, R_n is the net radiation flux, H is the sensible heat flux, Q_b is the heat flux from the water to the lake bed, A_w is net advection of energy due to interaction with the land surface, inflows and/or outflows, and $\frac{\Delta Q_s}{dt}$ is the heat stored in the control volume over the specified time interval (Figure 2.2).

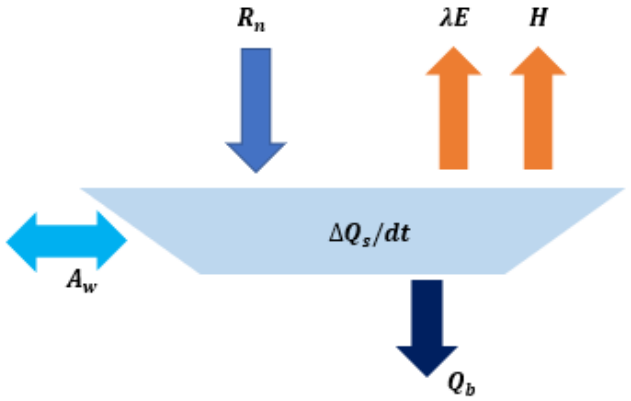

Figure 2.2 – Energy balance conceptual diagram

Surface Energy Balance

Reducing Equation 2.2 to a surface energy balance is much more common because it eliminates half the required inputs. In this case, the control volume becomes an infinitesimally thin portion of the water column near the center of the lake or reservoir with no subsurface or advection components:

$$\lambda E = R_n - H - Q_x \; , \quad (2.3)$$

where Q_x is the heat storage flux from the surface into the water column.

Bowen Ratio Energy Balance (BREB)

The Bowen Ratio Energy Balance (BREB) method uses the ratio between sensible and latent heat to help calculate evaporation:

$$\beta = \frac{H}{\lambda E} = c_\beta \, p \, \frac{(T_s - T)}{(e_w - e_a)} \; , \quad (2.4)$$

where β is the Bowen ratio (dimensionless), c_β is the empirical constant determined by Bowen (0.61 $^{o}C^{-1}$), p is the atmospheric pressure (kPa), T_s is the water surface temperature (^{o}C), T is the air temperature (^{o}C), e_w is the saturation vapour pressure at the water surface temperature (Pa), and e_a is the actual vapour pressure of the air temperature (Pa). Incorporating the Bowen ratio into the energy balance equation and rearranging to solve for evaporation yields the following equation:

$$E = \frac{R_n - Q_x - A_w - Q_b}{\rho_w (L_v (1 + \beta) + C_w T_s)} \; , \quad (2.5)$$

where ρ_w is the density of water (kg m^{-3}), L_v is the latent heat of vapourization (J kg^{-1}), C_w is the specific heat capacity of water (J kg^{-1} $^{o}C^{-1}$). If all flux inputs are in W m^{-2}, then evaporation is in m s^{-1}.

BREB is frequently used as a reference for which to compare other methods, despite the fact that it is not a direct measurement (Majidi et al., 2015; Rosenberry et al., 2007; Winter et al., 1995). The main benefit of this method is that it does not require any aerodynamic variables; however, problems can arise due to the surface temperature and energy flux data requirements, very small vapour pressure deficits, or the desire for shorter timescale estimates (Andreasen et al., 2017). Still, it is considered one of the most reliable methods for quantifying open water evaporation.

Quantifying Heat Storage

Quantifying heat storage for energy balance approaches is highlighted as a particular challenge throughout the literature (Andreasen et al., 2017; McJannet et al., 2011). The preferred method of calculating the heat storage flux involves averaging temperature profile data over time (Blanken et al., 2000; Tanny et al., 2008; Winter et al., 2003). Since temperature profile data is not consistently available, heat storage is often calculated as the residual of the surface energy balance or using empirical methods driven by net radiation and/or surface temperatures (Duan & Bastiaanssen, 2015). Some researchers have recommended avoiding the use of energy balance related models at time scales of less than 10 days (Andreasen et al., 2017); however, this may not address the need to improve the frequency of current estimates. Others have used running mean bulk water temperatures as a way of avoiding the extreme variations of the heat storage calculation without compromising the consideration of diurnal processes, but this was done in a very shallow (<1 m) environment (Riveros-Iregui et al., 2017). Alternative methods that do not require heat storage may be more favourable.

2.2.3 Mass Transfer Approaches

Many transfer functions have been developed for evaporation estimates based on Dalton-type equations (Dalton, 1802) that calculate evaporation (E) as a function of windspeed ($f(u)$) and the vapour pressure difference ($e_w - e_a$):

$$E = f(u)\,(e_w - e_a) \quad \text{..... (2.6)}$$

The vapour pressure values are typically calculated from measured temperature values using empirical equations. Adding local coefficients and additional variables can produce meaningful estimates.

Meyer Equation

One example of an empirical Dalton-type equation was proposed by Meyer (1915, 1942). The initial 1915 equation introduced an empirical constant that was dependent on the size and character of the water body, as well as the observation times for the vapour pressure measurements. In 1942, Meyer added elevation to approximate the effect of barometric pressure. The Prairie Provinces Water Board (PPWB) currently uses a metric conversion of this equation at a monthly time step (Martin, 1988):

$$E = C\ 0.750062\ (e_w - e_a)\ (1 + 6.2139e^{-2}\ U_{7.6})\ (1 + 3.28084e^{-5}\ z)\ , \ldots\ldots\ldots\ldots\ldots\ldots \quad (2.7)$$

where C is the empirical constant, the vapour pressure difference is in mbar, $U_{7.6}$ is windspeed adjusted to 7.6 m above the surface (km hr^{-1}), and z is elevation (m).

The value assigned to C is critical to the performance of the Meyer equation. A default value of 11 has historically been used with adjustments based on the measurement timing and the relative size and depth of the lake or reservoir. Further adaptations of the formula used a default coefficient of 10.1 for the Prairie Provinces, a coefficient as low as 9 for larger water bodies such as Lake Diefenbaker, and a coefficient as high as 12 for small dugouts (Woodvine, 1995). The vapour pressure difference is calculated from air temperature measurements and modelled surface temperatures. Monthly surface temperatures are modeled using the following empirical relationship:

$$T_s = 0.60\ T + B\ , \ldots\ldots\ldots\ldots\ldots\ldots\ldots\ldots\ldots\ldots\ldots\ldots\ldots\ldots\ldots\ldots\ldots\ldots\ldots\ldots\ldots\ldots \quad (2.8)$$

where T is the mean monthly air temperature and B is a set of monthly coefficients. Surface temperature measurements have previously been used to estimate evaporation at shorter time

steps (Cork, 1976). Despite the accessibility of Meyer's equation, the empirical nature of the basic equation limits applications at shorter timescales.

Bulk Transfer Equation

The Bulk Transfer method builds on simpler mass transfer approaches by adding Monin-Obukhov Similarity Theory to calculate the latent heat flux (λE):

$$\lambda E = \frac{-\kappa\, \rho_a\, L_v\, u_*\, (\overline{q} - \overline{q_s})}{\ln\left(\frac{h}{z_0}\right) - \psi} \quad \text{..... (2.9)}$$

where κ is the von Karman constant (~ 0.4), ρ_a is the air density (kg m^{-3}), u_* is the friction velocity of the wind (m s^{-1}), $\overline{q}$ is the mean specific humidity of the air (kg kg^{-1}), $\overline{q_s}$ is the mean specific humidity of the surface, often considered to be saturated (kg kg^{-1}), h is the measurement height of the wind (m), z_0 is the momentum roughness length (m) and ψ is a correction factor to account for the effects of atmospheric stability.

Bulk Transfer equations have successfully modelled evaporation at many lakes and reservoirs (Eichinger et al., 2003; Heikinheimo et al., 1999; Ikebuchi et al., 1988; Metzger et al., 2018; Wang et al., 2017). While the additional computation required can make this approach more complex than a simple Meyer approach, the absence of empirical local coefficients is beneficial for broader application. While much work has been done to optimize roughness lengths and stability correction factors (Abdelrady et al., 2016; Bouin et al., 2012; Heikinheimo et al., 1999; Xiao et al., 2013), a simplified version that assume constant neutral conditions has still performed well in at least one study (Eichinger et al., 2003).

2.2.4 Penman Combination Method

Combination methods incorporate energy balance and mass transfer components into a single evaporation estimate that does not require surface temperature. Penman (1948) was the first to propose this combination. Many adaptations have since followed; one iteration (Vardavas & Fountoulakis, 1996) recommended for lake evaporation applications (McMahon et al., 2013) is as follows:

$$E = \frac{\Delta}{\Delta + \gamma}(R_n - Q_x) + \frac{\gamma}{\Delta + \gamma}\, u\,(e_s - e_a)\,, \quad (2.10)$$

where Δ is the slope of the saturation vapour pressure curve (kPa $^{o}C^{-1}$), γ is the psychrometric constant (kPa $^{o}C^{-1}$), and e_s is the saturation vapour pressure of the air temperature (kPa).

Combination methods align well with monthly energy balance and eddy covariance measurements over lakes (Rosenberry et al., 2007; Tanny et al., 2008), but are sometimes avoided because of the difficulty in quantifying the heat flux term (Q_x) at shorter time scales (Assouline et al., 2008; McGloin et al., 2014a; Rosenberry et al., 2007). Despite the intended benefits of the combination method, the lake heat storage flux remains challenging to measure or model and can reduce the potential accuracy of the evaporation estimate.

2.2.5 Priestley-Taylor Method

The Priestley-Taylor method assumes equilibrium evaporation, where the vapour pressure deficit tends to zero. It can also be described as a variation of the Penman Combination approach that introduces an empirical factor (α) to the energy partitioning term of the equation:

$$\lambda E = \alpha \frac{\Delta}{\Delta+\gamma}(R_n - Q_x) \quad (2.11)$$

Since the energy term of Penman-based equations often far exceeds the effects of the second term, estimation accuracy can be maintained while reducing data requirements, even if equilibrium evaporation is occurring (Bailey et al., 1997). The empirical factor (α) is often assumed to be 1.26 in humid environments, including open water, but has been shown to vary seasonally (Assouline et al., 2016; De Bruin & Keijman, 1979). This multiplication of the energy partitioning term is necessary because mixing of dry air from the free atmosphere above the boundary layer creates a net surface-to-air vapour deficit (Bailey et al., 1997). As might be expected, the Priestley-Taylor method also aligns well with monthly energy balance measurements (Rosenberry et al., 2007; Slota, 2013). A modification of the Priestley-Taylor (where α = 1.66) is used by Alberta Irrigation for reservoir applications (Liu et al., 2014).

Ultimately, while surface temperature measurements are not required, this method can still be limited by the need to measure or model the storage heat flux.

2.2.6 Morton's Complementary Relationship Evaporation

Complimentary relationship evaporation is based on Bouchet's hypothesis, assuming potential evaporation is not independent of, but rather coupled with, actual evaporation in response to surface-atmosphere interactions (Bouchet, 1963). Over land, this is expressed as:

$$ETa + ETp = 2\,ETw\,, \quad \text{..... (2.12)}$$

where ETa is the actual evapotranspiration, ETp is the potential evapotranspiration, and ETw is the wet environment evapotranspiration. The hypothesis suggests that reduced ETa makes excess energy available for sensible heat fluxes that warm and dry the air, causing an increase in ETp. Accordingly, increased ETa makes less energy available for sensible heat fluxes and ETp decreases. If moisture becomes unlimited, but energy remains limited and all excess energy goes to sensible heat, $ETa = ETp = ETw$. As the water content of a surface increases, ETa increases and ETp decreases until the surface reaches ETw conditions: a hypothetical large area of saturated surface with unlimited water supply and fixed energy budget (Figure 2.3). Observational evidence to support this hypothesis has been published showing measurements from 25 basins across the United States resemble this theoretical plot (Ramírez et al., 2005).

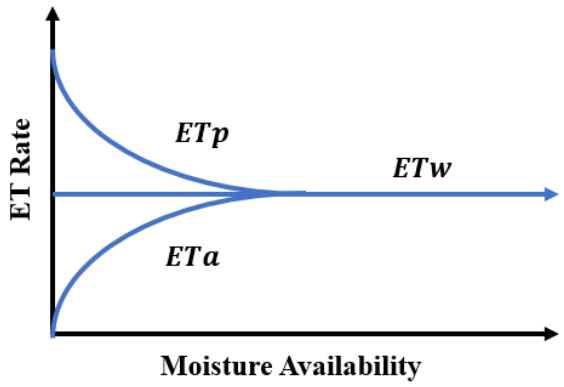

Figure 2.3 – The conceptualization of the complementary relationship for evapotranspiration

Morton developed models for evapotranspiration from land (Complementary Relationship Areal Evaporation – CRAE) and lake evaporation (Complementary Relationship Lake Evaporation – CRLE) based on this complimentary relationship (Morton, 1983a, 1983b, 1986). Both models use land-based data: elevation (z), latitude (d), average precipitation (P), temperature (T), humidity/dew point temperature (RH), and solar radiation/sunshine duration (SR). The main benefits of the Morton models are the use of land-based data and the lack of local coefficients. CRLE model results aligned well with monthly water-budget estimates for lakes of varying sizes around the world (McMahon et al., 2013; Morton, 1983b, 1986) and have become the standard evaporation estimation method for the Government of Alberta (Liu et al., 2014).

When applying the CRAE model in land environments, the desired ETa variable is calculated by rearranging Eqn. 2.12. ETp and ETw are calculated as:

$$ETp = R_T - F_T \lambda \left(T_p - T\right), \quad \text{..... (2.13)}$$

$$ETw = b_1 + b_2 R_{Tp} \left(1 + \frac{\gamma_p}{\Delta_p}\right), \quad \text{..... (2.14)}$$

where R_T is net radiation, F_T is a vapour transfer coefficient, λ is a heat transfer coefficient , T_p is potential/equilibrium temperature, b_1 and b_2 are constants, R_{Tp} is net radiation at T_p, γ_p is a psychrometric pressure constant, and Δ_p is the slope of the saturation vapour pressure curve at T_p . All these values are derived from the three meteorological inputs (T, RH, and SR) and the set station variables (z, d, and P).

Since the lake environment is not water-limited, the CRLE model does not consider ETa. Thus, ETw and ETp are referred to as Ew and Ep, respectively, and are calculated using adjusted emissivity, albedo and roughness constants to account for the different radiation absorption and vapour transfer characteristics over water. Three types of lake environments can be considered: shallow lakes, deep lakes and ponds. Morton defines shallow lakes as lakes where upwind transition effects are negligible and seasonal subsurface heat storage changes are insignificant; this includes lakes where only the annual evaporation is of interest (Morton, 1983b). Deep lake evaporation accounts for heat storage by routing delayed available solar and waterborne heat energy through a hypothetical heat reservoir using the lake delay time

(determined empirically from lake depth), and the storage constant (determined empirically from salinity). Pond evaporation includes an adjustment for the edge effects using the width of the lake along the dominant wind direction. These edge effects can be calculated for both shallow and deep lakes if desired using the same adjustment.

Concerns with Morton's method revolve around data inputs and applicable timescale. Firstly, radiation measurements are not readily available at all weather stations and modelling this input would be suspect since the Morton model is most sensitive to errors in this variable (Morton, 1983b). Secondly, Morton claims that the models can be applied at shorter timescales but warns against potential errors due to heat storage effects and only publishes monthly and annual estimates (Morton, 1983b, 1986). Thirdly, windspeed is not considered. Although Morton has argued this is unnecessary because of windspeed measurement sensitivity, the dominance of heat turbulence during high winds, and the partial offsetting of wind effects by surface temperature changes (Morton, 1983b), windspeed has been shown to be a dominant control for sub-daily (Assouline & Mahrer, 1993; Blanken et al., 2000; Bouin et al., 2012; Granger & Hedstrom, 2011; Tanny et al., 2008) and multi-day (Blanken et al., 2000, 2003; Shao et al., 2015; Xiao et al., 2018) evaporation from open water surfaces. Thus, the absence of windspeed in the Morton model may limit its application to shorter timescales.

2.3 Case for Eddy Covariance Measurements at Prairie Reservoirs

Eddy covariance (EC) is currently considered the most direct technique available for measuring evaporation. Its development began as early as the 1950s when an apparatus was described for the direct measurements of vertical heat transfer by eddies in the lower atmosphere (Swinbank, 1951). Forty years later, a study comparing EC to energy budget approaches (EB) over water surfaces claimed that EC was then able to estimate evaporation within 10% for 30 min periods and considered EC generally accurate but slightly overestimating EB (Stannard & Rosenberry, 1991). When testing EC over various land surfaces, another study found < 3% difference from water balance methods (WB) annually and claimed EB results were underestimates (Scott, 2010). EC has also shown good agreement with scintillometry measurements over water (McJannet et al., 2011). While these techniques can only be compared

against each other in order to determine relevant accuracies, EC has been well accepted in the scientific literature as the standard application throughout the world for over-lake measurements.

The EC technique involves two instruments: a sonic anemometer to measure the three components of the wind speed vector and a gas analyzer to capture the fluctuation of the gas in question. The sonic anemometer calculates three dimensional windspeeds and sonic air temperature from the speed of sound measured at each pulse interval. The gas analyzer detects water vapour concentrations based on the attenuation of an ultraviolet signal by the water vapour between the sensor pairs at the same interval. More detailed descriptions of the technique are available elsewhere (i.e. Burba, 2013). Measurement intervals are often between 10 and 20 Hz, providing detailed records of air movement at the site. The covariance of the instantaneous vertical wind speed fluctuation (ω') and instantaneous water vapour fluctuation (q') multiplied by the latent heat of vapourization (L_v) and the density of the air (ρ_a) provides the latent heat flux (λE) upwind of the site:

$$\lambda E = L_v \rho_a \overline{\omega' q'} \quad \text{..... (2.15)}$$

The volume of air upwind of the site that influences these measurements, referred to as footprint, varies according to the aerodynamic conditions. For lake and reservoir studies, this footprint should be exclusively over the water surface to avoid the influence of land surface effects on the eddy covariance measurements. A general rule-of-thumb is that the footprint extends upwind by a horizontal distance one hundred times the instrument height (Burba, 2013).

Eddy covariance systems have been deployed at many open water sites using a variety of installation strategies. Mounting platforms include fixed land-based towers (Blanken et al., 2000, 2011; Shao et al., 2015), stationary offshore towers (Assouline et al., 2008; Eichinger et al., 2003; Tanny et al., 2011), and moored buoys (Eugster et al., 2003; Granger & Hedstrom, 2010; Spence & Hedstrom, 2015). Moored buoys are very useful because they can be built with a fin that allows rotation of the buoy, so the instruments are almost always facing into the wind. This means the potential footprint extends in all directions and most of fluxes can be measured with limited interference from the instruments or mounting equipment.

While the use of eddy covariance method for open-water evaporation is growing, there were no direct measurements for Canadian Prairie lakes or reservoirs prior to this project. Eddy

covariance studies conducted across Canada on major lakes, including Great Slave Lake (Blanken et al., 2000), Great Bear Lake (Rouse et al., 2008), Lake Superior (Blanken et al., 2011), Lake Erie (Shao et al., 2015) and Lake Okanagan (Spence & Hedstrom, 2015), and small boreal forest lakes in northern Saskatchewan and the Northwest Territories (Granger & Hedstrom, 2010, 2011) demonstrate the success of this approach in a variety of settings. Direct measurement of evaporation from prairie water bodies is necessary to evaluate the accuracy of the numerous methods currently used in a Canadian Prairie context.

2.4 Recent Observations of Evaporation Controls over Open Water

Lake evaporation measurements using the eddy covariance method have provided detailed information about trends in evaporation drivers globally. Many different types of lakes have been studied, including a tiny reservoir in Australia (McGloin et al., 2014a), an even smaller humic chemically stratified boreal lake in Finland (Nordbo et al., 2011; Vesala et al., 2006), a lagoon in France (Bouin et al., 2012), the largest inland saline lake in China (Z. Li et al., 2016), large high altitude lakes in the Northwest Territories (Blanken et al., 2000; Rouse et al., 2008), and the Great Lakes (Blanken et al., 2011; Shao et al., 2015). The surface area (Woolway et al., 2018), depth (Panin et al., 2006; Wang et al., 2014), climate (Assouline et al., 2008; Woolway et al., 2018), and hydrologic connectivity (Rouse et al., 2008) of lakes influence the near-surface conditions that drive evaporation. Common observations from lake evaporation studies support the consideration of particular near-surface meteorological controls for this study.

Windspeed generally has a strong relationship to evaporation (Eichinger et al., 2003; Sun et al., 2018; Tanny et al., 2008). Diurnal evaporation is highly correlated with diurnal windspeeds at shallow lakes in arid (Assouline et al., 2008; Assouline & Mahrer, 1993), temperate (Bouin et al., 2012), and boreal environments (Granger & Hedstrom, 2011). The same relationship was observed at a large deep lake in Canada's subarctic (Blanken et al., 2000). Short-term evaporation episodes (where evaporation increases for a period of a few days) have been linked to periods of strong winds (Blanken et al., 2000, 2003; Shao et al., 2015; Xiao et al., 2018). This increase in wind can (1) dry the air and strengthen the surface temperature and vapour gradients, (2) mix warm surface waters and promote a release of stored energy, and (3) be triggered by periods of atmospheric instability.

Temperature and vapour pressure gradients between the water surface and the overlying air are also critical for lake evaporation. Diurnal variations in evaporation can be driven by the vapour pressure difference (Nordbo et al., 2011; Vesala et al., 2006), sometimes more than windspeed (Shao et al., 2015). In fact, at Thau Lagoon in France, it was determined that short term evaporation peaks were more driven by low humidity in the air increasing these gradients than high winds (Bouin et al., 2012). The product of windspeed and vapour pressure differences is routinely cited as a strong predictor of daily or sub-daily evaporation (Bouin et al., 2012; Mammarella et al., 2015; McGloin et al., 2014a; Potes et al., 2017; Salgado & Le Moigne, 2010; Shao et al., 2015). This finding supports pursuits of aerodynamic approaches such as the Bulk Transfer method for short-term estimates.

Heat storage and release tends to impact seasonal trends in evaporation and is closely related to water body depth. Shallow lakes often have peak evaporation that aligns with peak net radiation during summer months (Bouin et al., 2012; Mammarella et al., 2015; Nordbo et al., 2011; Shao et al., 2015; Tanny et al., 2011; Wang et al., 2014). This is because shallow lakes have a smaller volume which can absorb energy inputs more quickly and reflect these inputs in the surface temperature, creating relationships at weekly or longer periods (Granger & Hedstrom, 2011). In deeper lakes, heat takes longer to be distributed throughout the water body. This can lead to warmer fall surface temperatures driving higher evaporation in fall (Assouline & Mahrer, 1993). Peak seasonal evaporation in deep lakes can be delayed for several months from peak net radiation (Z. Li et al., 2016) and may even climax during the winter months (Blanken et al., 2011; Ikebuchi et al., 1988). One exception to this observed relationship comes from a study at Elephant Butte Reservoir, where near constant evaporation was observed throughout the season (Eichinger et al., 2003).

Trends in diurnal evaporation also vary between lakes but are fundamentally different than evaporation over unsaturated land surfaces. This difference between land and water evaporation is demonstrated by the study of an ephemeral lake in China (Zhao & Liu, 2018). When the land surface was exposed, peak daily evaporation occurred during peak daily net radiation and was reduced to zero overnight. Once the area became flooded, evaporation peaked later in the day and continued overnight. Diurnal evaporation from open water is consistently out of phase with net radiation, peaking in the afternoon (Assouline et al., 2008; Liu et al., 2015; Mammarella et al., 2015; Sun et al., 2018; Wang et al., 2017) or evening (Potes et al., 2017;

Salgado & Le Moigne, 2010). Some studies have also recorded significant nighttime evaporation (Beyrich et al., 2006; Shao et al., 2015; Stannard & Rosenberry, 1991; Wang et al., 2014), which authors have suggested is from overnight mixing in shallow lakes (Stannard & Rosenberry, 1991). Double evaporation peaks were also reported at Lake Kinneret in response to diurnal net radiation peaks in the afternoon and diurnal windspeed peaks in the evening (Lensky et al., 2018). In all these cases, evaporation did not fall to zero overnight like evaporation over land because of the thermal properties of water that create a near constant vapour pressure.

2.5 Summary

Evaporation measurements are important for practical and research applications in water management. Evaporation comprises a large portion of the water lost from lakes and reservoirs and is predicted to increase due to climate change and increasing population demand. Unfortunately, practical estimates are often data limited and no previous direct open water evaporation measurements were found to validate practical estimation methods in the Canadian Prairies. This is problematic for organizations that must rely on these methods with varying inputs and assumptions for water management decisions in an often water-stressed region. Eddy covariance techniques for direct evaporation measurements are well established in the literature and can be implemented to fill this first major gap.

Additionally, while many factors have been shown to impact evaporation processes at other water bodies around the world, the key controls driving evaporation at small prairie reservoirs have not been explored fully. Collecting over-lake meteorological data and comparing it to direct evaporation measurements is required to better understand these controls. Evaluating how these findings compare with present estimation practices is the first step required to improve future estimation approaches.

3 Methods

This chapter outlines the methods used to achieve each of the three objectives of this study: (1) collect high-frequency eddy covariance evaporation measurements and meteorological data at two prairie reservoirs during the open water season; (2) determine the main controls on open water evaporation at the reservoirs; and (3) evaluate the performance of several common estimation methods using measured and calculated variables from moored buoy and land stations.

3.1 Objective 1: Create Prairie Reservoir Evaporation Dataset

3.1.1 Data Collection

Field data were collected at two reservoirs during the 2016 and 2017 open water seasons (May-October): Val Marie Reservoir (49.3079^{o} N, 107.8128^{o} W) and Shellmouth Reservoir (51.1056^{o} N, 101.4328^{o} W) (Figure 3.1). These reservoirs were selected by the Prairie Provinces Water Board. Both reservoirs are reasonably accessible from Saskatoon, while still representing some of the variation in geography and reservoir characteristics found in the Prairies Provinces.

Val Marie Reservoir (also called Newton Lake) is located along the Frenchman River at a surface elevation near 803 m a.s.l. and has a surface area of approximately 5 km^2 (Figure 3.2). During the study years, depths near the center of the reservoir measured 3.5 – 4.0 m. Val Marie Reservoir was created in 1937 for municipal water use and crop irrigation and designated as a Migratory Bird Sanctuary on November 3, 1948 (Environment and Climate Change Canada, 2017). Water levels are managed by the local Technical Services Branch of Agriculture and Agri-Food Canada (AAFC). This organization was formerly known as the Prairie Farm Rehabilitation Administration (PFRA). The surrounding landscape consists of rolling hills, with the land used mainly for cattle pasture and agricultural crops.

Shellmouth Reservoir (also called Lake of the Prairies) is a long and narrow water body on the Assiniboine River surrounded by a steep bank and rolling forested terrain with agricultural

crops dominating the uplands (Figure 3.2). It is larger and deeper than the Val Marie Reservoir with depths near 10 m and a surface area of greater than 50 square kilometers spanning nearly 40 km of the river's length. The surface elevation during the study years was approximately 427 m a.s.l. The reservoir was created by the construction of the Shellmouth Dam between 1964 and 1972 (Province of Manitoba, 2017). Water levels are regulated at the dam to help protect Brandon, Portage la Prairie, Winnipeg and surrounding communities from flooding (Province of Manitoba, 2017). The reservoir has also developed a secondary function as a tourist and recreation destination in conjunction with the neighboring Asessippi Ski Resort.

Three stations were established during this study: two moored buoys (one in each reservoir) and a land-based weather station near the Val Marie Reservoir (2017 season only). Instrumentation details for all stations can be found in Table 3.1. Buoys were accessed by driving from a local boat launch in a 3 m inflatable boat with a 4 hp motor. Regular site visits were scheduled to download data and perform routine maintenance on equipment (details in Appendix A).

The two reservoir sites used repurposed buoys from previous studies by partners at Environment and Climate Change Canada (ECCC). The Val Marie buoy (Figure 3.3) consisted of a tripod mounted on three pontoons, previously used for a project in Prince Albert National Park (Granger & Hedstrom, 2010). The Shellmouth buoy (Figure 3.4), designed by Axys Technologies for ocean waters, was previously deployed at Lake Okanagan (Spence & Hedstrom, 2015). Both buoys were designed with a fin opposite the eddy covariance instrumentation to allow for constant rotation to align these instruments with the changing wind direction. This reduces contamination from equipment interfering with wind before it reaches the sensor but requires additional corrections to account for the movement of the buoy.

Secondary buoys made of a string with five to seven temperature sensors attached at predetermined depths were moored nearby for calculation of the heat storage term. The sensors were removed for data download at the end of each season. Unfortunately, not all sensors were recovered after the 2017 season: the wire used to attach the sensors to the rope appeared to have worn through the plastic loop of the sensor cover. Additional temperature depth-profile measurements were also made from the boat during select site visits (see measurements in Appendix B).

The land station was located at the southwest corner of the local AAFC yard site (49.2471^{o} N, 107.7207^{o} W) and consisted of a large tripod with meteorological instruments (Figure 3.5). The purpose of this site was to provide local weather data in addition to the nearest ECCC weather station (Val Marie Southeast: 49.06^{o} N, 107.59^{o} W), which is located approximately 30 km southeast of the reservoir. Data was stored on a local data logger and downloaded during monthly site visits. This was not considered necessary at Shellmouth Reservoir, since the nearest ECCC weather station (Roblin: 51.18^{o} N, 101.36^{o} W) was within 10 km of the moored buoy.

Perhaps the greatest challenge of the field campaign occurred when the buoy at Val Marie was discovered overturned in June 2016. A review of the card (which could still be read, despite being submerged for weeks) revealed low winds during the time that the buoy became inverted, implying an act of vandalism may have been the cause of the damage. Additional signage and communications with contacts at AAFC were pursued to discourage a repeat event. The new buoy, consisting of a square floating platform constructed of 2.5 x 15 x 180 cm wooden deck boards secured atop four pontoons (Figure 3.6), was operational by mid-August 2016. The sturdier, elevated platform allowed for minimal wave-induced motion and greater ease of access during site visits.

Additional data gaps resulted from challenges related to equipment failure and data storage issues (Figure 3.7). Weather forced some maintenance trips to be delayed due to high winds that would have made attending to the buoy from the boat impractical. Equipment failure included a krypton hygrometer at Shellmouth in June 2016 and a sonic anemometer at Val Marie in August of 2016. These were replaced, but data was lost for a period of a few weeks in each case. There were also two periods in 2017 when data card storage issues at Shellmouth meant the loss of 10Hz data that could not be recovered.

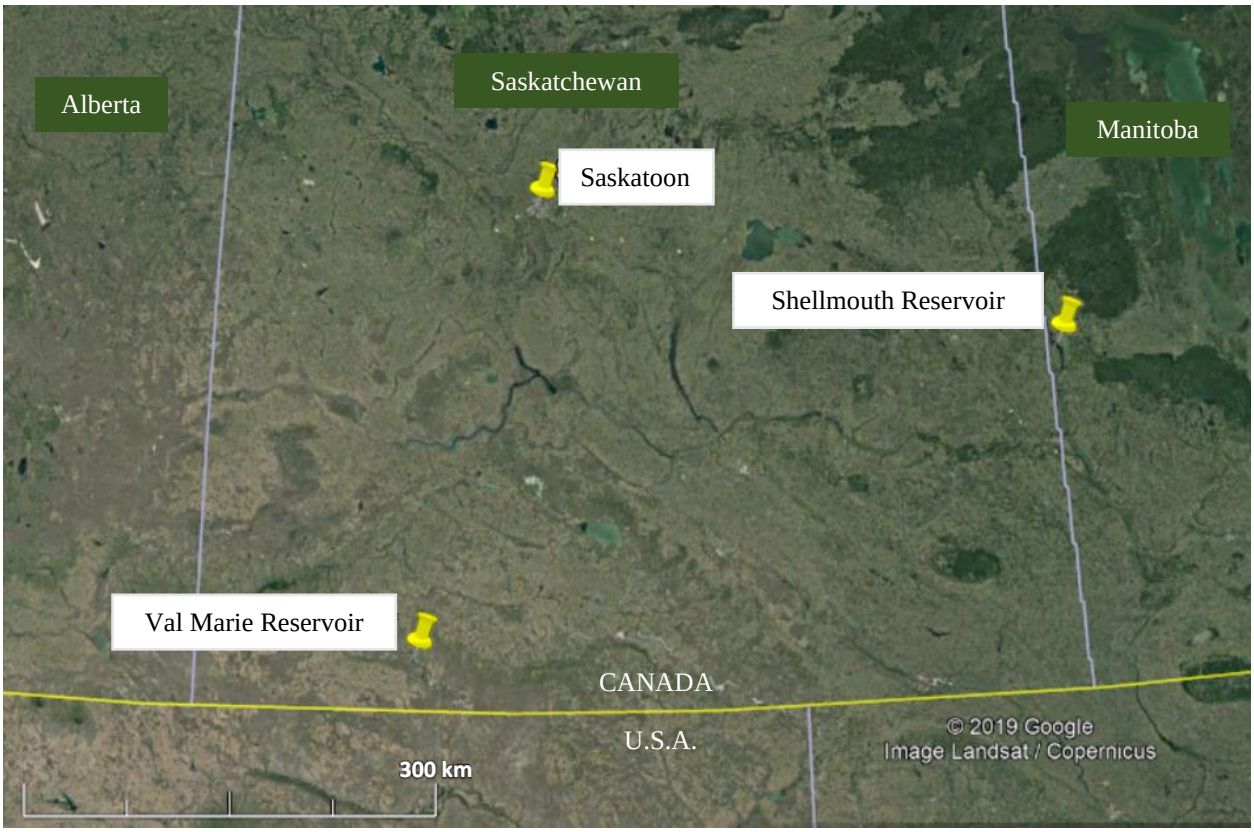

Figure 3.1 – Satellite imagery showing site locations relative to Saskatoon (Google Earth)

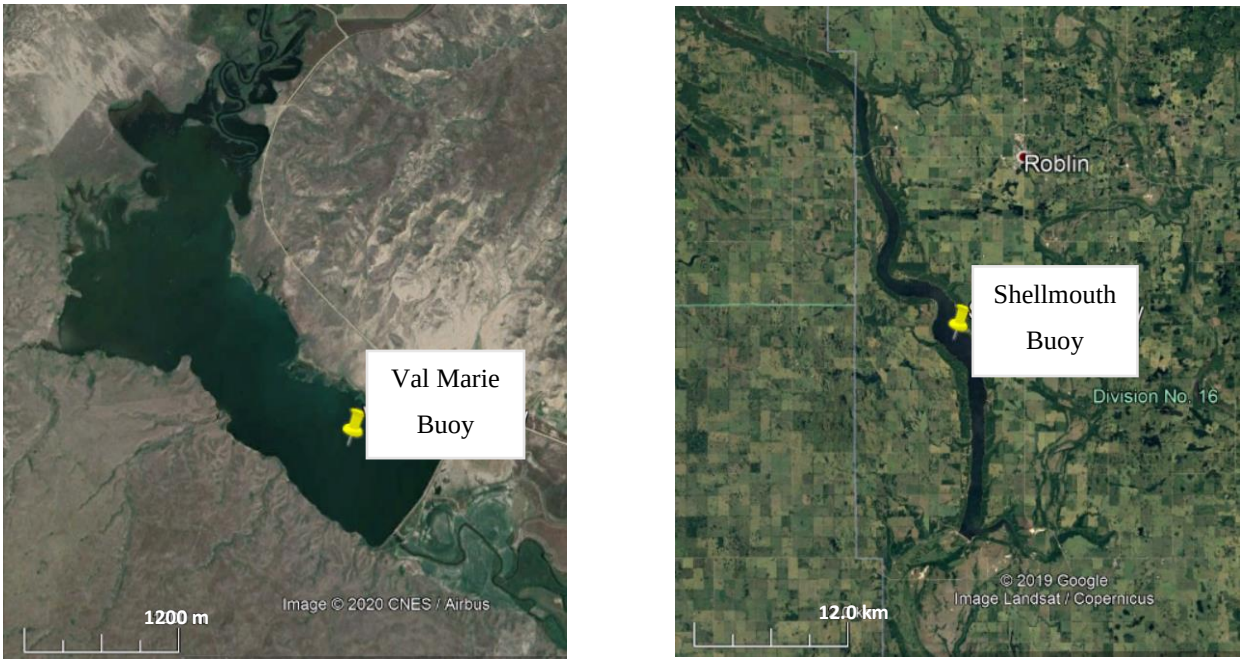

Figure 3.2 – Satellite imagery of Val Marie and Shellmouth Reservoirs (Google Earth)
Note: Buoy mooring locations indicated by the yellow pin.

Table 3.1 – Instruments installed at the reservoir stations for the 2016/2017 open-water seasons

Measurements	Shellmouth Buoy	Val Marie Buoy	Val Marie Land
3D wind speed	Campbell Scientific CSAT3 sonic anemometer		n/a
Vapour density	Campbell Scientific KH20 krypton hygrometer		n/a
Inertial Sensor	3DM-GX3-25 Attitude Heading Reference System (Val Marie upgraded to 3DM-GX4-25 post-tip)		n/a
Direction	KVH C100 Digital Compass	n/a*	n/a
Air temperature and relative humidity	Rotronic HC Temperature and Relative Humidity Probe, installed within 12 plate radiation shield	Vaisala HMP 45C Temperature and Relative Humidity Probe, installed within 12 plate radiation shield	
Surface temperature	Apogee SI-111 Infrared Radiometer		
Wind speed and direction	RM Young 05103 Wind Anemometer		
Water temperature	YSI Thermistors (on buoy - 50, 80, 100 cm) HOBO Thermistors (separate string - 25, 50, 75, 100, 200, 400, 600 cm)	HOBO Thermistors (separate string – 20, 50, 100, 200, 300 cm)	n/a
Atmospheric pressure	Vaisala PTB201 Barometric Pressure Sensor	RM Young 61205V Barometric Pressure Sensor (pre-tip) Vaisala PTA-427 Barometric Pressure Transducer (post-tip)	n/a
Net radiation	n/a	Kipp & Zonen NR-Lite Net Radiometer	
Incoming shortwave radiation	LI-COR Li-200SA Pyranometer	n/a	n/a
Incoming shortwave and longwave radiation	n/a	n/a	Hukseflux 2-component net radiometer
Rainfall	n/a	n/a	Tipping Bucket Gauge

* Val Marie buoy system recorded direction from inertial sensor

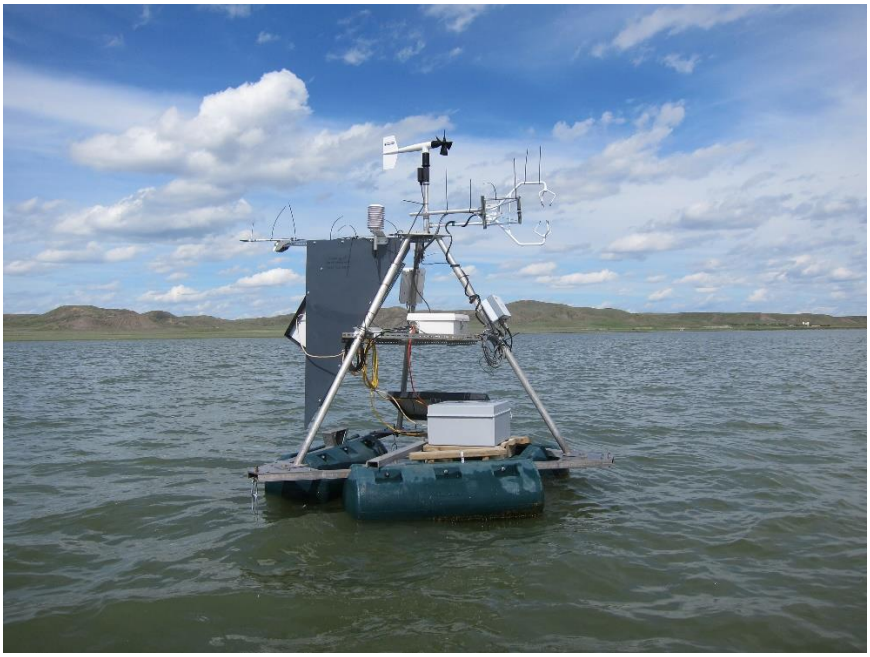

Figure 3.3 – Photo of the original Val Marie Buoy (May 2016)

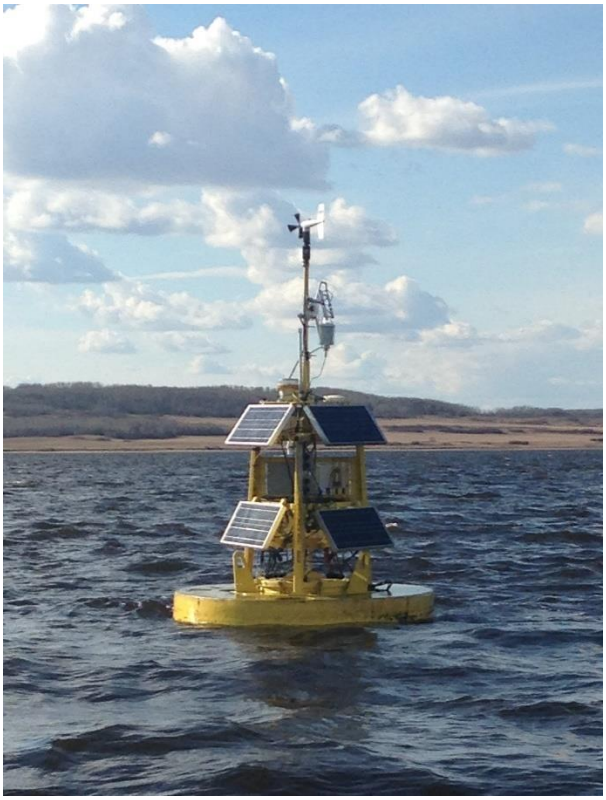

Figure 3.4 – Photo of the Shellmouth buoy (June 2016)

Figure 3.5 – Photo of land station near Val Marie Reservoir (May 2017)

Figure 3.6 – Photo of new buoy on Val Marie Reservoir (August 2016)

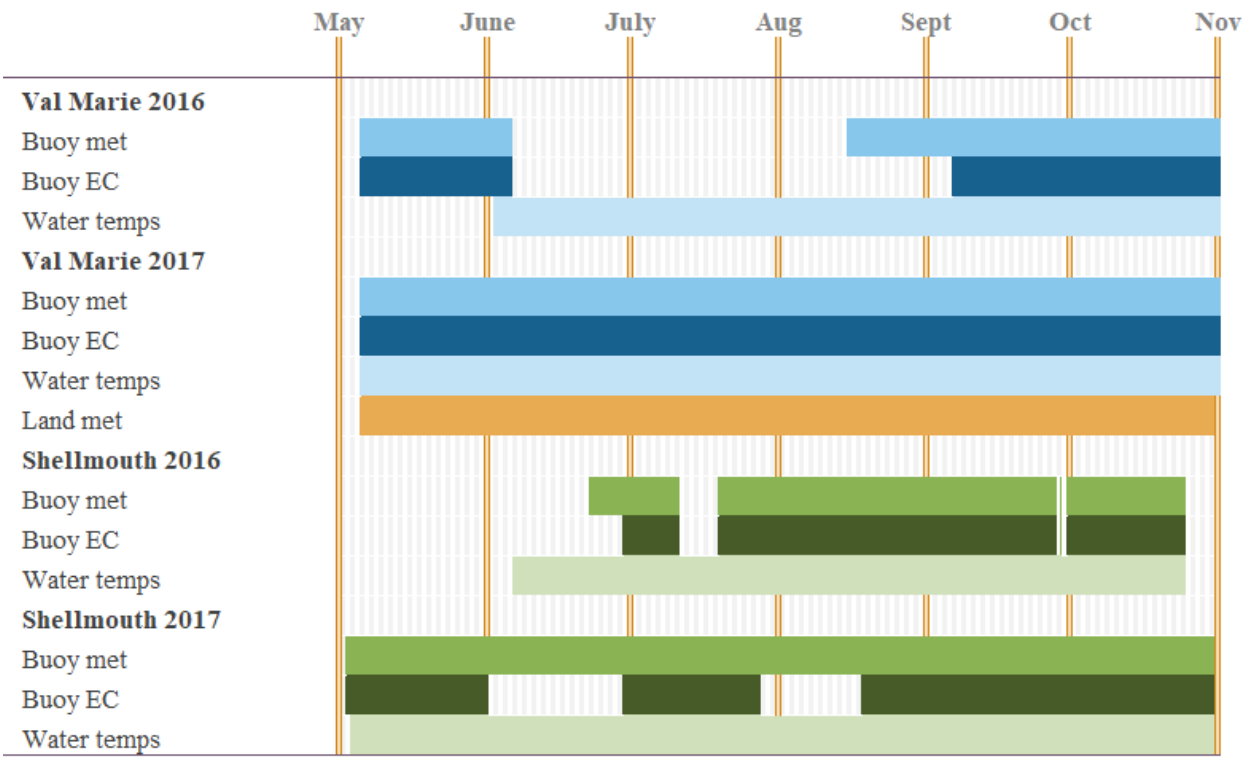

Figure 3.7 – Time series of data collection days at Val Marie and Shellmouth Reservoirs during the 2016 and 2017 open-water seasons.
Note: Val Marie 2016 data gap was from damage and rebuilding of the buoy and CSAT issues. Shellmouth 2016 EC measurement delay was from Krypton issues. Shellmouth 2016 and 2017 gaps were from data storage issues.

3.1.2 Data Processing

Meteorological data and evaporation data were processed separately using a combination of Matlab (R2018a, The MathWorks, Inc., Natick, Massachusetts, United States) and EddyPro (v6.2.2, LI-COR Inc., Lincoln, Nebraska, United States) software. Meteorological data processing involved removal of extreme outliers, rotating wind directions to the earth coordinate system, and calculation of basic statistics. Evaporation data required corrections before accurate measurements could be presented. First, the wind vectors were corrected for the buoy motion to obtain the true vertical wind speed relative to the earth. Second, standard corrections were performed to eliminate lags, spikes, and interference in the data. Third, corrected latent heat fluxes were filtered and filled using buoy meteorological data. This resulted in 30 min average fluxes that were then converted into daily, weekly and monthly depths of evaporation. Stages of the evaporation data processing are explained below.

Motion correction accounts for the wave-induced motion of the buoys using data from the inertial sensor. These movements contaminate the vertical wind vector measurements needed for the eddy covariance calculation. Motion correction algorithms have been shown to produce nearly identical flux data on moored ocean buoys as neighbouring stationary tower mounted eddy covariance systems (Flugge et al., 2016). Motion corrections have been successfully carried out using Matlab scripts for similar studies by researchers at ECCC (Granger & Hedstrom, 2011) using coordinate rotation methods outlined in the literature (Edson et al., 1998; Miller et al., 2008). Adaptations of these scripts were used to perform the motion correction at 10 Hz for this study.

The main equation used in the motion correction rotates the wind vectors measured by the anemometer and accounts for additional linear and angular velocities of the buoy platform measured by the motion sensor:

$$U = T_{ea}U_a + T_{ep}\left(\int \ddot{x}_p\, dt + \Omega_p\, r_p\right), \quad \text{(3.1)}$$

where U is the corrected windspeed, U_a is the measured windspeed, T_{ea} is the transformation matrix from the anemometer to the earth, T_{ep} is the transformation matrix from the platform to the earth, $\int \ddot{x}_p\, dt$ is the platform linear velocity, Ω_p is the platform angular velocity, and the r_p is

the position vector from the motion sensor to the anemometer (Miller et al., 2008). For this project, linear platform velocity assumed negligible and the motion sensor and the anemometer were assumed collinear. The second assumption means the following single transformation matrix can be used to transform both the measured wind vectors and angular velocities into the earth coordinate system:

$$T\ (\Phi, \theta, \Psi),$$

$$= A(\Psi)A(\theta)A(\Phi),$$

$$= \begin{bmatrix} \cos(\Psi) & \sin(\Psi) & 0 \\ -\sin(\Psi) & \cos(\Psi) & 0 \\ 0 & 0 & 1 \end{bmatrix} \begin{bmatrix} \cos(\theta) & 0 & \sin(\theta) \\ 0 & 1 & 0 \\ -\sin(\theta) & 0 & \cos(\theta) \end{bmatrix} \begin{bmatrix} 1 & 0 & 0 \\ 0 & \cos(\Phi) & -\sin(\Phi) \\ 0 & \sin(\Phi) & \cos(\Phi) \end{bmatrix},$$

$$= \begin{bmatrix} \cos(\Psi)\cos(\theta) & \sin(\Psi)\cos(\Phi) + \cos(\Psi)\sin(\theta)\sin(\Phi) & -\sin(\Psi)\sin(\Phi) + \cos(\Psi)\sin(\theta)\cos(\Phi) \\ -\sin(\Psi)\cos(\theta) & \cos(\Psi)\cos(\Phi) - \sin(\Psi)\sin(\theta)\sin(\Phi) & -\sin(\theta)\cos(\Phi)\sin(\Psi) - \sin(\Phi)\cos(\Psi) \\ -\sin(\theta) & \cos(\theta)\sin() & \cos(\theta)\cos(\Phi) \end{bmatrix}, \quad \text{..... (3.2)}$$

where Φ is the roll (positive port up), θ is the pitch (positive bow forward), and Ψ is the yaw (positive clockwise) (Edson et al., 1998).

Motion-corrected eddy covariance data were then processed fully using EddyPro Software. This program performs additional corrections, including sonic anemometer tilt correction, de-trending of raw time series, compensation of lag between sonic anemometer and water vapour analyzer, and adds a quality control flag based on the data characteristics (LI-COR Inc. 2018). This is standard procedure for other eddy covariance flux measurements collected at the University of Saskatchewan and, as such, default settings were used for consistency unless site specific information was available (details in Appendix C).

Latent and sensible heat fluxes were excluded from any further analysis if they were outside the set upper (400 W/m^2 for Val Marie, 225 W/m^2 for Shellmouth) and lower (-50 W/m^2 for both sites) limits or if they were assigned a quality control value of two or greater for

EddyPro processing. Excluded values were filled using dynamic linear regression with 30 min mean windspeed and vapour pressure differences (Taylor et al., 2007). These inputs were determined after preliminary examination of evaporation controls detailed in Appendix D. Gaps > 2 days were not filled. Weekly and monthly evaporation depths were calculated by summing daily depths.

3.2 Objective 2: Examine Evaporation Controls

Some potential controls of lake and reservoir evaporation cannot be directly measured and must be calculated separately. Three areas of potential controls were chosen for further examination at the study reservoirs based on various practical estimation requirements and observations from previous studies. These areas are: (1) temperature and moisture gradients, (2) aerodynamic effects, and (3) surface energy balance components. Calculations and adjustments of specific factors related to these three areas are explained below.

3.2.1 Temperature and Moisture Gradients

Temperature gradients were calculated as the difference between the water surface temperature (T_s) and air temperature (T) measured at the buoys divided by the height (h) of the air temperature sensor above the water. Moisture gradients were calculated as the vapour pressure difference ($e_w - e_a$) between the vapour pressure of the water surface (e_w) and the actual vapour pressure of the air (e_a) divided by the height (h) of the air temperature sensor above the water. Both diurnal and seasonal variations were considered.

3.2.2 Aerodynamic Effects

Windspeed Height Adjustment

Comparing windspeed measurements from land and over-lake stations is helpful for exploring the usefulness of land data inputs to evaporation models. Windspeeds measured at different heights must be standardized when comparing sites because windspeeds increase logarithmically with height above the surface. Windspeeds collected at the reservoirs were

adjusted to the height of the ECCC weather station windspeeds (10 m) using the following formula:

$$U_{h1} = U\left(\frac{h1}{h}\right)^{0.25}, \quad (3.3)$$

where U is the measured windspeed at height h, and U_{h1} is the calculated windspeed at height $h1$, where $h1$ is 10 m. This is the same formula used by PPWB for windspeed height adjustments for the Meyer approach (Liu et al., 2014).

Atmospheric Stability

Stability can be quantified using several approaches. For this study, the zeta stability value (ζ) from Monin-Obukhov Stability Theory is used because it is a standard output from the EddyPro processing step. Zeta is a non-dimensional value obtained by dividing the measurement height (h) by the Obukhov length (L). The Obukhov length can be interpreted as an estimate of how high the stable air mass extends from the earth's surface into the atmosphere and is calculated using the following equation:

$$L = \frac{-{u_*}^3 \theta_0}{\kappa g \overline{\omega' \theta'}}, \quad (3.4)$$

where u_* is the friction velocity, θ_0 is the potential temperature at the surface, κ is the von Karman constant (~ 0.4), g is the acceleration due to gravity, and $\overline{\omega' \theta'}$ is the surface kinematic heat flux. The resulting zeta values can be categorized as stable ($\zeta > 0$), unstable ($\zeta < 0$) or neutral ($\zeta \sim 0$).

Surface Roughness

Since the surface roughness can affect evaporation rates, some measure of this effect should also be considered. This was approximated as the mean wind speed normalized by the

friction velocity (U/u_*). Higher values indicate a smoother surface with less shear created by roughness effects.

3.2.3 Heat Storage

Heat storage was calculated from the depth-weighted mean of all available water temperature measurements at both reservoirs as follows:

$$Q_x = C_w \rho_w Z \frac{dT_w}{dt}, \quad \text{..... (3.5)}$$

where Z is the reservoir depth (m) and dT_w/dt is the difference in the depth-weighted mean water temperature for the given time period (°C). T_w was calculated by first assigning the mean temperature of each pendant for the desired time step (i.e. hourly, daily, or weekly) to a section of water that extends to the midpoints between that pendant and the pendant above and below that pendant. These mean temperatures were then multiplied by the depth of the section, added together, and divided by the reservoir depth. Reservoir depth (Z) was obtained by relating daily reported water elevations from the Water Survey of Canada to mean lakebed elevations determined using depth measurements from field visits (Appendix B). Lakebed elevations were assumed constant for the entire study and daily depths were applied to the entire day.

3.3 Objective 3: Evaluate Practical Estimation Approaches

3.3.1 Application of Selected Approaches

Four practical estimation approaches were selected for preliminary evaluation. The Meyer (Martin, 1988) and Morton (1983) approaches were selected because they are commonly used in the Prairie Provinces. The Penman (1948) approach was selected because it includes the heat storage variable and is regularly applied successfully in the literature (Rosenberry et al. 2007, Tanny et al. 2011, Wang et al. 2017, Zola et al. 2019). The Bulk Transfer method was the final method selected because it includes stability and surface roughness parameters and also estimates evaporation well in other studies (Eichinger et al., 2003; Heikinheimo et al., 1999;

Ikebuchi et al., 1988; Metzger et al., 2018; Wang et al., 2017). These methods are hereafter referred to as Meyer, Morton, Penman and Bulk Transfer. Estimation approaches were compared with the most complete evaporation dataset collected at Val Marie in 2017.

Before considering evaporation models with all the available data collected during this study, it is important to confirm that standard methods require improvements. Morton and Meyer methods were developed for use with weather station data from land stations exclusively. Mean temperature, relative humidity, and windspeed (Meyer only) inputs from the Val Marie Southeast weather stations were used. Solar radiation was modeled for Morton (details in Section 3.3.2) since it is not measured at Val Marie Southeast. In order to apply Meyer to timescales shorter than monthly, measured surface temperatures were used following methods of a previous study at Val Marie (Cork, 1976).

The effect of using land-based vs over-lake driving data was also explored for the Penman and Bulk Transfer models. Daily mean inputs were used for the land-based estimates because it is more reasonable to infer relationships between land and reservoir variables at this timescale. Net radiation and heat storage were modeled for the Penman land-based scenario (details in Section 3.3.2).

Models driven with over-lake data were run hourly and summed daily in order to avoid issues that could result from averaging due to the coupling of similar variables and differing diurnal cycles of other variables (Riveros-Iregui et al., 2017). Multiple time steps were considered for each approach. Estimates of monthly, weekly and daily evaporation were calculated when possible. In addition, the effect of using different time steps was compared by running the models (1) at each time step and (2) by aggregating daily and/or hourly estimates to the larger time steps.

In addition, the best model and best available inputs were used to fill large gaps and questionable evaporation measurements. The best model was determined based on both correlation and mean differences at multiple time scales. This was a logical step to add after the preliminary evaluation revealed an opportunity to gap fill (details in Chapter 5).

3.3.2 Modelling Missing Data

The following models would be required to use the selected evaporation estimation approaches under circumstances where only ECCC land station data is available. As such, a number of assumptions were made about model parameters etc. These assumptions were not intended to provide the most accurate model, but rather a more realistic model that would be created in these data-limited circumstances to show how the selected evaporation estimation approaches might perform given only the most readily available resources.

Solar Radiation Model

Incoming solar radiation is a main input into the Morton equation. The Clear Sky model was chosen for this variable (Allen et al., 2006). Clear Sky radiation is calculated from Global Extraterrestrial radiation for a given latitude using air temperature (T), humidity (RH), and air pressure (P) inputs. These inputs were taken from the ECCC weather stations (Val Marie Southeast and Roblin) since these are consistently available. The Clear Sky model was applied to the Val Marie land station for approximate calibration. It was found that adding a 0.75 transmissivity factor to account for partial cloud cover resulted in a reasonable fit to the measured incoming solar radiation at the land station (plots in Appendix E). This factor was assumed constant for both years at both sites.

Net Radiation Model

Net radiation was also modeled for use in the Penman equation. The above-mentioned Clear Sky model with 0.75 cloud-cover factor was used for short-wave incoming radiation. Short-wave outgoing radiation was assumed to be the short-wave incoming radiation multiplied by a water albedo of 0.05 (McMahon et al., 2013). Long-wave incoming radiation was calculated using Brutsaert's model:

$$LW_{in} = 1.24 \left(\frac{10\, e_a}{T+273.15}\right)^{\frac{1}{7}} \sigma \, (T + 273.15)^4 \, , \quad (3.6)$$

where σ is the Stefan Boltzmann constant (5.67e8). Long-wave outgoing radiation was calculated using the Stefan Boltzmann equation:

$$LW_{out} = \varepsilon\, \sigma\, (T_s + 273.15)^4 \text{ , ... (3.7)}$$

with the emissivity of water (ε) assumed equal to 0.97 (McMahon et al., 2013) and the surface temperature (T_0) assumed equal to the land station air temperature. Net radiation model results aligned well enough with measurements at Val Marie buoy and land station in 2017 to be used as evaporation model inputs (Appendix E).

Heat Storage Model

Heat storage is also a requirement for the Penman model. The net radiation model was used as an input into a hysteresis model for heat storage previously proposed (Duan & Bastiaanssen, 2015):

$$Q_x = aR_n + b + c\, \frac{dR_n}{dt} \text{ , ... (3.8)}$$

where a, b, and c are coefficients and $\frac{dR_n}{dt}$ is the difference in net radiation over the given time period. Ideally, local coefficients would be determined, but mean values from the twenty-two study lakes from around the world were used. While determining local coefficients and stronger relationships between land and reservoir variables would clearly produce stronger models, the goal of this application was to show how the selected models perform in a situation where only land station data is available, and assumptions must be made.

3.4 Summary

Evaporation and meteorological data were collected from moored buoys at Val Marie and Shellmouth Reservoirs during the 2016 and 2017 open water seasons (May to October). Additional data was collected from a land station near the town of Val Marie in 2017. Direct evaporation measurements were made using the eddy covariance technique, processed to account

for buoy motion and standard flux corrections, then filtered and filled using dynamic linear regression. Three groups of evaporation controls were selected for examination (temperature and moisture gradients, aerodynamic effects, and heat storage) and additional calculations required to examine these controls were presented. Preliminary evaluation of four practical estimation approaches (Meyer, Morton, Penman and Bulk Transfer) followed using a combination of land-based and over-lake inputs at multiple timescales to demonstrate the effects of various driving data. Assumptions and models required for the four practical estimation approaches were also presented. Results and discussion for the first two objectives of this study (creating the evaporation dataset and evaluating evaporation controls) can be found in Chapter 4. Results and discussion of the third objective (evaluate practical estimation approaches) can be found in Chapter 5.

4 Evaporation Measurements and Meteorological Controls

This chapter examines observations recorded at Val Marie and Shellmouth Reservoirs during the 2016 and 2017 open water seasons (May to October), addressing the first two objectives of this study. This is achieved by (1) establishing background meteorological conditions, (2) discussing local meteorological conditions, daily evaporation values, and evaporation drivers, (3) comparing meteorological driving data collected over-lake vs land, and (4) comparing measured evaporation data and trends from this study to relevant literature.

4.1 Background Meteorology

The Canadian Prairies typically experience warm summers and cold dry winters with peak precipitation occurring in June. This pattern is present in the Climate Normals for the ECCC weather stations near the study reservoirs (Figure 4.1). Climate Normals for Val Marie Reservoir were taken from the Val Marie Southeast station (49.06^{o} N, 107.59^{o} W, approximately 30 km SE of the reservoir). Climate Normals were not available for the station nearest Shellmouth Reservoir (Roblin, 51.18^{o} N, 101.36^{o} W, approximately 10 km NE of the reservoir), so the second nearest station (Langenburg, 50.90^{o} N, 101.72^{o} W, approximately 30 km SW of the reservoir) was used. Average annual precipitation is 353 mm for Val Marie and 464 mm for Shellmouth. Daily average temperatures range from -10.8 ^{o}C in January to 18.5 ^{o}C in July for Val Marie and -16.6 ^{o}C in January to 17.7 ^{o}C in July for Shellmouth.

Monthly precipitation and temperature averages for the study years were obtained from the Val Marie Southeast and Roblin stations. Both sites had higher than normal precipitation in 2016 (517 mm and 550 mm, respectively) and lower than normal precipitation in 2017 (150 mm and 249 mm, respectively). July 2017 was a particularly hot and dry month at Val Marie, where the daily maximum temperature exceeded 30 ^{o}C for 17 of 31 days and only 9.1 mm rainfall was recorded.

The predominant wind directions during the open water periods were observed to align with the reservoir valleys. At the Val Marie buoy, these winds were NW and SE in origin (Figure 4.2). Fetch distances from the buoy to the reservoir edge were approximately 2.8 km to the NW and 0.6 km to the SE (refer to Figure 3.2). At the Shellmouth buoy, the predominant winds were from the WNW and SSE directions (Figure 4.2). Fetch distances from the buoy to the reservoir edge were approximately 1.6 km to the WNW and 2.3 km to the SSE.

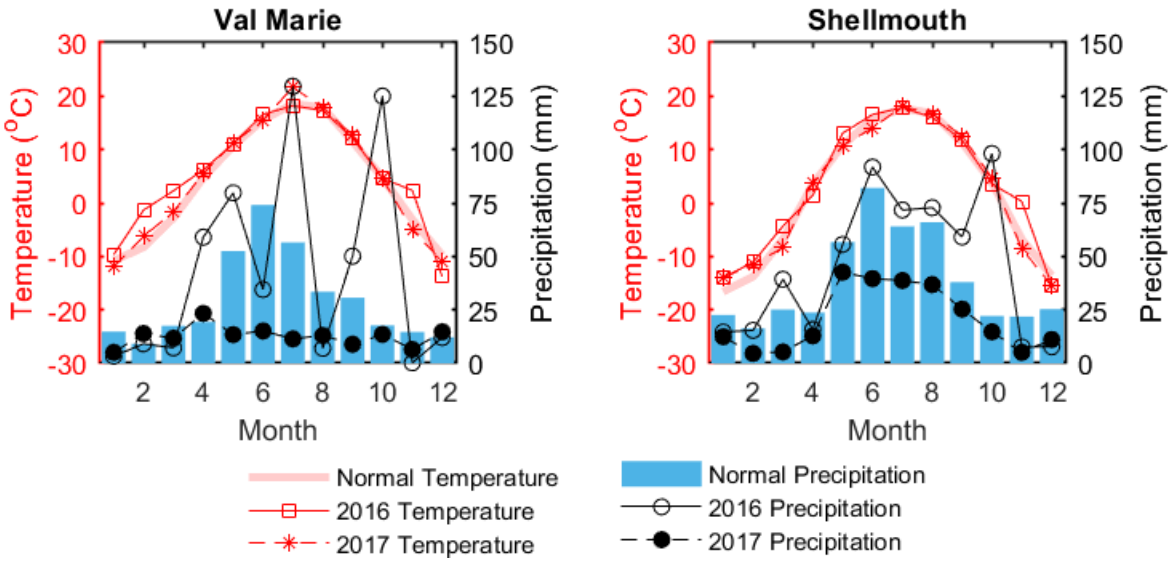

Figure 4.1 – Average daily temperatures and total precipitation for each month of the year at the nearest ECCC weather stations to each reservoir.
Note: Normals are 30-year averages for 1981-2010.

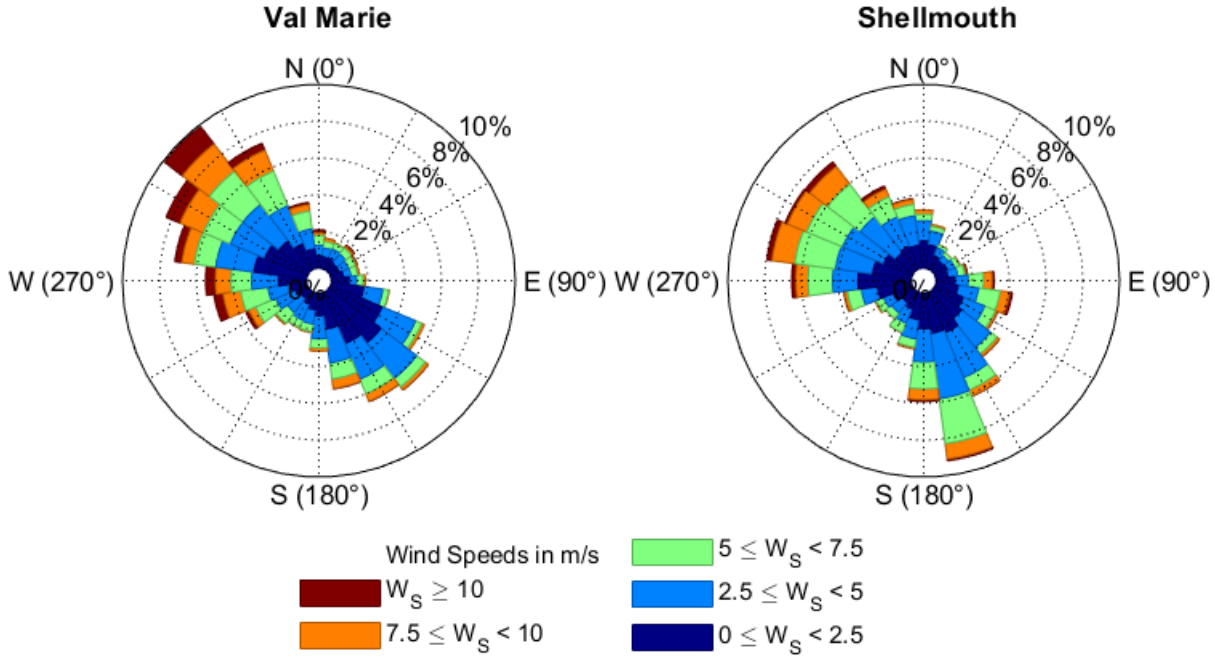

Figure 4.2 – Average wind speeds and directions measured every 15 minutes at the buoys.
Note: Predominant winds align with reservoir valley orientation

4.2 Measured Evaporation and Its Drivers

4.2.1 Daily Evaporation and Meteorological Conditions

Val Marie Reservoir

Evaporation measurements at Val Marie for the 2016 season averaged 3.0 mm/d (Figure 4.3a). The highest daily evaporation rate was recorded on May 9th (9.2 mm/d) with smaller peaks in late August and early October. Generally, daily evaporation rates remain relatively high (9 % of days measured > 5.0 mm/d even without mid-summer measurements) and display a large amount of variability (std dev = 2.1 mm/d). Evaporation during the 2017 open water period averaged 4.0 mm/d (std dev 1.8 mm/d) and represents the most complete dataset of the field study (Figure 4.4a). Peak daily evaporation occurred on June 10th (9.6 mm/d) with smaller peaks throughout the season, including one in early October similar to that observed in 2016.

Windspeeds at Val Marie (Figure 4.3b and Figure 4.4b) were strong and highly variable during both years (hourly mean 4.3 m/s, range 0.1 – 17.2 m/s, std dev 2.8 m/s). Seasonally, windspeeds were higher in spring and fall than summer. Hourly mean air temperature measurements at the Val Marie buoy ranged from -8.6 to 34.6 ^{o}C. There was gradual warming throughout the month of May, gradual cooling through late August and September, and rapid cooling in early October (Figure 4.3c and Figure 4.4c). Surface temperatures followed the same seasonal pattern (Figure 4.3d and Figure 4.4d). Daily averages and ranges of relative humidity, net radiation and atmospheric pressure measurements at Val Marie Reservoir can be viewed in the remaining panels of Figure 4.3 and Figure 4.4.

Shellmouth Reservoir

Evaporation measurements at Shellmouth Reservoir during the 2016 open water season averaged 0.43 mm/d (std dev 0.38 mm/d) from June 23rd to October 25th (Figure 4.5a). Peak daily evaporation was 1.7 mm/d on September 25th with smaller peaks throughout the year. Evaporation measurements during the 2017 open water season began earlier in the season but sustained two large gaps in the summer months because of data logger complications (Figure 4.6a). Daily average evaporation rates were slightly higher than 2016 rates at 0.47 mm/d (std dev

0.43 mm/d). Peak daily evaporation was on May 24th (1.9 mm/d), with additional peaks observed in July, September and October.

The observed rates of evaporation were much lower than expected and are believed to be a result of technical errors with the buoy system. Numerous in-season checks were made to validate data from the buoy and components of the eddy covariance measurements were validated independently (plots in Appendix F). It is apparent that there were calibration issues with the KH20 gas analyzer starting partway through the 2016 season, but this cannot fully explain the low flux outputs recorded since there were no calibration issues at the beginning of 2016 and low flux outputs were also recorded then. The remaining thesis will continue to examine factors related to evaporation at Shellmouth but will not further analyze the evaporation measurements themselves.

Conditions at Shellmouth were also quite windy (Figure 4.5b and Figure 4.6b). Windspeeds measured during 2016 and 2017 at the buoy averaged 3.9 m/s hourly (range 0.1 – 16.3 m/s, std dev 2.4 m/s). Seasonally, windspeeds were lower during summer months as compared to spring and fall averages. Hourly mean air temperatures at the Shellmouth buoy ranged from -6.6 – 30.4 ºC. Gradual cooling throughout September in both years was followed by an abrupt temperature drop in early October 2016 and continued gradual cooling in October 2017 (Figure 4.5c and Figure 4.6c). Surface water temperatures followed a similar pattern but sustained much smaller daily fluctuations (Figure 4.5d and Figure 4.6d). Daily averages and ranges of relative humidity, net radiation and atmospheric pressure measurements at Shellmouth Reservoir can be observed in the remaining panels of Figure 4.5 and Figure 4.6. A net radiation model (described in Section 3.3.2) and atmospheric pressure from the Roblin land station are presented as dashed lines in the two bottom panels of Figure 4.5 and Figure 4.6 because the local measurements of these variables were also believed to be incorrectly measured.

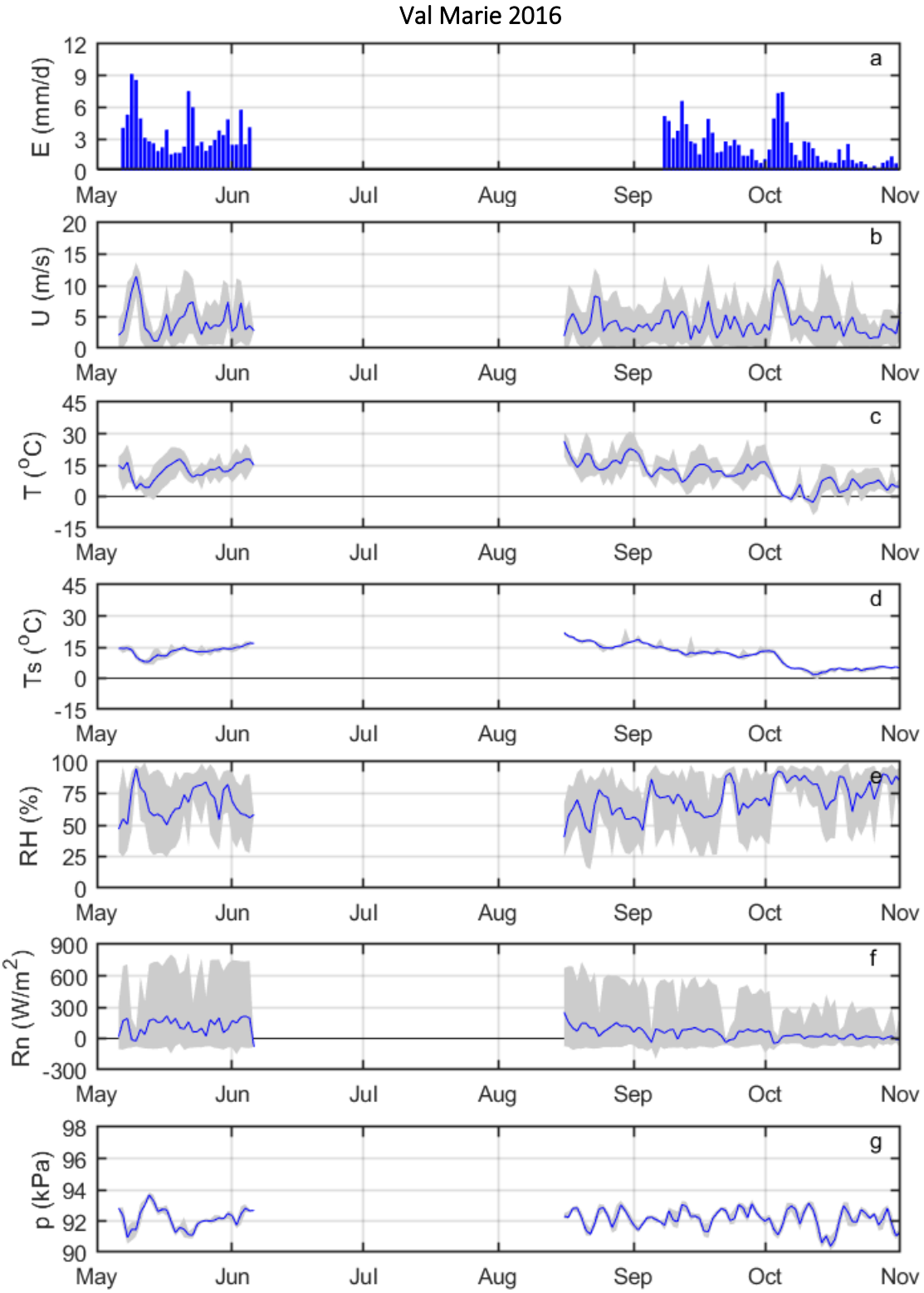

Figure 4.3 – Daily evaporation and local conditions measured at the Val Marie buoy 2016.
Note: Evaporation bars are filtered and filled daily, solid lines are daily means and shaded areas are daily ranges. The summertime gap is from buoy damage and reconstruction.

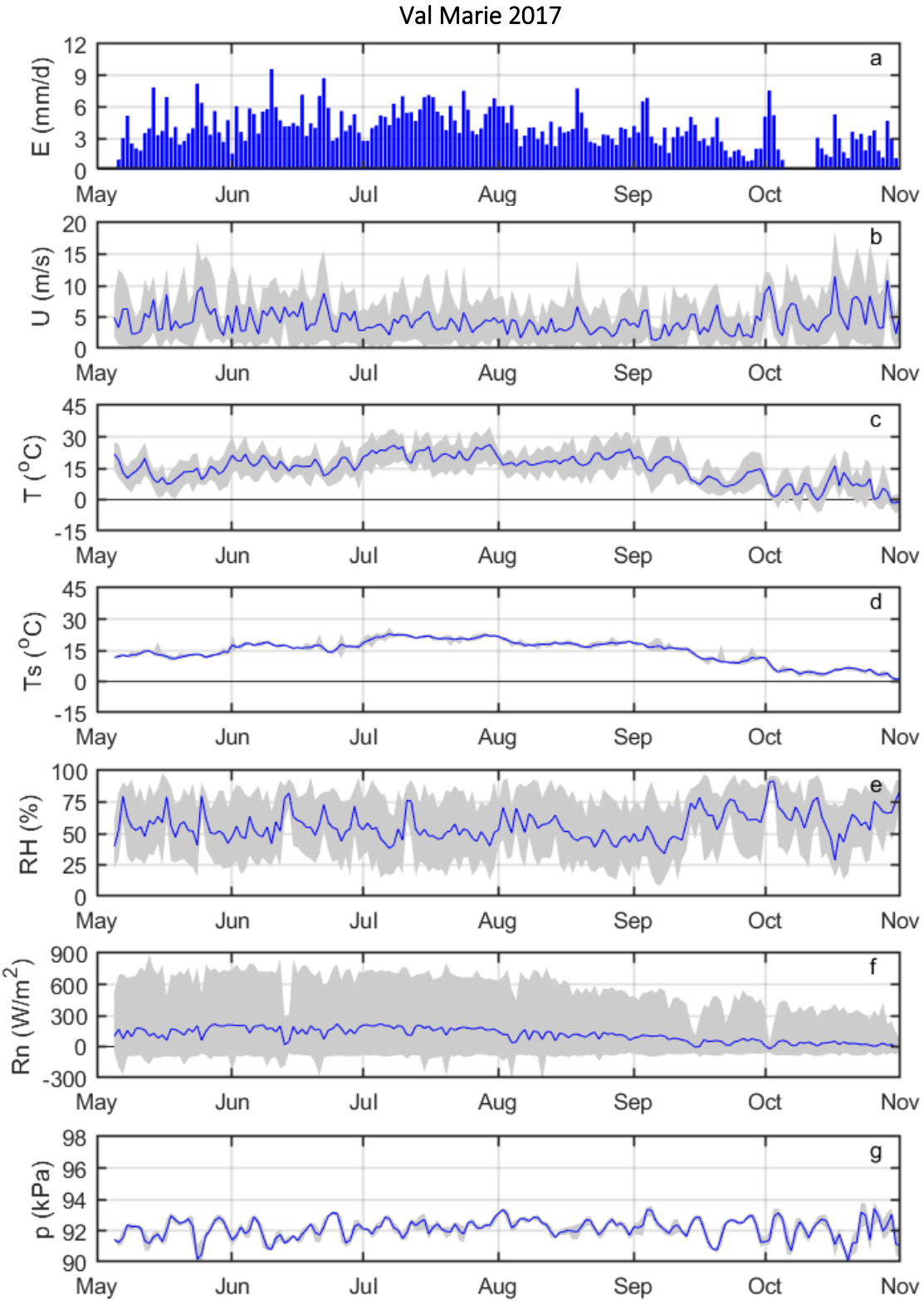

Figure 4.4 – Daily evaporation and local conditions measured at the Val Marie buoy 2017.
Note: Evaporation bars are filtered and filled daily, solid lines are daily means and shaded areas are daily ranges.

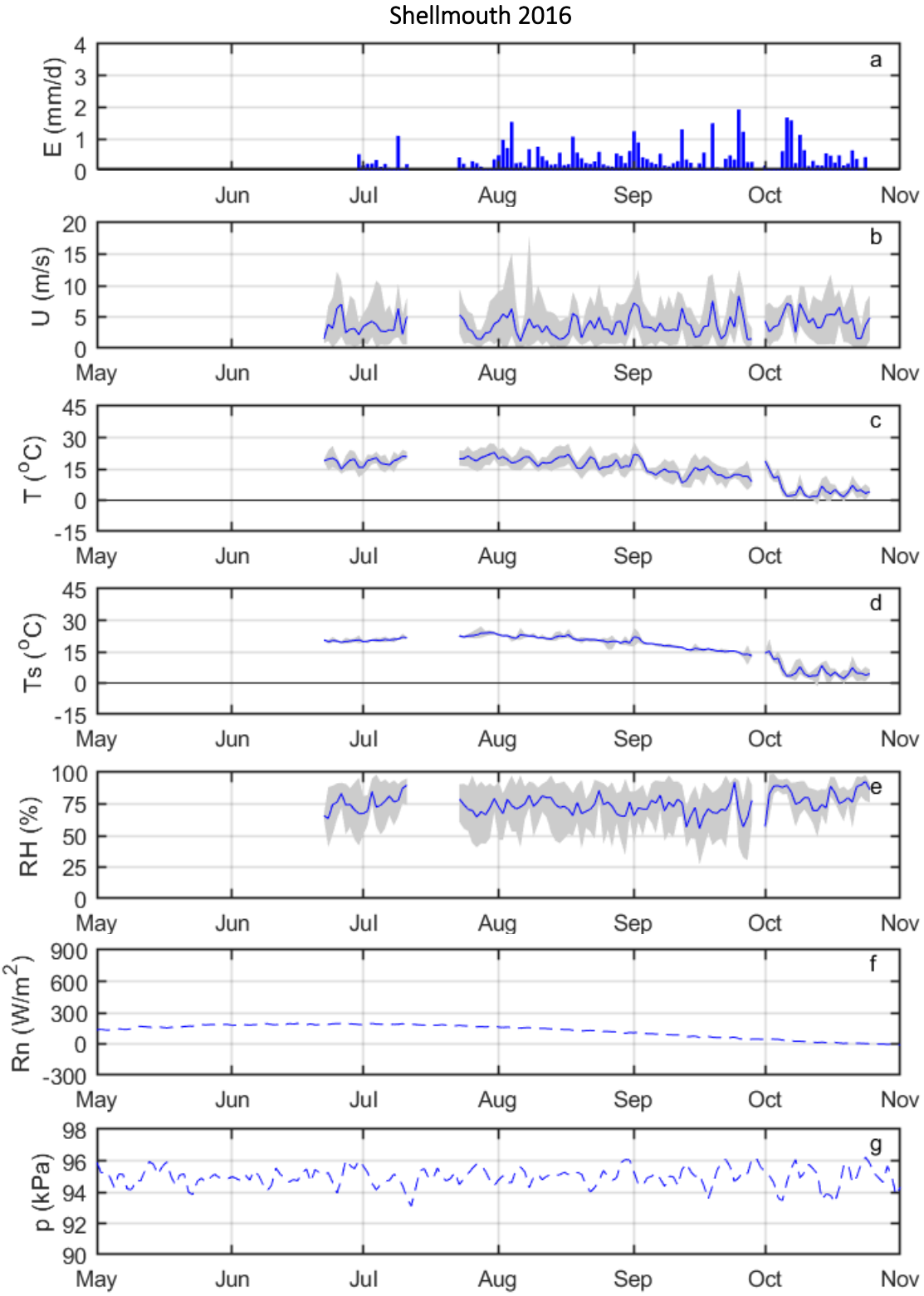

Figure 4.5 – Daily evaporation and local conditions measured at the Shellmouth buoy 2016.
Note: Evaporation bars are filtered and filled daily, solid lines are daily means, shaded areas are daily ranges, and dashed lines are modeled/measured elsewhere. Data gaps are from storage issues.

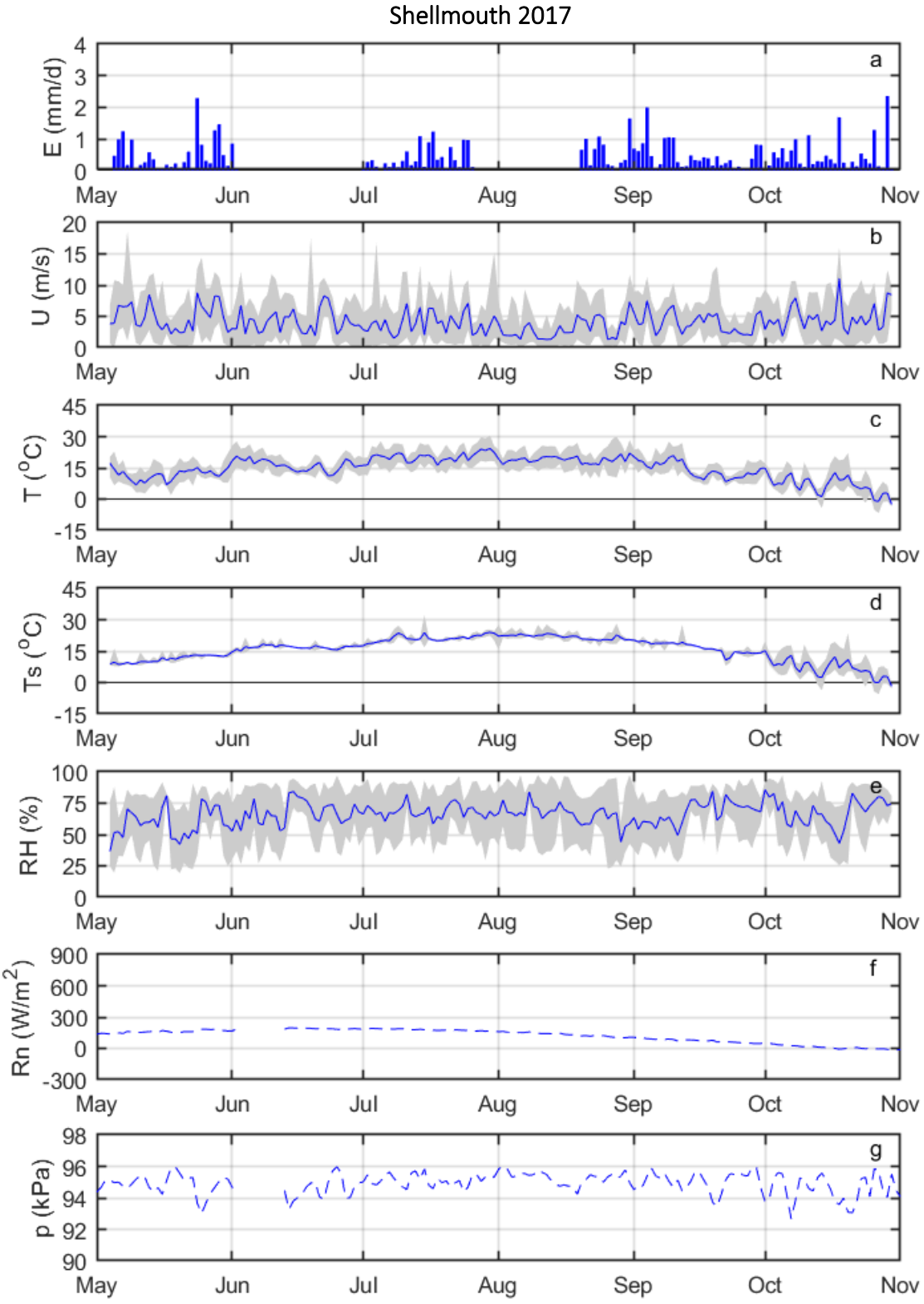

Figure 4.6 – Daily evaporation and local conditions measured at the Shellmouth buoy 2017.
Note: Evaporation bars are filtered and filled daily, solid lines are daily means, shaded areas are daily ranges, and dashed lines are modeled/measured elsewhere. Data gaps are from storage issues.

4.2.2 Gradients of Temperature and Water Vapour Pressure

The observed gradients of temperature and water vapour pressure over the lake surface provide insight regarding the mechanisms of evaporation. While temperature gradients indicate the strength of sensible heat exchange, they also play a role in determining the atmospheric stability over the water surface. Vapour pressure gradients are cited as key drivers of evaporation at other lakes (Nordbo et al., 2011; Shao et al., 2015) and are required inputs for aerodynamic evaporation estimates (such as the Meyer formula and Bulk Transfer approach). Gradients of temperature and water vapour pressure at Val Marie and Shellmouth Reservoirs were examined individually in this section following Figure 4.7 to Figure 4.12 depicting (1) diurnal temperature patterns by month, (2) diurnal vapour pressure, windspeed and evaporation patterns by month and (3) seasonal temperature and vapour pressure gradients.

Val Marie Reservoir

Mean diurnal patterns of air and water temperatures at Val Marie during 2016 and 2017 are plotted for the months of May through October (Figure 4.7a-f). Additionally, temperatures measured at the Val Marie Southeast land station are included here. Generally, both water and air temperatures peak during the afternoon and cool in the evening. Due to the large heat capacity of water, the variation in water temperatures throughout the day are minimal compared to air temperatures and do not reach a maximum until approximately 18h. The reservoir also has a moderating effect on the air temperature: air temperatures measured at the buoy are slightly less extreme and delayed (peaking at approximately 18h) than air temperatures measured at the Val Marie Southeast land station (peaking at approximately 15h). The result is a consistently positive temperature gradient overnight and throughout the morning (unstable atmospheric conditions), followed by a consistently negative temperature gradient during the afternoon and early evening (stable atmospheric conditions). Seasonally, the pattern is similar between months, but noticeable amplitude differences occur in response to weakening solar radiation in the shoulder seasons.

The measured vapour pressure gradients exhibit a different diurnal pattern: gradients are consistently positive and are highest throughout the afternoon and early evening (Figure 4.8a-f). This pattern has been observed previously (Vesala et al., 2006) and aligns well with diurnal evaporation and windspeed patterns, a correlation that is also commonly observed (Blanken et

al., 2011; Bouin et al., 2012; Granger & Hedstrom, 2011; Mammarella et al., 2015; McGloin et al., 2014a; Potes et al., 2017; Salgado & Le Moigne, 2010; Shao et al., 2015; Xiao et al., 2018). The positive vapour pressure gradient over Val Marie Reservoir continues to drive evaporation overnight because the vapour pressure of the saturated water surface is always higher than the overlying air (vapour pressure increases with both heat and water content). During the day, when the temperature of the water surface increases, the vapour pressure of the air that is in contact with the water also increases. At the same time, the overlying air warms up and becomes less humid. The increased afternoon wind speeds may also contribute to the drying of the overlying air. The combination of increased vapour pressure at the water surface and decreased water vapour pressure of the overlying air increases the afternoon gradient resulting in higher evaporation rates at this time of day.

Despite the relatively consistent, diurnal temperature pattern, the daily average temperature gradient at Val Marie Reservoir alternates frequently between warmer air and water surfaces throughout the open water season (Figure 4.9a), presumably depending on synoptic conditions. Daily average vapour pressure gradients are always positive and peak in July (Figure 4.9b). From a seasonal perspective, the magnitude of daily evaporation follows a very similar trend as vapour pressure differences with little relationship between evaporation and temperature gradients (Figure 4.9c).

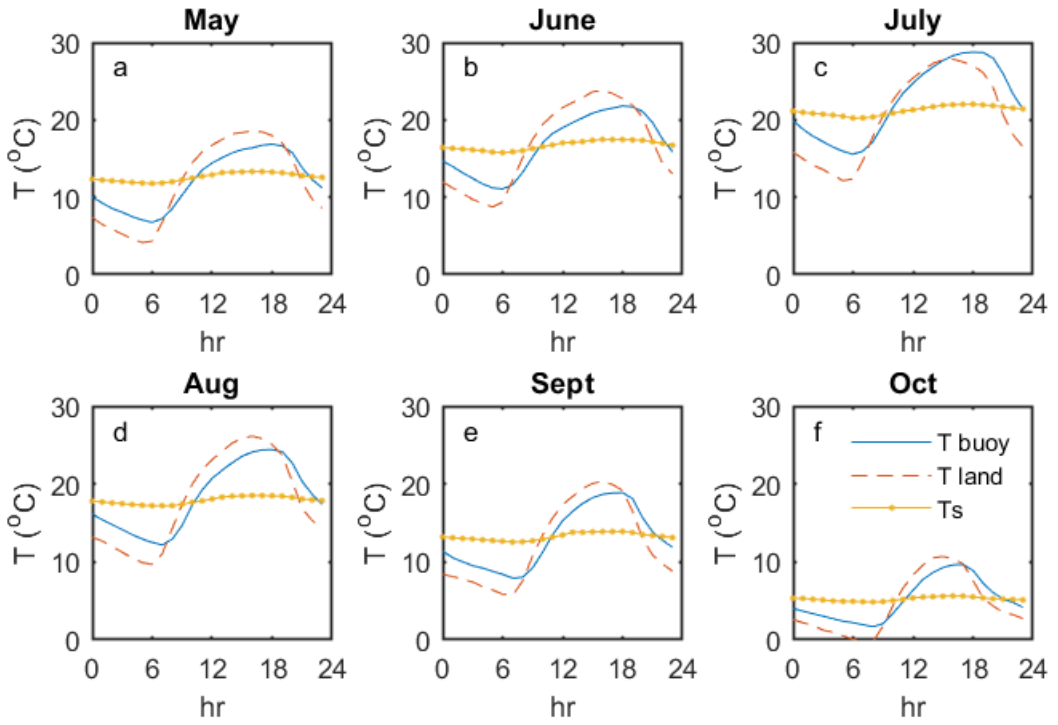

Figure 4.7 – Monthly mean diurnal air temperatures (T buoy and T Land) and surface water temperatures (Ts) at Val Marie Reservoir 2016 and 2017

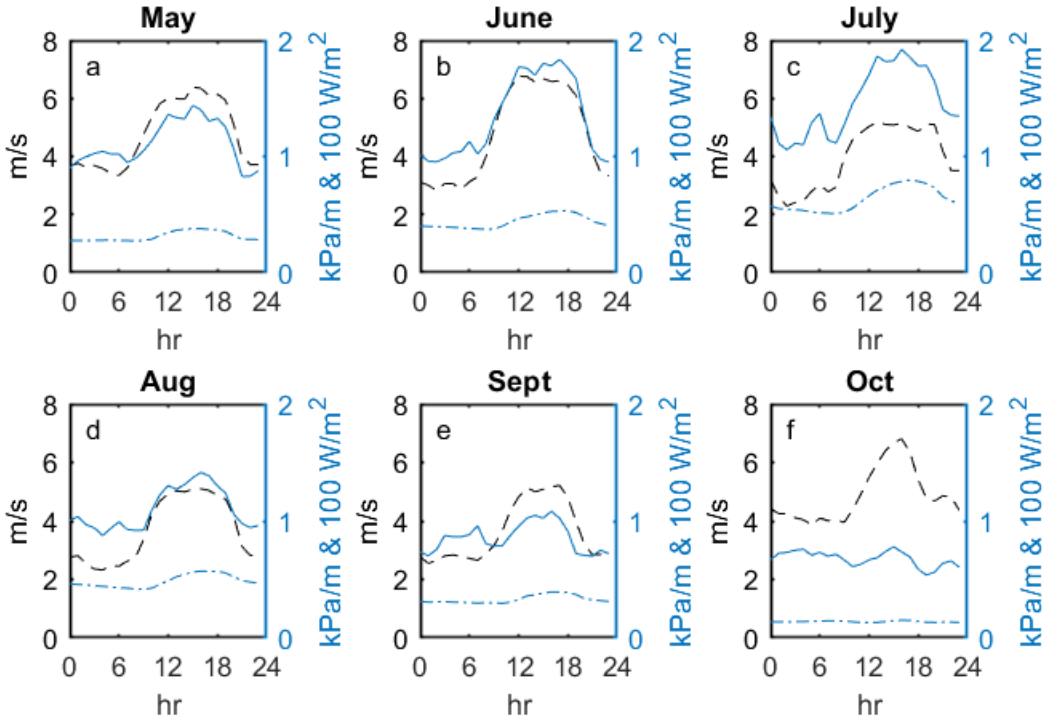

Figure 4.8 – Monthly mean diurnal latent heat flux (solid blue line), windspeed (dashed black line) and vapour pressure gradient (dotted blue line) at Val Marie Reservoir 2016 and 2017

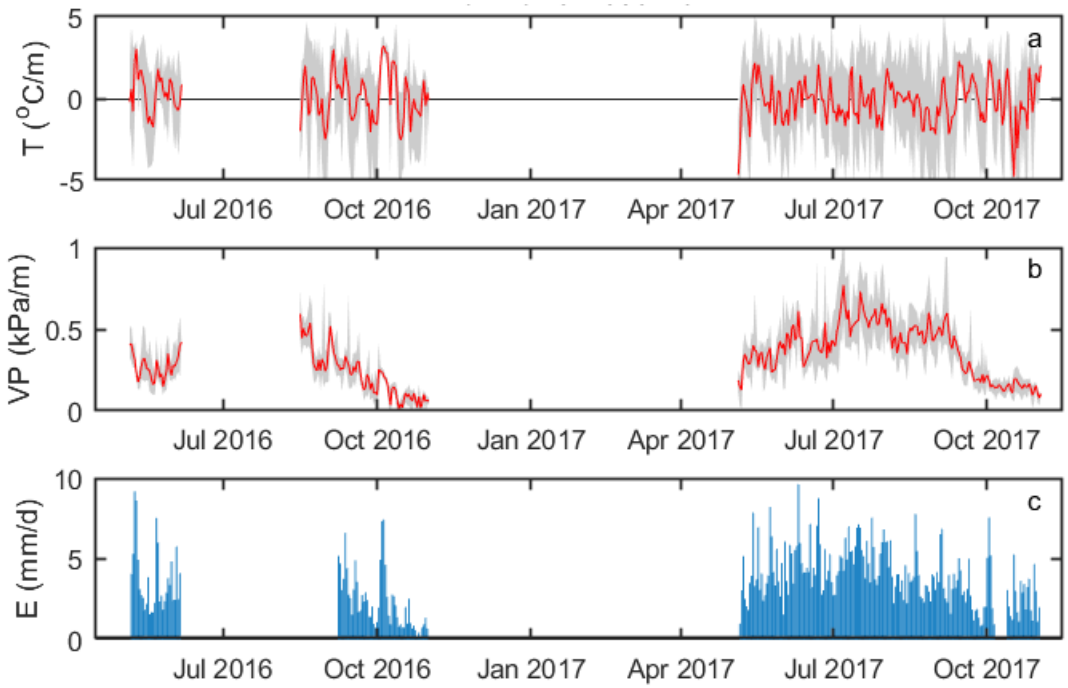

Figure 4.9 – Temperature gradients (T) and Vapour pressure gradients (VP) compared to daily evaporation rates (E) for Val Marie Reservoir 2016 and 2017
Note: Red lines are daily means and grey shading is daily ranges for gradients

Shellmouth Reservoir

Mean diurnal temperature trends for each month at Shellmouth Reservoir also show greater variation in air temperatures compared to water surface temperatures and a slight moderating effect on the air temperatures measured at the buoy (Figure 4.10a-f). Water surface temperatures increase during the spring and early summer months until they are consistently warmer than air temperatures throughout the entire day in August and September. In October, surface temperatures sync up with overlying air temperatures. This pattern is different from the one observed at Val Marie. Algae observed on the surface of Shellmouth Reservoir during the summer months may contribute to the surface warming since algae affects the absorption of incoming radiation (Andrade et al., 2019). This can both increase surface temperature and reduce depth penetration of solar energy, altering the subsurface warming and mixing processes. In the case of a humic lake, reduced water clarity resulted in a shallower mixed layer and increased longwave and turbulent heat loss (Heiskanen et al., 2015). It should be noted that algae was also observed on the surface of Val Marie Reservoir during the summer months, so it's presence alone cannot explain the surface warming at Shellmouth. A more likely explanation is that Shellmouth Reservoir is much deeper than Val Marie Reservoir and takes longer to build and release heat throughout the season. This is discussed further in Section 4.2.4.

Diurnal trends at Shellmouth Reservoir show vapour pressure gradients and windspeeds peak in the afternoon (Figure 4.11a-f). Daily average temperature gradients at Shellmouth were relatively strong with surface temperatures greater than air temperatures most of the summer (Figure 4.12a) and peaking in September both years. Vapour pressure gradients were highest in late summer/early fall (Figure 4.12b). The prevalence of strong positive vapour pressure gradients should result in higher evaporation rates.

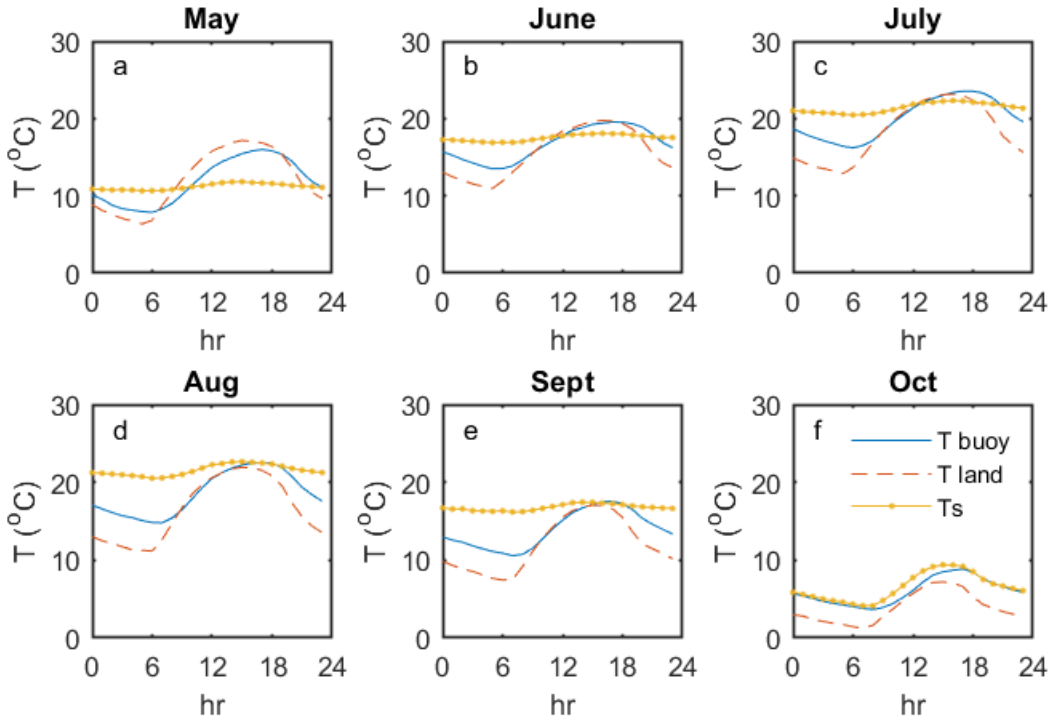

Figure 4.10 – Monthly mean diurnal air temperatures (T buoy and T Land) and surface water temperatures (Ts) at Shellmouth Reservoir 2016 and 2017

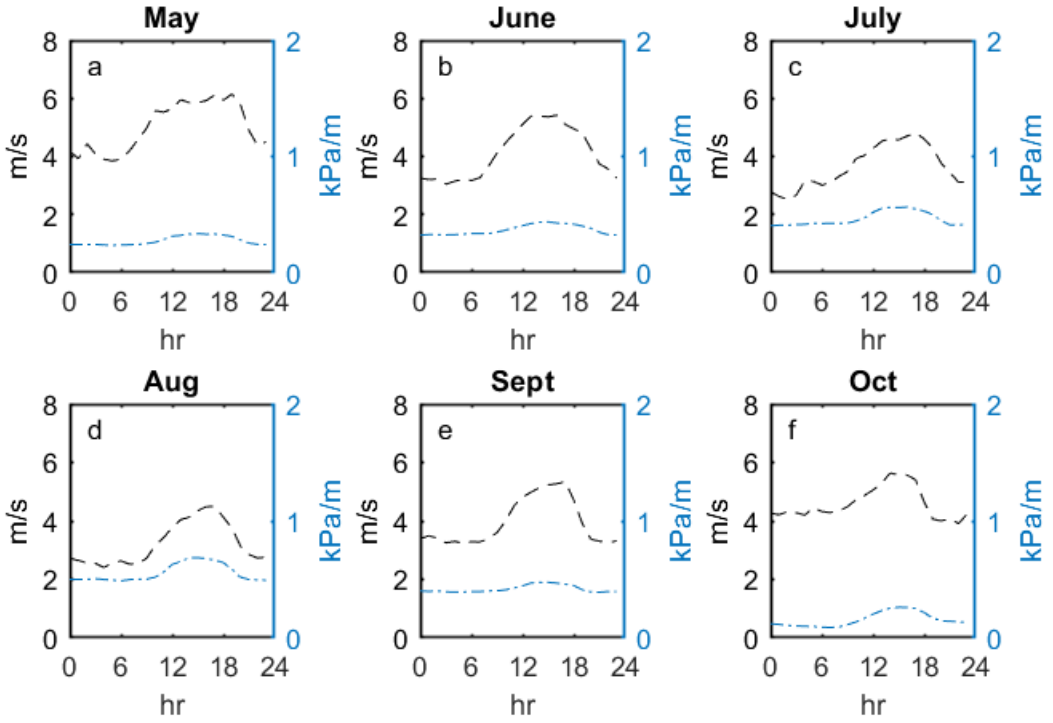

Figure 4.11 – Monthly mean windspeed (dashed black line) and vapour pressure gradient (dotted blue line) at Shellmouth Reservoirs 2016 and 2017

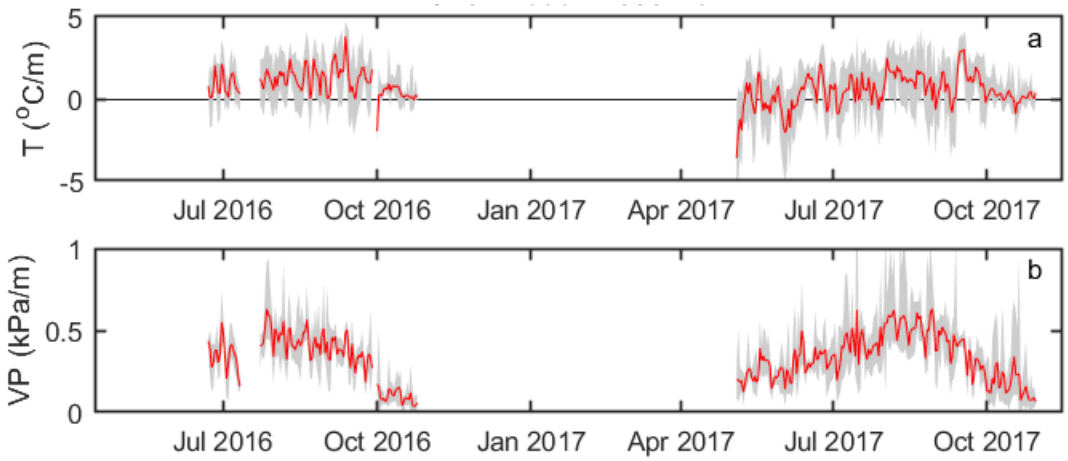

Figure 4.12 – Temperature gradients (T) and Vapour pressure gradients (VP) for Shellmouth Reservoir 2016 and 2017
Note: Red lines are daily means and grey shading is daily ranges for gradients

4.2.3 Aerodynamic Forcing

Val Marie Reservoir

A frequency histogram of hourly windspeeds (Figure 4.13a) reveals that low to moderate windspeeds of 1-3 m/s are most common at Val Marie Reservoir, but stronger winds are also commonly observed. Generally, there is a near-linear increase in the latent heat flux with increasing wind speed (Figure 4.13c), suggesting that windspeed is a key driver of evaporation. Indeed, it can also be noted at the daily scale that windspeed has the strongest relationship with evaporation ($R^2 = 0.30$) of any single variable measured at Val Marie Reservoir (see Figure 4.3 and Figure 4.4 and Appendix D). However, at weekly timescales, the correlation between evaporation and windspeed is decreased ($R^2 = 0.03$), and the correlation with temperature related variables becomes stronger (details in Appendix D).

Atmospheric conditions (Figure 4.13d) are generally unstable at lower windspeeds (<5 m/s). This is also seen in Figure 4.7 and Figure 4.8 where during the evenings, when windspeeds are typically the lightest, the water temperature is warmer than the overlying air. During these light wind conditions, the stability values are highly variable but then tend towards neutral as windspeeds increase to value greater than 5 m/s.

Surface roughness effects are presented as the mean wind speed normalized by the friction velocity, i.e. U/u* (Figure 4.10g). Higher values indicate a smoother surface and less shear created by roughness effects. Relative surface roughness decreases as windspeeds increase from 0-3 m/s, decreases to approximately 8 m/s and increases again when windspeeds exceed 8 m/s due to the influence of surface waves. The initial low values indicating rough conditions are likely due to poorly sampled momentum fluxes at low wind speeds.

The observed relationship between windspeed and evaporation partially explains the high rates of evaporation measured in early October of both years. During this period, windspeeds exceeded 5 m/s for multiple days. This persistent air movement cools the near surface layer while removing existing moisture, thus increasing the moisture and temperature gradients. In order to properly capture this high evaporation event, whether in measurement or modelling scenarios, short-term windspeeds are extremely useful. Previous studies have linked cold fronts with high evaporation events (Blanken et al., 2000; McGloin et al., 2015; Xiao et al., 2018). Cold

fronts are characterized by wind gusts, a sudden drop in temperature, cloudy conditions, precipitation events, and a drop then rise in atmospheric pressure. At Val Marie Reservoir, all cold front characteristics are present in the data in early October (Figure 4.3 and Figure 4.4), suggesting that the link between cold fronts and high evaporation events is active here. This release of energy was cited as the main energy source for evaporation during fall at a small Minnesota lake (Xiao et al., 2018) and may explain the high evaporation rates measured in early October at Val Marie.

Shellmouth Reservoir

At Shellmouth Reservoir, conditions are generally unstable at low windspeeds (approximately 5 m/s) then settles to neutral conditions as windspeeds increase (Figure 4.13e). Shellmouth Reservoir's apparent surface roughness (Figure 4.13g) decreases up to wind speeds of approximately 3 m/s, then increases with wind speed up to approximately 8m/s windspeeds and decreases rapidly thereafter. This may be related to high sensitivity to the motion of the buoy or different wave pattern development over the larger reservoir. Further investigation into surface roughness conditions at Shellmouth could also be helpful for future evaporation estimates.

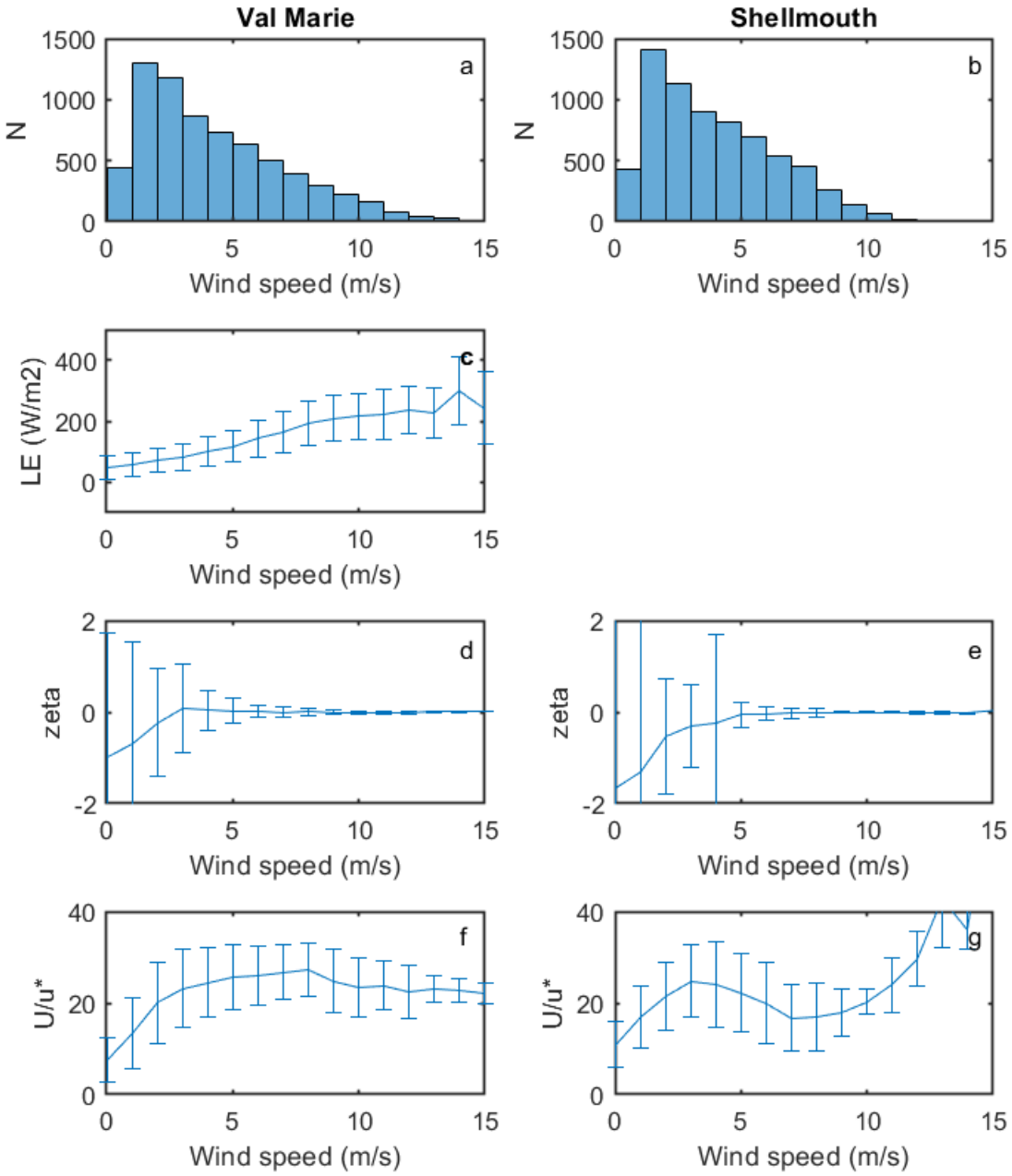

Figure 4.13 – Frequency of wind speeds measured at the Val Marie and Shellmouth buoys compared to evaporation, stability and surface roughness changes with increasing wind speeds using hourly averaged data.

Note: Data are 15 min values bin-averaged with a bin size of 1 m/s

4.2.4 Surface Energy Partitioning and Heat Storage

Much of the solar radiation received at the water surface is absorbed and therefore goes into warming up the reservoir. In this study, thermistor strings were used to record the accumulation of heat within the water body (Figure 4.14 to Figure 4.16 and Figure 4.20 to Figure 4.22). These temperature measurements allowed for heat storage calculations (Figure 4.17) and surface energy balance partitioning (Figure 4.18, Figure 4.19, Figure 4.23 and Figure 4.24). The effect on heat storage on the evaporation measurements at Val Marie Reservoir and more probable evaporation rates than those measured at Shellmouth Reservoir are discussed.

Val Marie Reservoir

Surface temperatures throughout the season loosely follow variations in air temperatures measured at the buoy (Figure 4.14a and Figure 4.15a). Sub-surface temperatures measurements at Val Marie show a well-mixed water column in 2016 when five thermistors (0.2 m, 0.5 m, 1.0 m, 2.0 m and 3.0 m depths) were retrieved from the reservoir at the end of the season (Figure 4.14b). During the 2017 season, only two thermistors (0.5 m, 1.0 m, and 2.0 m depths) were retrieved. Since the water column was so well mixed in 2016, it was determined reasonable to apply the 2.0 m temperature measurement to the remaining 1-2 m of water below (Figure 4.15b). In 2016, hourly mean depth-weighted water temperatures peaked at 23.6 ^{o}C the evening of July 25th, 2016 and dropped as low as 3.1 ^{o}C the morning of October 13th, 2016. In 2017 temperatures had already warmed up to 12.8 ^{o}C when measurements began at noon on May 6th, 2017. Ranges in 2017 were very similar to 2016: hourly mean depth-weighted water temperatures peaked at 24.5 ^{o}C the evening of July 9th, 2017 and dropped as low as 1.2 ^{o}C the morning of November 2nd, 2017.

Even though the lake appeared to be well-mixed, weak diurnal stratification and mixing patterns were observed during some calm summer days. An example of this is shown for Aug 13-18, 2016 (Figure 4.16). For each subsequent warm, relatively calm day, the peak afternoon water temperature increased by approximately 1 degree Celsius, creating a 2- to 4-degree difference between the top and bottom of the water column, then partially mixed overnight. Once the wind picked up on the 18th, the surface cooled, causing a temporary inversion, followed by full mixing of the measured water column.

Seasonally, cumulative heat storage gradually builds throughout the summer months, diminishes during fall, and experiences an abrupt release in early October of both years (Figure 4.17). This energy storage is responsible for a minor delay of a few weeks between peak evaporation and peak net radiation. This subtle effect of seasonal heat storage at Val Marie is supported by literature: while large deep lakes can have a delay in peak evaporation up to five months after peak summer radiation and air temperatures (Blanken et al., 2011), shallower lake evaporation is more tightly coupled to radiation and overlying air temperatures (Lenters et al., 2005; Wang et al., 2014). Val Marie is a moderately shallow lake compared to other study lakes and should be expected to have a moderate delay in peak evaporation. This is discussed further in Section 4.4.

The surface energy balance at Val Marie is dominated by the latent heat flux (Figure 4.18a-b). The sum of the three surface energy components (latent heat flux, sensible heat flux and heat storage flux) agrees reasonably with the measured and modelled net radiation, however, large variations at the weekly timescale are still present (Figure 4.19a-b). Increasing the timescale to 10 days and two weeks (not shown) did little to improve the agreement.

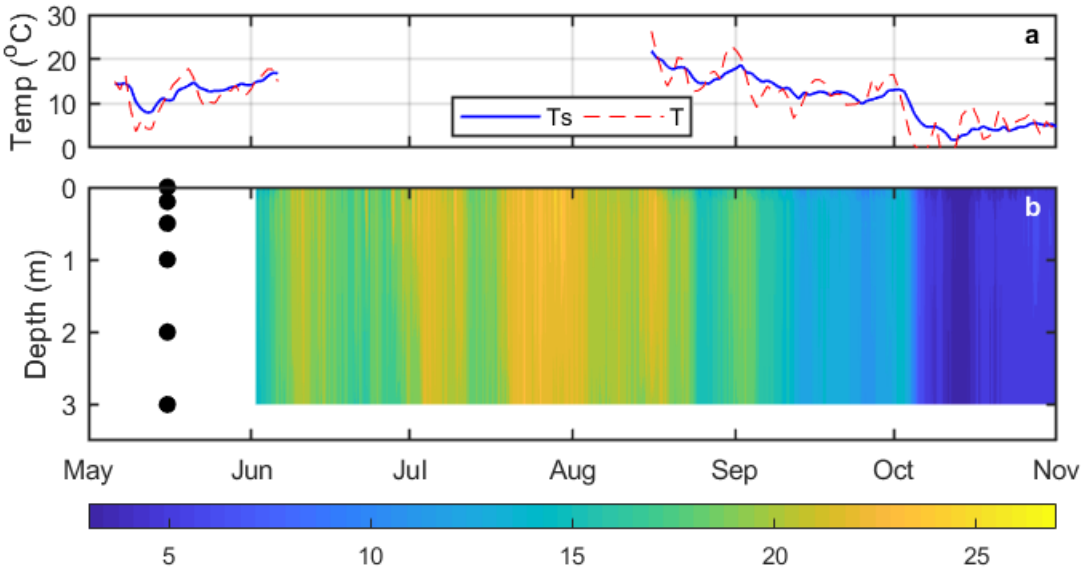

Figure 4.14 – Daily mean surface temperatures (Ts), daily mean air temperatures (T) and 15min mean water temperatures (panel b) measured at Val Marie Reservoir in 2016
Note: Sensor depths indicated by black circles

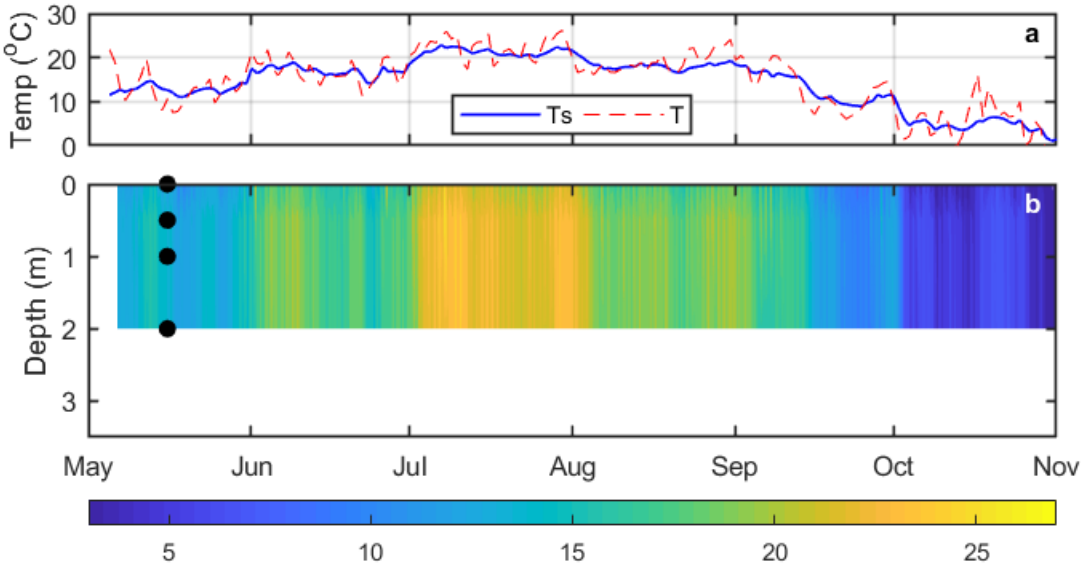

Figure 4.15 – Daily mean surface temperatures (Ts), daily mean air temperatures (T) and 15min mean water temperatures (panel b) measured at Val Marie Reservoir in 2017
Note: Sensor depths indicated by black circles

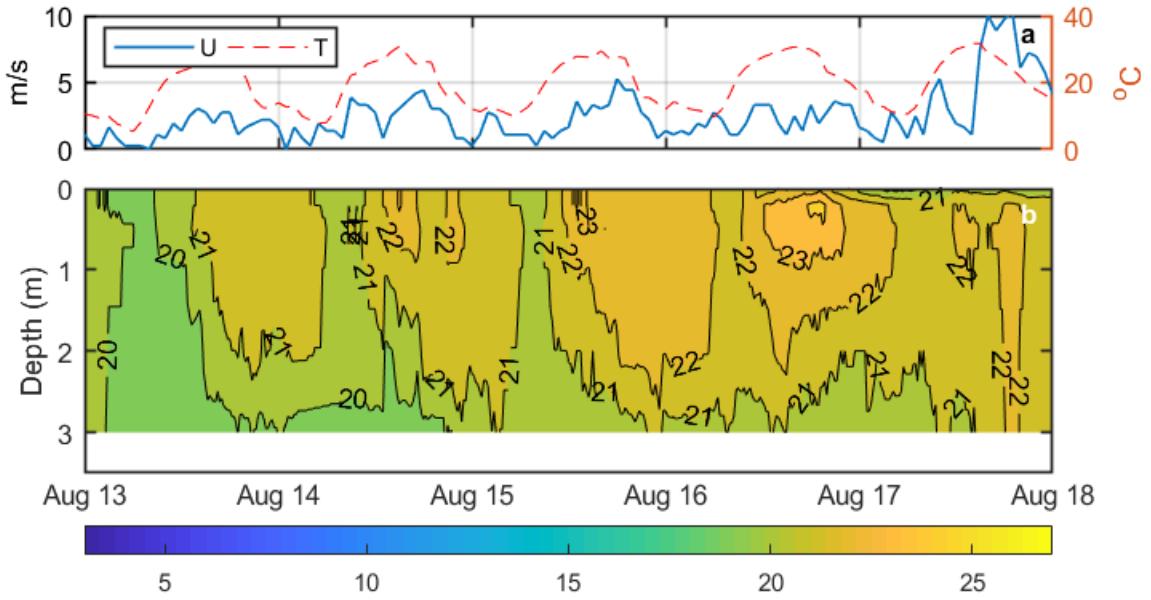

Figure 4.16 – Hourly windspeeds (U), hourly air temperatures (T) and 15min mean water temperatures (panel b) measured at Val Marie Reservoir Aug 13-18, 2016
Note: Hourly data from Val Marie Southeast weather station in place of over-lake data gap while buoy repaired

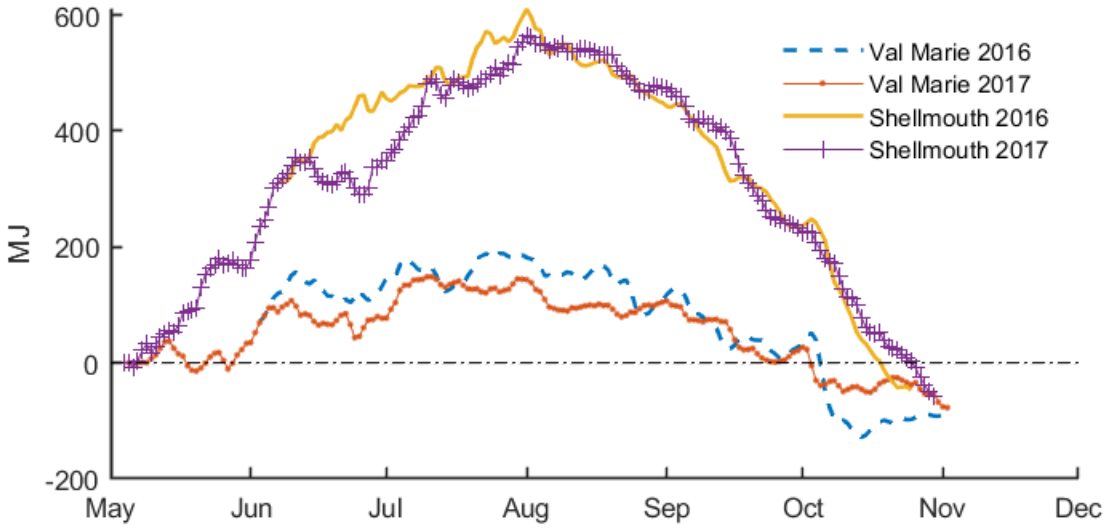

Figure 4.17 – Cumulative heat storage calculated daily for Shellmouth and Val Marie Reservoirs during the 2016 and 2017 open water seasons
Note: Values for 2016 are offset to start at roughly the same level as the same date in 2017 for comparison

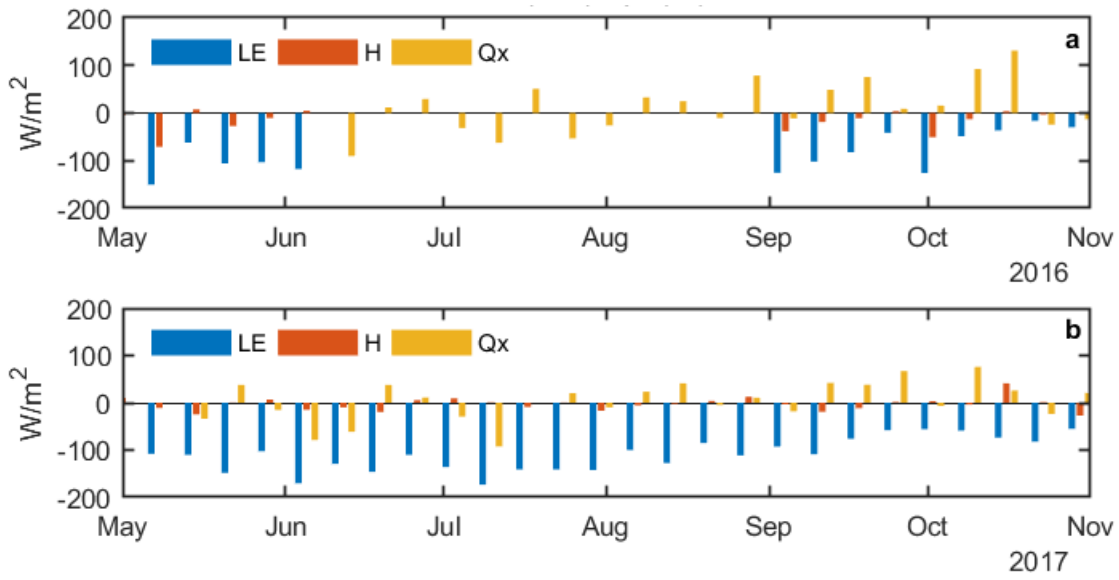

Figure 4.18 – Weekly surface energy balances at Val Marie Reservoir during the 2016 and 2017 open water seasons

Note: Surface energy balance components are latent heat (LE), sensible heat (H) and lake heat storage (Qx) fluxes

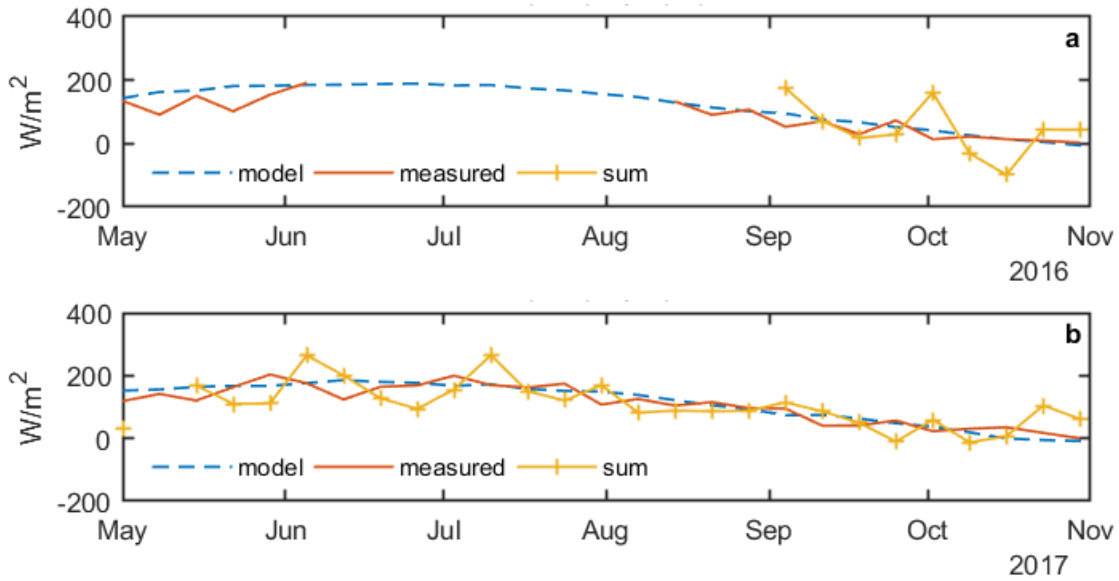

Figure 4.19 – Weekly net radiation calculated for Val Marie Reservoir during the 2016 and 2017 open water seasons

Note: The sum presented is the sum of latent heat (LE), sensible heat (H), and reservoir heat storage (Qx) fluxes

Shellmouth Reservoir

Water temperatures measured at Shellmouth Reservoir showed gradual, well-mixed warming and cooling phases (Figure 4.20b and Figure 4.21b). While ten thermistors were available for 2016 (0.2 m, 0.5 m, 0.75 m, 1.0 m, 2.0 m, 4.0 m, and 6.0 m depths on the thermistor string and 0.5 m, 0.8 m and 1.0 m depths attached to the buoy), only five were recovered in 2017 (0.25 m and 6.0 m depths on the thermistor string and 0.5 m, 0.8 m and 1.0 m depths attached to the buoy). Similar to Val Marie, the 2016 temperatures indicated a well-mixed water column and most of the temperature variation was observed in the top meter. As such, the limited depth measurements in 2017 were deemed sufficient for calculating an estimate of lake heat storage. Hourly mean depth-weighted temperatures in 2016 range from 24.0 ^{o}C on the evening of July 31st, 2016 to 6.5 ^{o}C on the morning of October 25th, 2016. In 2017, hourly mean depth-weighted temperatures peaked at 23.7 ^{o}C on the evening of July 30th, 2016 and dropped as low as 6.0 ^{o}C the morning of October 30th, 2017. Surface temperatures loosely followed air temperatures in the spring warming period (2017), were consistently warmer than air temperatures by late June (2016) or early July (2017) and synced with air temperatures in early October (2016 and 2017).

Short-term warming and mixing were observed during calm summer days (Figure 4.22). Similar to Val Marie Reservoir, warming resulted in a 2- to 4-degree top to bottom temperature difference during the day with mild mixing overnight and full mixing during wind events. Unlike the shallower Val Marie Reservoir, this stratification was restricted to within the first few meters of the surface and the rest of the measured water column was fully mixed.

Cumulative heat storage at Shellmouth Reservoir was much larger than at Val Marie Reservoir and peaked mid-summer both study years (Figure 4.17). One difference is the loss and recovery during cooler temperatures in June 2017. Such high volumes of stored energy in Shellmouth should contribute to larger fluxes in fall and a large delay in peak evaporation from peak net radiation, but fluxes remain low throughout both open-water seasons (Figure 4.5a and Figure 4.6a).

At Shellmouth, the measured surface energy balance is dominated by heat storage fluxes with very low sensible and latent heat values (Figure 4.23a-b). The sum of the three surface energy components measured at the Shellmouth buoy is approximately 100 Wm^{-2} lower on average than the net radiation model (Figure 4.24a-b). This supports the claim that the evaporation measurements at Shellmouth are unrealistically low.

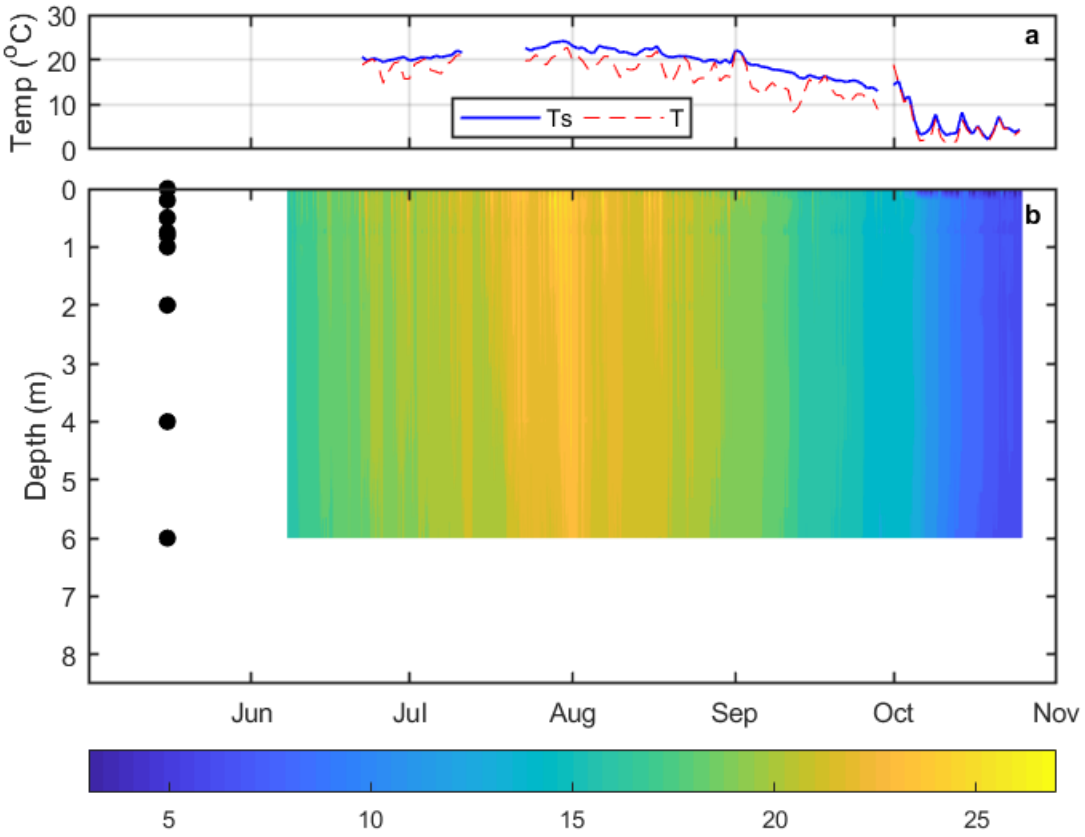

Figure 4.20 – Daily mean surface temperatures (Ts), daily mean air temperatures (T) and 15min mean water temperatures (panel b) measured at Shellmouth Reservoir in 2016
Note: Sensor depths indicated by black circles

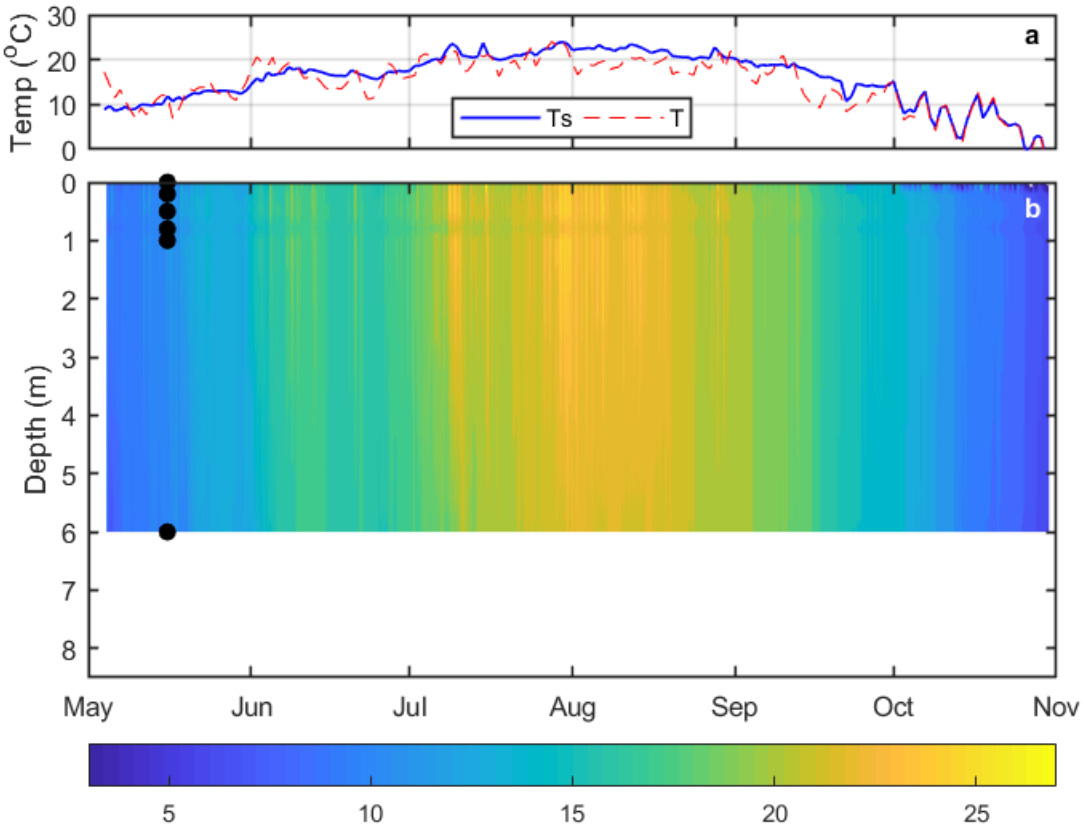

Figure 4.21 – Daily mean surface temperatures (Ts), daily mean air temperatures (T) and 15min mean water temperatures (panel b) measured at Shellmouth Reservoir in 2017
Note: Sensor depths indicated by black circles

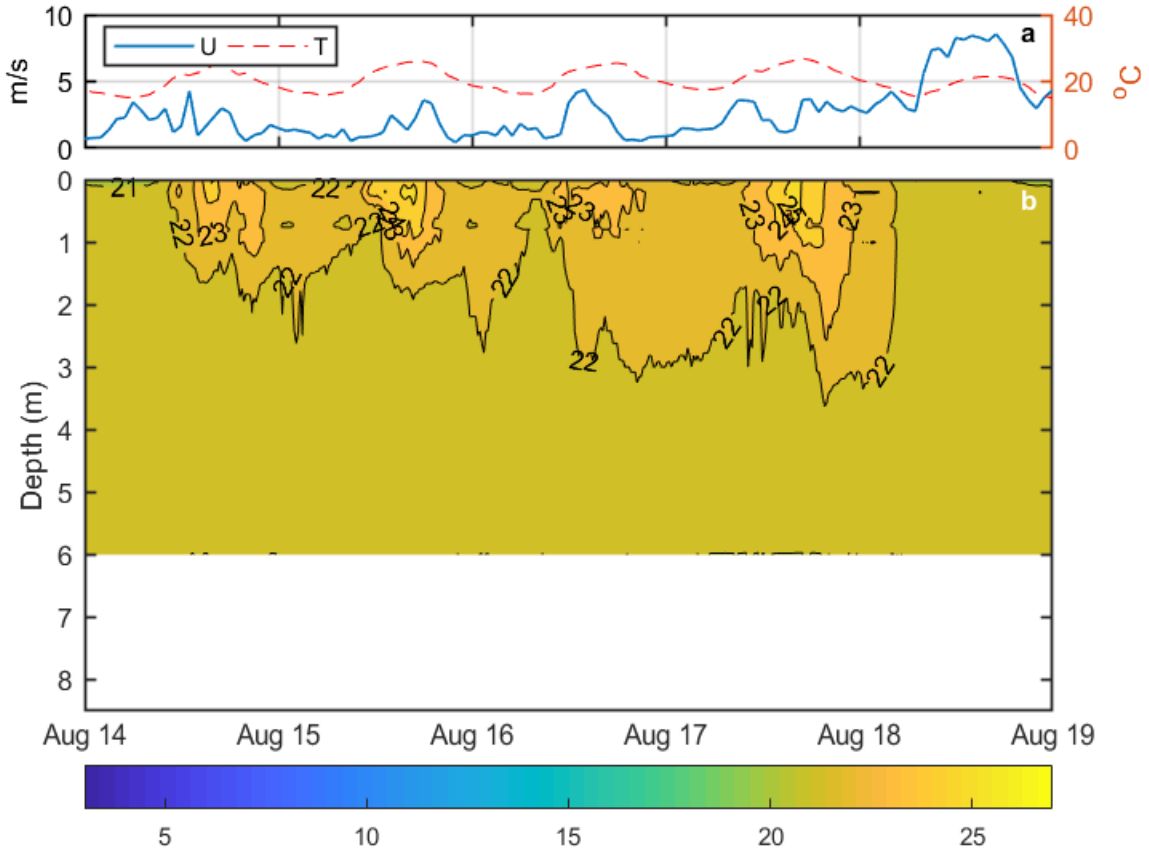

Figure 4.22 – Hourly windspeeds (U), hourly air temperatures (T) and 15min mean water temperatures (panel b) measured at Shellmouth Reservoir Aug 14-19, 2016

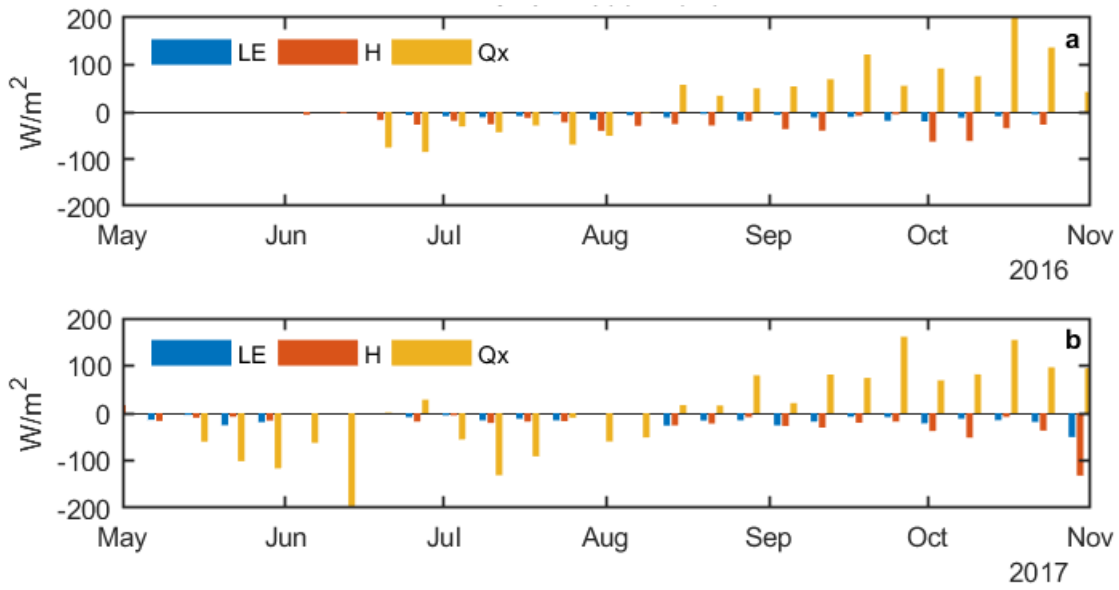

Figure 4.23 – Weekly surface energy balances at Shellmouth Reservoir during the 2016 and 2017 open water seasons

Note: Surface energy balance components are latent heat (LE), sensible heat (H) and lake heat storage (Qx) fluxes

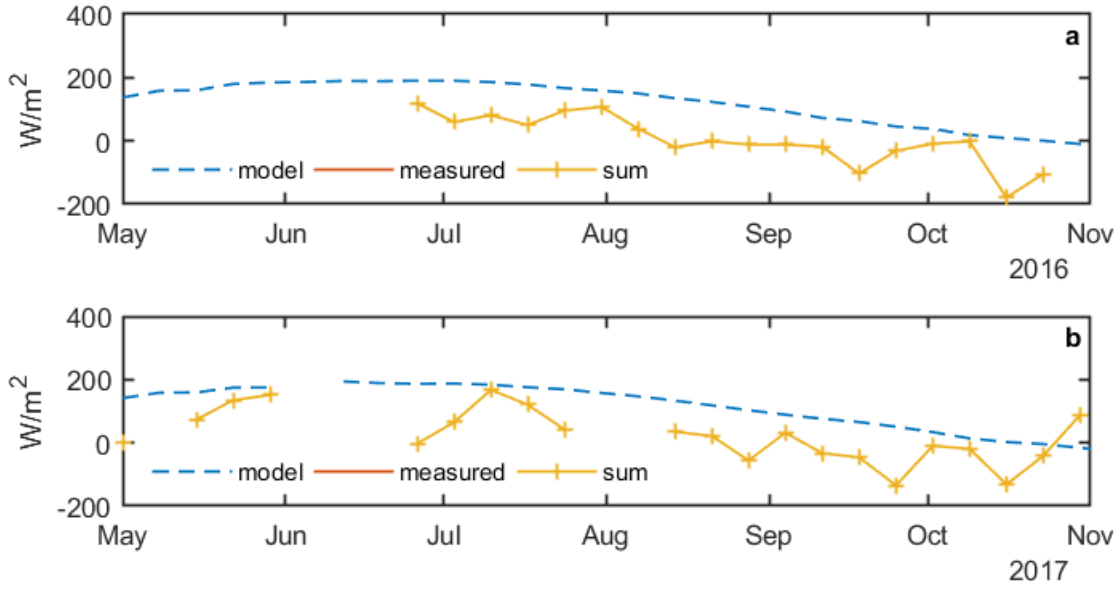

Figure 4.24 – Weekly net radiation calculated for Shellmouth Reservoir during the 2016 and 2017 open water seasons

Note: The sum presented is the sum of latent heat (LE), sensible heat (H), and reservoir heat storage (Qx) fluxes

4.3 Driving Meteorological Data: Measurement Over Land vs. Water

Accurate measurements of windspeed and water surface temperature are important for driving evaporation estimates. These are often inaccessible or significantly different from data at land stations. While equations have been proposed for estimating hourly windspeed (Granger & Hedstrom, 2011) and monthly surface temperature (Piccolroaz et al., 2018; Wiens & Godwin, 1978; Woodvine, 1995) from land station data, these cannot be relied upon in all circumstances because of variability in local conditions. In this section, observations of daily mean windspeed, temperature and vapour pressure at the buoys and land stations are compared (Figure 4.25) and the implications of the differences discussed.

Val Marie Reservoir

Weather data from the Val Marie buoy were compared to two land stations: Val Marie Land Station (this study, 2017 only) and Val Marie Southeast (ECCC weather station, 2016 and 2017). Daily average wind speeds, air temperatures, surface temperatures, and actual vapour pressure of the air were compared where available (Figure 4.25). Wind speeds are compared at an equivalent height of 10 m and show consistently higher winds over the water than either land station (details in Section 3.2.1). Daily average air temperatures are very similar on land and water, while surface temperatures vary. Vapour pressure is also slightly higher over the water surface. These differences are a result of the different thermal properties of land and water; which ultimately result in different diurnal air temperature patterns over land vs water (as discussed in Section 4.2.2). Thus, using land-based temperature measurements at sub-daily timescales would be inappropriate. Measuring or modeling over-lake windspeeds, temperatures and humidity conditions remains an important step in estimating evaporation.

Shellmouth Reservoir

Three meteorological variables were measured at both the Shellmouth buoy and nearby Roblin weather station: air temperature, relative humidity and windspeed. Daily average wind speeds (adjusted to 10 m height) show the same relationship trajectory as at Val Marie with over-lake winds higher than land-based wind measurements. Air temperatures are warmer and vapour

pressure is higher over the water than the land station. These observations suggest a general daily windspeed relationship could be used if over-lake measurements are unavailable, but that daily air temperature would not be appropriate for over-lake application. Air temperatures at Shellmouth Reservoir are warmer compared to the nearby Roblin station. This is likely due to the valley vs upland locations of the two stations. The different relationships between lake and land measurements at the two reservoirs highlight the need to improve modeling and measurements since not all lakes will have the same relationship with land-based measurements.

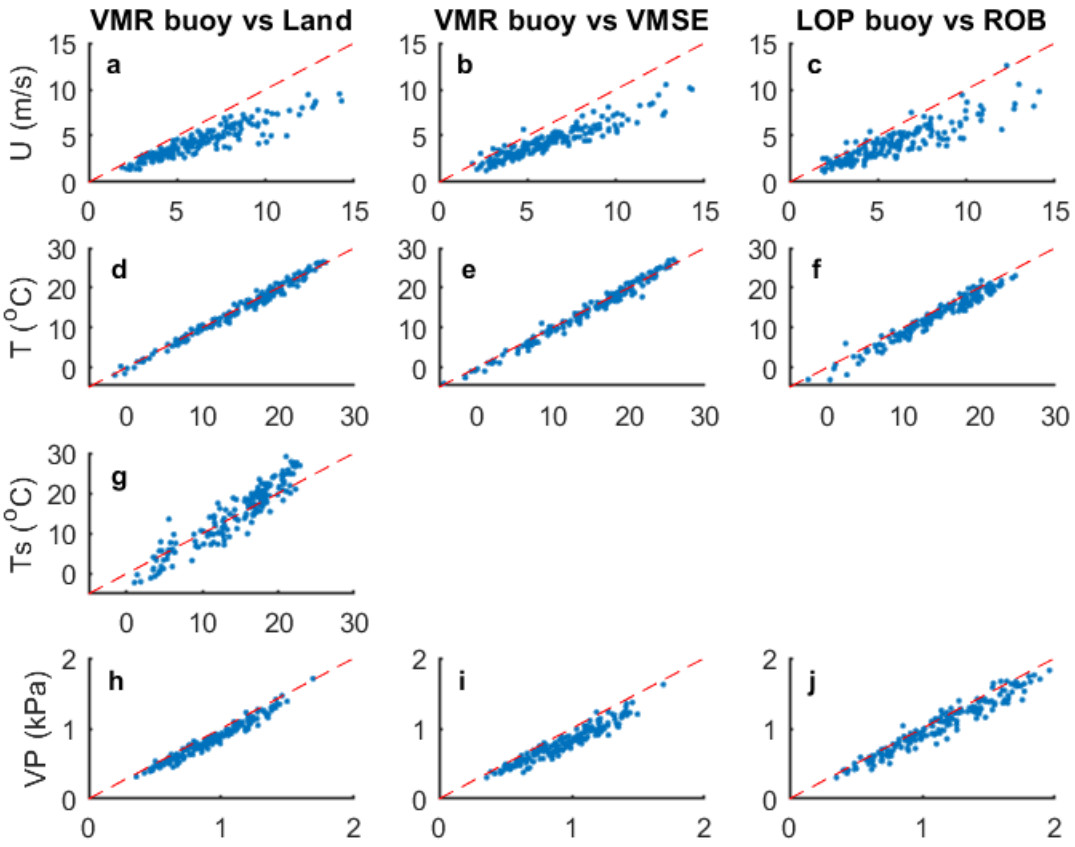

Figure 4.25 – Comparison of daily average meteorological values measured at both local buoy (x-axes) and nearby land stations (y-axes).
Note: Dashed lines show 1:1 relationship. Wind speeds from the buoys and Val Marie land station are adjusted to 10 m height to match weather stations using Eqn. 3.3. Site abbreviations are as follows: VMR (Val Marie buoy), Land (Val Marie land station), VMSE (Val Marie Southeast weather station), LOP (Shellmouth buoy), ROB (Roblin weather station).

4.4 Comparison with Literature

Val Marie Reservoir

The mean evaporation measurements at Val Marie Reservoir resemble historical evaporation estimates for Saskatchewan lakes and reservoirs. A 1975 study using pan evaporation estimated 4.2 mm/d on average from Apr 28 to Oct 7 (Cork, 1976). The same study compared the pan evaporation estimates with the Meyer formula (using measured surface temperature inputs) for two 10-day periods each in the spring and fall, resulting in estimates averaging 3.8 mm/d and 3.9 mm/d, respectively. Another study at Weyburn Reservoir, SK reported evaporation rates of 3.49 – 8.81 inches/month (3.0 – 7.2 mm/d or 5.1 mm/d when averaging all methods used) during the summers (May to Sept) of 1966 and 1967 using a variety of estimation approaches (Buckler & Quine, 1971). Estimates for Last Mountain Lake, SK (mean depth 7.6 m) in 1973 and 1977 averaged 2.1 mm/d annually or 3.7 mm/d during the open water season (May to Oct) using water budget and Morton equations (Morton 1986).

These values also fall in the range of what is expected based on previous eddy covariance measurements at lakes and reservoirs around the world (Table 4.1). These rates are clearly affected by water body size, climate, and timing of the measurements (i.e. short-term, open-water season, or annual). Larger lakes (surface areas 350-82,000 km^2, average depths 20-400 m) in various climates measured annual average evaporation near 2 mm/d, while some smaller lakes (surface areas < 10 km^2, average depths <8 m) measured annual average evaporation closer to 4 mm/d. The highest evaporation rates reported (~6 mm/d) were from summertime measurements at smaller water bodies in arid climates (Eshkol Reservoir in Israel and Island Lake in Nebraska) and the lowest evaporation rates reported (< 1 mm/d) were at Great Bear Lake (Northwest Territories, Canada), but summertime measurements at small northern European lakes were consistently 2 mm/d or less. A lake of similar size to Val Marie Reservoir (Lake Merasjarvi in northern Sweden) measured approximately 2.0 mm/d of evaporation during the open water season (Jonsson et al., 2008). As a relatively small and shallow water body in a semi-arid climate, it follows that Val Marie Reservoir would experience higher evaporation than both a slightly smaller, deeper boreal lake and the mean of the larger lakes but fall in the middle of the smaller lakes' range.

Shellmouth Reservoir

While it makes sense for evaporation at Shellmouth Reservoir to be lower than at Val Marie Reservoir due to water volume, these values are much smaller than expected. No studies presented in Table 4.1 measured evaporation rates this low. A slightly larger lake (~120 km^2, 12 m average depth) in boreal Saskatchewan measured approximately 2.5 mm/d during the open water season (Granger and Hedstrom 2010). Based on the trends discussed for Val Marie Reservoir, it would follow that Shellmouth should have higher evaporation than this lake because it is smaller and located in a slightly drier climate. High winds, periods of instability, consistently positive temperatures and vapour pressure gradients, and a large heat storage build-up and release should also contribute to increased evaporation.

Table 4.1 – Summary of published evaporation measurements using eddy covariance technique sorted by surface area

Note: Approximate mean evaporation (~) is estimated from reported flux values (mean W/m^2), long term evaporation (i.e. mm/year) and/or published figures.
** denotes surface areas estimated using Google Earth Pro measurement tools*

Water Body	Location	Climate	Surface Area (km2)	Mean Depth (m)	Max Depth (m)	Measurement Dates	Mean Evap (mm/d)	Reference(s)
Lake Superior	Canada/USA	Cold continental, Temperate	82100	148	406	2008 – 2012	~1.5	(Blanken et al. 2011; Spence et al. 2013)
Great Bear Lake	Northwest Territories, Canada	Subarctic	31000	72	413	2004 & 2005 open water seasons	0.43	(Rouse et al., 2008)
Great Slave Lake	Northwest Territories, Canada	Subarctic, Dfc/Dsc	27200	41	614	1997 –1999 open water seasons	~2.2	(Blanken et al., 2000; Rouse et al., 2003, 2008)
Lake Erie	Ohio, USA	Warm summer continental	25700	5.1	n/a	Oct 2011 – Sep 2013	~1.9	(Shao et al., 2015)
Qinghai Lake	Tibetan Plateau, China	Temperate, Cold semi-arid	4400	n/a	26	May 2013 – May 2015	~2.3	(X.-Y. Li et al., 2016)
Taihu Lake (three sites)	Eastern China	Humid subtropical	2400	1.9	2.6	Jun 2010 – Jun 2012, Aug 2011 – Jun 2012, Dec 2011 – Jun 2012	n/a	(Wang et al., 2014; Xiao et al., 2013)
Poyang Lake	Yangtze River Basin, China	Subtropical monsoon	1000-3000	<8.4	n/a	Jan – Dec 2014	n/a	(Zhao & Liu, 2018)
Biwa Lake	Japan	Cfa, subtropical	680	41	104	1985	~2.4	(Ikebuchi et al., 1988)
Eastmain-1 Reservoir	Quebec, Canada	Continental subarctic	627	6	n/a	2008-2012	~1.6	(Strachan et al., 2016)

Water Body	Location	Climate	Surface Area (km2)	Mean Depth (m)	Max Depth (m)	Measurement Dates	Mean Evap (mm/d)	Reference(s)
Dead Sea	Jordan	Arid	600	200	300	Mar 2014 – Mar 2015	~2.7	(Metzger et al., 2018)
Ngoring Lake	Tibetan Plateau, China	Cold semi-arid continental	610	17	32	Jul – Nov 2011	~2.5	(Z. Li et al., 2016)
Lac Leman (Lake Geneva)	Switzerland	Oceanic temperate	582	3	n/a	Aug - Oct 2006	~1.5	(Assouline et al., 2008; Vercauteren et al., 2009)
Lake Okanagan	British Columbia, Canada	Humid continental	348	76	242	Jul 2011 – May 2014	~2.1	(Spence & Hedstrom, 2015)
Erhai Lake	Southern China	Semi-arid	256.5	10	n/a	Apr – Nov 2012	~3.6	(Liu et al., 2015)
Alqueva Reservoir	Portugal	Semi-arid	250	16.5	65	Jul – Sep 2007 June – Oct 2014	~6.5	(Potes et al., 2017; Salgado & Le Moigne, 2010)
Lake Kinneret (Sea of Galilee)	Israel	Mediterranean	166	25	n.a	May – June, Sept – Oct 1990	~5.0	(Assouline & Mahrer, 1993)
Elephant Butte Reservoir	New Mexico, USA	Cold desert	148	n/a	n/a	Jul 2001 – Apr 2002	~3.0	(Eichinger et al., 2003)
Ross Barnett Reservoir	Mississippi, USA	Cfa, Temperate	134	5	11	Sep 2007 – Feb 2008, Sep 2008 – Mar 2008, 2008 – 2009	~2.7	(Liu et al., 2009, 2012)
Crean Lake	Saskatchewan, Canada	Boreal	120*	12	25	2005 – 2008 open water seasons	~2.5	(Granger & Hedstrom, 2010)
Thau Lagoon	France	Csa	75	4	11	Mar – Nov 2009	~2.9	(Bouin et al., 2012)

Water Body	Location	Climate	Surface Area (km2)	Mean Depth (m)	Max Depth (m)	Measurement Dates	Mean Evap (mm/d)	Reference(s)
Tamnaren Lake	Sweden	Warm summer continental	37	2.0	n/a	Jun 1994, Jun – Jul 1995 (1-2-day periods)	n/a	(Heikinheimo et al., 1999)
Scharmultzelsee	Germany	Maritime temperate	12.1	9.8	31	May – Jun 2003	n/a	(Beyrich et al., 2006)
White Bear Lake	Minnesota, USA	Temperate	9.7	<10	25	2014 – 2016	~1.8	(Xiao et al., 2018)
Lake Merasjarvi	northern Sweden	Subarctic	3.8	5.1	17	Jun – Oct 2005	~2.0	(Jonsson et al., 2008)
Island Lake	Nebraska, USA	Semi-arid	2.25	0.85	1.75	Aug 1988	~ 6.0	(Stannard & Rosenberry, 1991)
Kossenblatter See	Germany	Maritime temperate	1.86	2.1	4	May – Jun 1998	n/a	(Beyrich et al., 2006; Panin et al., 2006)
Toolik Lake	Alaska, USA	Subarctic	1.5	7	25	Jul 1995	n/a	(Eugster et al., 2003)
Yindeertu Lake	Badain Jaran Desert, China	Cold desert	1.03	5.6	9.4	Mar 2012 – Mar 2013	4.0	(Sun et al., 2018)
unnamed (near Nam Co Lake)	Tibetan Plateau, China	Plateau	1.0	n/a	14	Apr – Nov 2012, Apr – Nov 2013	~3.8	(Wang et al., 2017)
Landing Lake	Northwest Territories, Canada	Subarctic	1*	3.5	n/a	2007 – 2008 open water seasons	~3.0	(Granger & Hedstrom, 2010)
Kuivajarvi	Finland	Boreal	0.63	6.4	13.2	Aug – Oct 2010, Jun – Oct 2011	~1.5	(Mammarella et al., 2015)

Water Body	Location	Climate	Surface Area (km2)	Mean Depth (m)	Max Depth (m)	Measurement Dates	Mean Evap (mm/d)	Reference(s)
Eshkol Reservoir	Israel	Csa, Mediterranean	0.36	3.5	n/a	Jul – Sep 2005, May – Sep 2008 (non-continuous days)	~6.0	(Assouline et al., 2008; Tanny et al., 2008, 2011)
Williams Lake	Minnesota, USA	Temperate	0.34	5.2	9.3	Apr 1992, Apr 1993, Jul 1993, Oct 1993, Apr 1994	n/a	(Anderson et al., 1999)
Soppensee	Switzerland	Temperate	0.25	12	27	Sep 1998 (4 days)	~1.5	(Eugster et al., 2003)
Logan's Dam	Queensland, Australia	Humid subtropical	0.17	n/a	6	Nov 2009 (18 days), Mar 2010 – Feb 2011	~4.0	(McGloin, McGowan, McJannet, Cook, et al., 2014; McJannet et al., 2011)
Valkea-Kotinen	Finland	Dfc, continental subarctic	0.04	2.5	6.5	2003 & 2005 – 2007 open water periods (Apr/May – Oct/Nov)	~1.5	(Nordbo et al., 2011; Vesala et al., 2006)

4.5 Summary

This chapter has presented and discussed observations recorded at Val Marie and Shellmouth Reservoirs during the 2016 and 2017 open water seasons (May to October). The 2016 season was abnormally wet, while the 2017 season was abnormally dry at both sites. Both sites experienced periods of high winds, the strongest of which aligned with the reservoir valleys. Conditions were often unstable at both reservoirs until winds exceeded approximately 5 m/s. Sub-surface temperatures from both reservoirs revealed generally well-mixed water columns that experienced periods of diurnal stratification during calm summer days.

Daily evaporation at Val Marie Reservoir averaged 3.0 mm/d in 2016 (missing large portion of summer evaporation) and 4.0 mm/d in 2017 (full open-water season). Seasonal evaporation was highest during the summer months, but the highest single day of evaporation in both years (>9.0 mm/d) occurred in the spring. A multi-day spike in evaporation was also observed in early October both years during a period of high winds and rapid cooling. Short-term evaporation at Val Marie Reservoir is aerodynamically driven with daily and sub-daily evaporation rates highly correlated to both windspeeds and vapour pressure gradients. These three components (evaporation, windspeed and vapour pressure gradients) all peak in the afternoon. Seasonal evaporation is affected slightly by heat storage, which shifts peak evaporation a few weeks later than peak net radiation. These findings echo observations at other water bodies in various climates.

Mean daily evaporation at Shellmouth Reservoir was unreasonably low (0.43 mm/d in 2016 and 0.47 mm/d in 2017) and is thought to be inaccurate based on comparison with other studies, a large (~100 W/m^2) surface energy balance gap, and challenges presented by the system used at the Shellmouth buoy. Despite the poor evaporation data, the meteorological data collected from this site remains valuable for practical estimates and future study. Conditions at Shellmouth were affected by the reservoir's relatively large heat storage. Surface temperatures were consistently warmer than air temperatures throughout the summer months and remained warm into September. The combination of high winds, strong temperature and vapour pressure gradients, and heat storage should lead to much higher evaporation rates.

Most land-based measurements are not adequate approximations for over-lake conditions at these reservoirs. The one exception was Val Marie air temperatures at daily or greater time steps. Air temperatures at Shellmouth were warmer than those measured at the land station. At both sites, windspeeds over the water were stronger than land winds and humidity (and therefore vapour pressure) was also higher. In order to approximate over-lake conditions, additional work to establish relationships and test models for land vs lake conditions at different sites would be beneficial.

The mean evaporation rates measured at Val Marie Reservoir resemble rates published in other studies. This includes studies using other methods to estimate evaporation at small Saskatchewan reservoir. Evaporation rates were also logical when compared to studies using the eddy covariance technique to measure evaporation at water bodies around the world by considering climate, depth and seasonal characteristics. The dataset from Val Marie Reservoir can now be confidently used to validate driving data and practical estimation techniques.

5 Practical Estimates of Lake Evaporation

Part of the motivation behind collecting the eddy covariance measurements was to begin evaluating existing evaporation estimation methods. This chapter addresses the third objective of this study by (1) evaluating methods commonly used in the Prairie Provinces (Meyer and Morton) and alternate approaches commonly found in the literature (Penman and Bulk Transfer), (2) comparing the performance of these models at different time steps, (3) examining the effect of using land-based vs over-lake driving data, and (4) suggesting the most appropriate method for filling large gaps in the reservoir evaporation data. Since 2017 at Val Marie Reservoir yielded the most complete season of data, it has been used for evaluating selected estimation methods.

5.1 Evaluation of Four Practical Estimation Methods

5.1.1 Empirical Bulk Transfer Approach: Meyer

The Meyer equation is an empirical bulk transfer approach (Meyer, 1915, 1942). It is commonly used in the Prairie Provinces where numerous adjustments to Meyer's original form have been made (Liu et al., 2014; Martin, 1988; Wiens & Godwin, 1978; Woodvine, 1995). The equation requires measurements of local windspeed, air temperature and relative humidity. These measurements are used to calculate the product of windspeed and the vapour pressure difference between the water surface and the overlying air ($e_w - e_a$). In order to approximate the surface temperature for the saturated water vapour pressure calculation, monthly coefficients are used to relate land-based air temperature measurements to water surface temperatures. Measurements of surface temperatures have been used for shorter than monthly timescales (Cork, 1976). The product of windspeed and vapour pressure difference is then multiplied by an elevation factor and an empirical coefficient that can be adjusted based on the relative size of the reservoir. The main appeal of the Meyer equation is the limited data requirements. The main issue with the Meyer equation is its empiricism, which often requires local coefficients to improve estimation results.

For the application at Val Marie in 2017, a metric conversion form of the Meyer equation was used (Martin, 1988) with the recommended coefficient (C) of 10.1 (Woodvine, 1995). Since land-based measurements are most commonly available, wind, air temperature and relative humidity measurements from the Val Marie Southeast land station were used as the main inputs. In order to compare the Meyer equation at shorter timescales surface temperature measurements from the buoy were also considered. This allowed for two monthly (Ts model and Ts measured), one weekly (Ts measured), and one daily (Ts measured) estimate of evaporation using the Meyer approach.

The Meyer evaporation estimates (lines) are compared with measurements (bars) in Figure 5.1. The monthly estimate using modeled surface temperatures (yellow dashed line) overestimates monthly measured evaporation (mean difference = 44.6 mm). Using measured surface temperatures improved the monthly estimates considerably, but July and August evaporation are still overestimated, and October evaporation is underestimated (mean difference = 13.2 mm). Weekly and daily evaporation estimates using measured surface temperatures also overestimate summer and underestimate fall evaporation, but the overall fit of the model is good.

There is a strong linear relationship between the Meyer estimates and evaporation measurements, but a seasonal bias (Table 5.1). The correlation is likely due to the inclusion of the two strongest controls on evaporation at Val Marie Reservoir: windspeed and vapour pressure difference. Estimates might be improved by determining local coefficients for Val Marie Reservoir, both to relate air temperature to water surface temperature and obtain a more appropriate C value but calculating yet another set of local coefficients limits the application of this approach. Other Dalton type equations have performed better after parameter optimization (Wang et al., 2019), but the best models in comparison studies of evaporation (most at time-steps of 10-days to 1 month) often include heat storage (Duan & Bastiaanssen, 2017; Slota, 2013; Wang et al., 2019; Zolá et al., 2019). While the use of a locally measured surface temperature can account for some of the effects of heat storage, the relationship is not perfect. The absence of a heat storage term in the Meyer equation may explain the slight seasonal over/under-estimation bias.

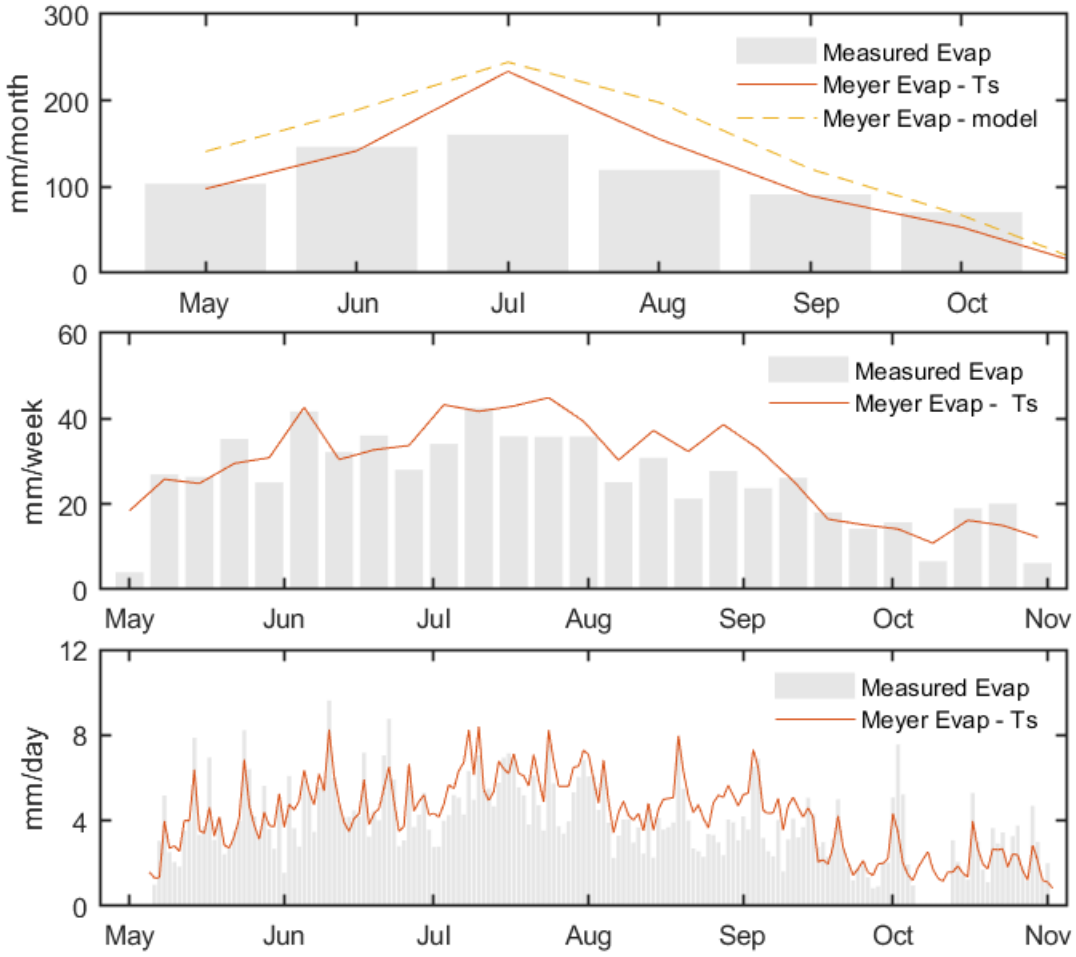

Figure 5.1 – Monthly, weekly, and daily Meyer evaporation estimates compared to eddy covariance measurements at Val Marie Reservoir 2017

Note: Estimation meteorological inputs are from the Val Marie Southeast land station only (model - yellow dashed line) or include buoy surface temperature measurements (Ts – red solid line)

Table 5.1 – Statistics relating the models presented in this chapter to measured evaporation at monthly, weekly and daily time steps. Chosen statistics are adjusted R^2 values, root mean squared error, and mean difference between the model and evaporation measurements

Model	R2	RMSE (mm)	Mean Diff (mm)
Monthly			
Meyer – Ts modelled	0.82	14.3	13.2
Meyer – Ts measured	0.89	11.4	44.6
Morton Shallow Lake	0.81	14.7	5.7
Penman – land model	0.89	11.3	8.4
Penman – buoy inputs	0.85	13.1	24.0
Bulk Transfer – land model	0.90	10.8	23.7
Bulk Transfer – buoy inputs	1.00	2.0	-1.0
Bulk Transfer – buoy inputs + stability	1.00	2.0	-1.0
Weekly			
Meyer – Ts measured	0.74	5.3	3.1
Morton Shallow Lake	0.57	6.8	1.9
Penman – land model	0.73	6.8	1.6
Penman – buoy inputs	0.77	6.3	4.6
Bulk Transfer – land model	0.66	7.6	5.2
Bulk Transfer – buoy inputs	0.97	2.1	0.5
Bulk Transfer – buoy inputs + stability	0.98	1.8	-0.2
Daily			
Meyer – Ts measured	0.68	1.1	0.4
Penman – land model	0.28	1.6	0.3
Penman – buoy inputs	0.28	1.6	0.8
Bulk Transfer – land model	0.26	1.6	0.7
Bulk Transfer – buoy inputs	0.86	0.7	0.08
Bulk Transfer – buoy inputs + stability	0.88	0.7	-0.04

5.1.2 Complementary Approach: Morton

Morton developed evaporation models for both land and water surfaces based on the complementary approach first proposed by Bouchet (1963). The complementary approach assumes actual and potential evaporation are dependent on one another and respond to surface-atmospheric interactions. Three models were developed by Morton for water bodies treated as fully saturated surfaces (potential evaporation = actual evaporation): pond evaporation, shallow lake evaporation, and deep lake evaporation (Morton, 1983b, 1986). The Morton methods are commonly used because they use routinely measured (air temperature and relative humidity or dew point temperature) and easily modeled (incoming solar radiation or sunshine hours) land station inputs. Shallow lake evaporation can be thought of as the base model. Pond evaporation includes additional calculations for the effects of adjacent land on evaporation and deep lake evaporation includes additional calculations to account for heat storage. One summary of evaporation estimation methods ranked Morton methods as the most appropriate for open water evaporation (McMahon et al., 2013).

The shallow lake evaporation model was applied to Val Marie Reservoir 2017 data using an Excel VBA script (Morton_2.xls, Version 2.0, 2014) for calculating weekly and monthly shallow lake evaporation that was available from Alberta Environment. Mean air temperature and relative humidity measurements were taken from the ECCC Val Marie Southeast land station. Incoming solar radiation was modeled using the Clear Sky radiation model (Allen et al., 2006) with a 0.75 transmittance factor as described in Section 3.3.2.

Monthly and weekly shallow lake evaporation estimates (lines) are presented alongside measured evaporation (bars) in Figure 5.2. Similar to Meyer estimates of evaporation, the Morton shallow lake model estimates tend to have a slight seasonal bias, but the overall magnitude of the estimates is an improvement from the Meyer estimates (Table 5.1). Additionally, a two-week lag is evident in the weekly measurements compared to weekly estimates, reducing the strength of the linear relationship. This difference might be reduced by applying Morton's deep lake evaporation version to account for the heat storage affect observed at Val Marie Reservoir (Morton, 1986). In fact, it is recommended most lakes be treated as a deep lake; the shallow lake model was determined most appropriate for annual evaporation estimates where heat storage is not a factor (McMahon et al., 2013). Applying the deep lake

model at Val Marie Reservoir would require additional modelling that is outside the scope of this study, but highly recommended for future work.

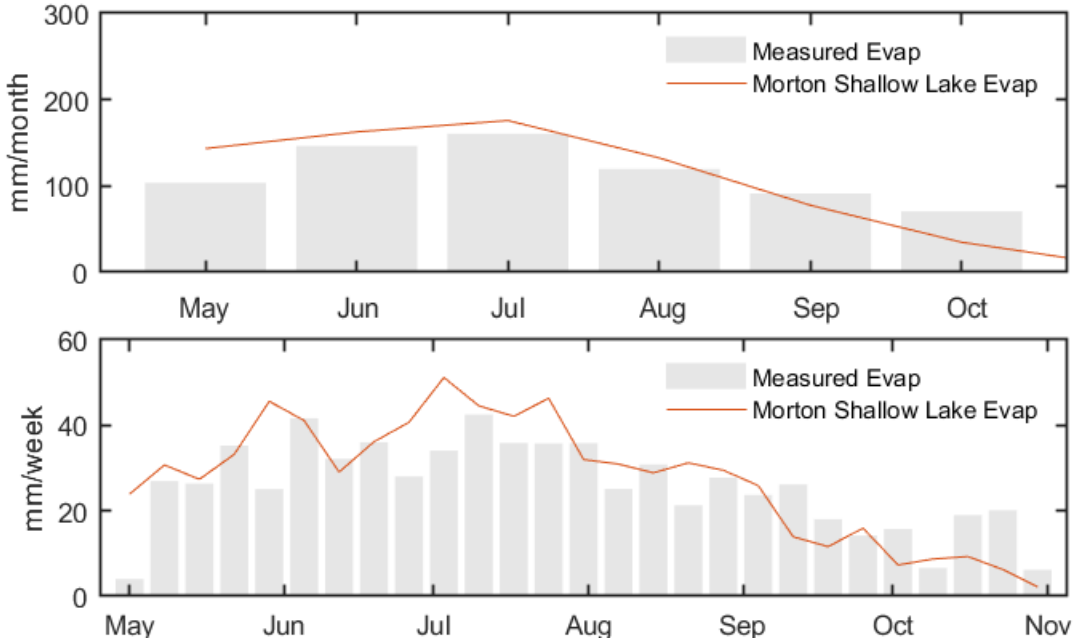

Figure 5.2 – Monthly and weekly Morton shallow lake evaporation estimates compared to eddy covariance measurements at Val Marie Reservoir 2017
Note: Estimation meteorological inputs are air temperature and relative humidity data from the Val Marie Southeast land station and a Clear Sky radiation model using data from the same station

5.1.3 Combination Method: Penman

The Penman equation is a common combination method (meaning it includes a bulk transfer and an energy component) that has performed well in other estimation method comparison studies of lake evaporation (Rosenberry et al. 2007, Tanny et al. 2011, Wang et al. 2018, Zola et al. 2019). The inclusion of the energy component may help with to estimate the seasonal pattern better than equations that do not consider heat storage of the reservoir. This equation requires more inputs than the previous two approaches discussed (net radiation, heat storage, windspeed, air temperature, relative humidity, atmospheric pressure, and assumed roughness heights and resistance terms), but the key benefit is that surface temperature is not required.

For Val Marie 2017 estimates, both land-based and over-lake measurements were considered. The first estimate only considered land-based measurements from the Val Marie Southeast land station since these are what would normally be available. Daily mean land-based measurements were used because they have stronger relationships with over-lake conditions than hourly means due to the different diurnal patterns over land vs water as discussed in Section 4.2.2. Mean air temperatures, relative humidity and atmospheric pressure were assumed equal to over-lake conditions based on observations in Section 4.3. Windspeed at the 10 m measurements height from the land station were used as is because these measurements were almost 1:1 with the over-lake measurements before the height adjustment (not shown). Net radiation was modelled using the approach outlined in Section 4.2.4. Subsurface heat storage was modelled assuming a hysteretic relationship between the modeled net radiation and heat storage and used mean coefficients for the monthly relationships observed at twenty-two lakes (Duan & Bastiaanssen, 2015) also outlined in Section 4.2.4.

Attempting to estimate evaporation using land-based inputs to model over-lake conditions results in slight overestimates at all three timescales (Table 5.1). Daily estimates were poorly fitted to the measurements ($R^2 = 0.28$), but the relationship improved for weekly ($R^2 = 0.73$) and monthly ($R^2 = 0.89$) estimates. Using time-matched means as opposed to daily aggregated evaporation to get weekly and monthly evaporation reduces the estimates slightly (not shown).

Over-lake estimates were then used to see if they could explain the discrepancies between the measurements and the Penman models. When using hourly mean buoy measurements to

calculate hourly evaporation which were aggregated to daily, weekly, and monthly time steps, the Penman approach still overestimated evaporation (Figure 5.3).

The main challenge with any energy balance approach is the measuring and/or modelling of the heat storage component. Having measured heat storage is highly unlikely in most scenarios, so pursuing this avenue is not very practical or beneficial. Additionally, there is basically no correlation between heat storage and evaporation at Val Marie Reservoir at shorter than weekly timescales (Appendix D).

Another issue with the Penman equation is that it uses the vapour pressure deficit of the air ($e_s - e_a$) instead of the vapour pressure difference between the water surface and the air ($e_w - e_a$). These two quantities do not have the same relationship with evaporation at Val Marie Reservoir. The vapour pressure deficit is more variable and very poorly correlated to evaporation measurements at hourly ($R^2 = 0.00$), daily ($R^2 = 0.00$), and weekly ($R^2 = 0.16$) time steps (Appendix D). This variability may also contribute to the extremes in the daily estimates. Alternatively, the vapour pressure difference has an increasing correlation with longer time steps (hourly $R^2 = 0.07$, daily $R^2 = 0.19$, weekly $R^2 = 0.58$) and becomes the strongest predictor of evaporation at Val Marie Reservoir when combined with windspeed measurements (hourly $R^2 = 0.33$, daily $R^2 = 0.52$, weekly $R^2 = 0.80$). These relationships support the investigation of a non-empirical aerodynamic approach.

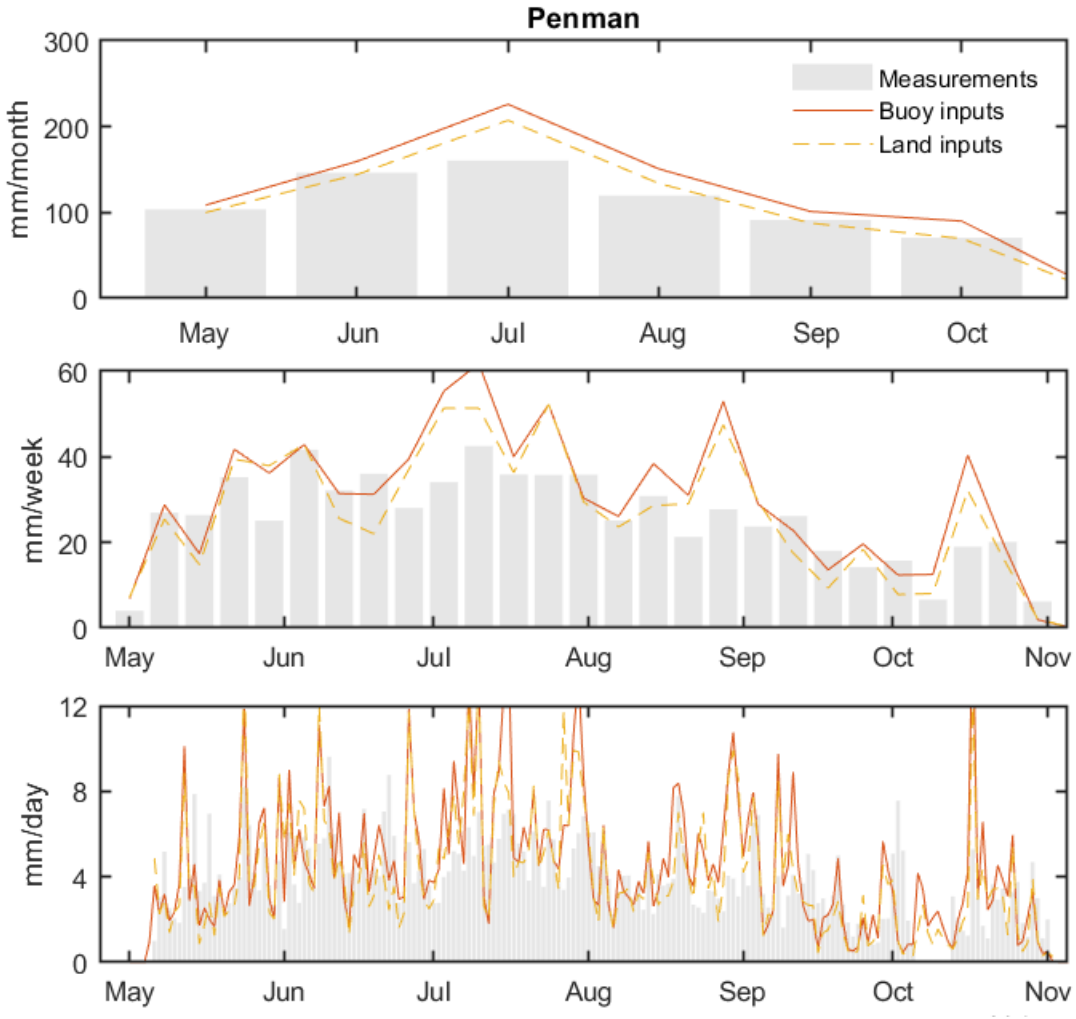

Figure 5.3 – Monthly, weekly, and daily Penman evaporation estimates using over-lake (buoy) and land-based inputs compared to eddy covariance measurements at Val Marie Reservoir 2017
Note: Buoy inputs are run hourly and aggregated to each time step, land inputs are run daily and aggregated to each time step

5.1.4 Bulk Transfer Method

Another commonly used and high performing estimation approach from the literature is the Bulk Transfer method (Eichinger et al., 2003; Heikinheimo et al., 1999; Ikebuchi et al., 1988; Metzger et al., 2018; Wang et al., 2017). This variation avoids the empiricism of equations like Meyer and can consider both surface roughness variations and atmospheric stability. Input requirements are high (windspeed, air temperature, surface temperature, relative humidity, atmospheric pressure, and surface roughness lengths), and additional calculations are sometimes required (i.e. friction velocity, absolute humidity, stability factors), making this method slightly more complicated.

This method was first applied at Val Marie 2017 using only land-based estimates measurements from the Val Marie Southeast land station since these are what would normally be available. Daily mean land-based measurements were used because they have stronger relationships with over-lake conditions than hourly means due to the different diurnal patterns over land vs water as discussed in Section 4.2.2. Mean air temperatures, relative humidity and atmospheric pressure were assumed equal to over-lake conditions based on observations in Section 4.3. Windspeed at the 10 m measurements height from the land station were used as is because these measurements were almost 1:1 with the 2 m over-lake measurements. Mean daily surface temperatures were assumed equal to mean daily air temperatures. The roughness lengths for momentum and vapour were set to 0.2 mm and 0.1 mm, respectively, following suggestions from literature (Abdelrady et al., 2016). Neutral conditions were assumed when using daily mean inputs since previous results showed consistent diurnal changes in stability (4.2.2). Estimates were run daily and aggregated to weekly and monthly estimates. Results are presented in Figure 5.4.

Using land inputs and models as described resulted in overestimates with poor daily correlation ($R^2 = 0.28$). Correlation improved with weekly ($R^2 = 0.77$) and monthly ($R^2 = 0.90$) timescales. Running estimates using time-matched inputs (i.e. weekly mean windspeeds) produced nearly identical results (not shown).

Over-lake evaporation estimates were run hourly and then aggregated to daily, weekly and monthly time-steps. The Bulk Transfer model using over-lake inputs is extremely close to the measured evaporation. Daily, weekly, and monthly estimates have strong linear relationships and low mean differences compared to evaporation measurements at these time scales (Table

5.1). Using time-matched inputs (not shown) resulted in slightly lower evaporation estimates. Ignoring stability (also not shown) resulted in slightly higher evaporation estimates.

These results show that the Bulk Transfer approach can accurately model evaporation using over-lake inputs. Since it is more likely that land stations will remain the most common source of meteorological data, exploring the land vs water relationships of windspeed and surface temperature would be particularly useful. If over-lake conditions can be accurately modeled, then the Bulk Transfer model should be used to estimate evaporation from reservoirs.

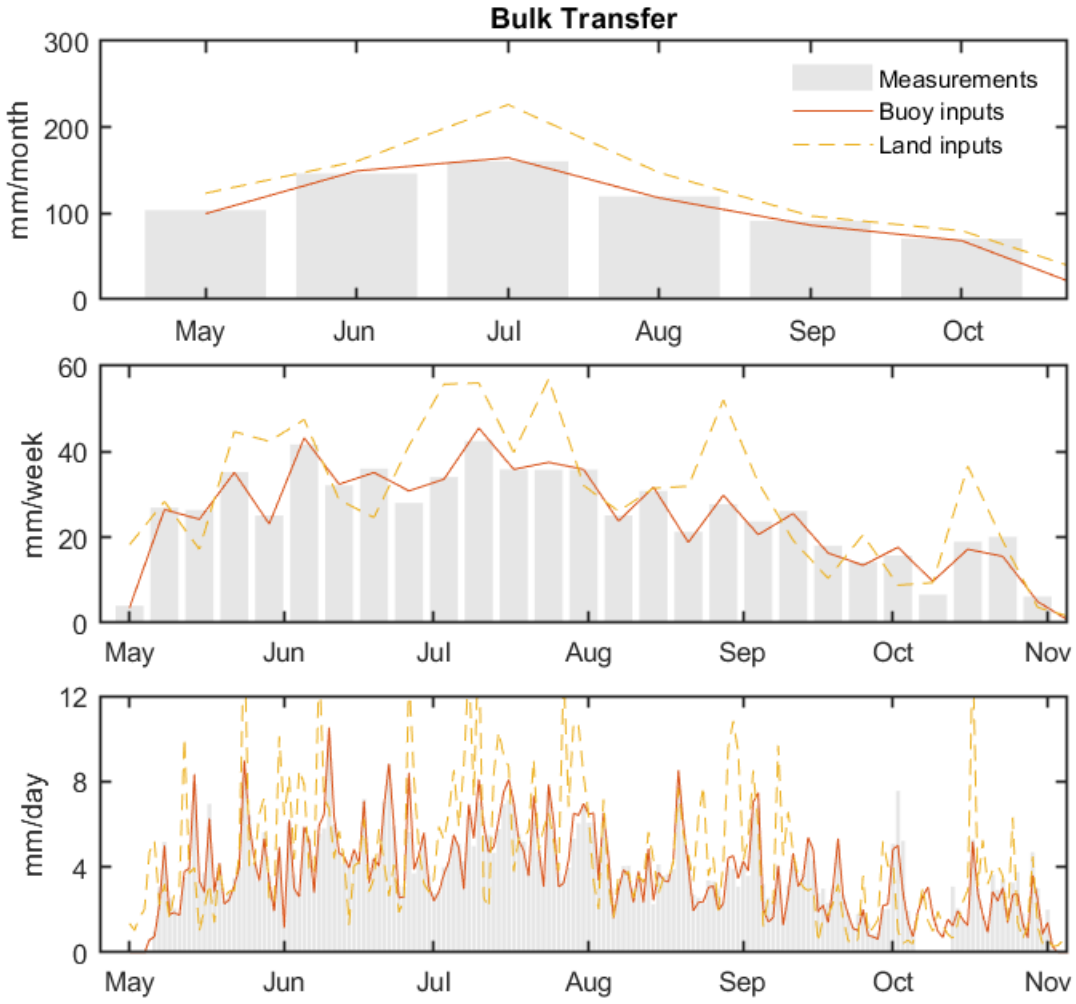

Figure 5.4 – Monthly, weekly, and daily Bulk Transfer evaporation estimates using over-lake (buoy) and land-based inputs compared to eddy covariance measurements at Val Marie Reservoir 2017

Note: Buoy estimates are run hourly with the stability factor and aggregated to each time step, land estimates are run daily without the stability factor and aggregated to each time step

5.2 Proposed Gap Filling Approach

Bulk Transfer estimates performed the best of the four methods considered. As such, it can be used to fill large gaps in the evaporation dataset. It is reasonable to apply this method to Shellmouth Reservoir as well as the Val Marie Reservoir 2016 data because Bulk Transfer or variations of aerodynamic approaches have successfully modelled evaporation at other sites and the transfer function inputs (windspeed and vapour pressure difference) are widely cited as the driving forces of evaporation in various settings (Assouline & Mahrer, 1993; Blanken et al., 2000; Mammarella et al., 2015; McGloin et al., 2014b; Nordbo et al., 2011; Shao et al., 2015; Xiao et al., 2018).

At Shellmouth Reservoir, sufficient over-lake data from the buoy was available to run the Bulk Transfer method for both years. However, for the 2016 summertime gap at the Val Marie buoy data were not available so daily mean air temperature, relative humidity and windspeed were taken from the Val Marie Southeast land station. Winds were adjusted for over-lake conditions by applying the measurements from the 10m measurement height, since the relationship of the 10m high winds at the land station had a near 1:1 relationship with the 2m high winds at the buoy. Daily mean surface temperature measurements were taken from the shallowest lake temperature pendent (20 cm).

The resulting Bulk Transfer model for Val Marie 2016 is presented in Figure 5.5a. Estimates for the summertime gap show highly variable daily evaporation rates and slightly reduced evaporation during the month of July when winds were lower on average (refer to Chapter 4). Estimates were also run for the late summer and fall and show strong correlation with measured daily evaporation, capturing short term peaks of evaporation during late August and early October cooling periods.

Bulk Transfer estimates at Shellmouth Reservoir suggest much higher evaporation (mean evaporation ~ 4 mm/d) than measured at the buoy (mean evaporation ~ 1 mm/d) during both 2016 and 2017 open water seasons. This fits with Table 4.1 rates from other lakes in similar climates of similar size. The higher rates are also more in line what was expected based on the high winds and strong temperature and vapour pressure gradients measured at the Shellmouth Reservoir buoy. There is no strong seasonal trend observed during 2016, but evaporation rates were higher in late August/early September of 2017. This corresponds with a warm and windy

end to the summer of 2017 (see Figure 4.6). It is recommended these estimates be considered over the questionable measurements from the Shellmouth buoy.

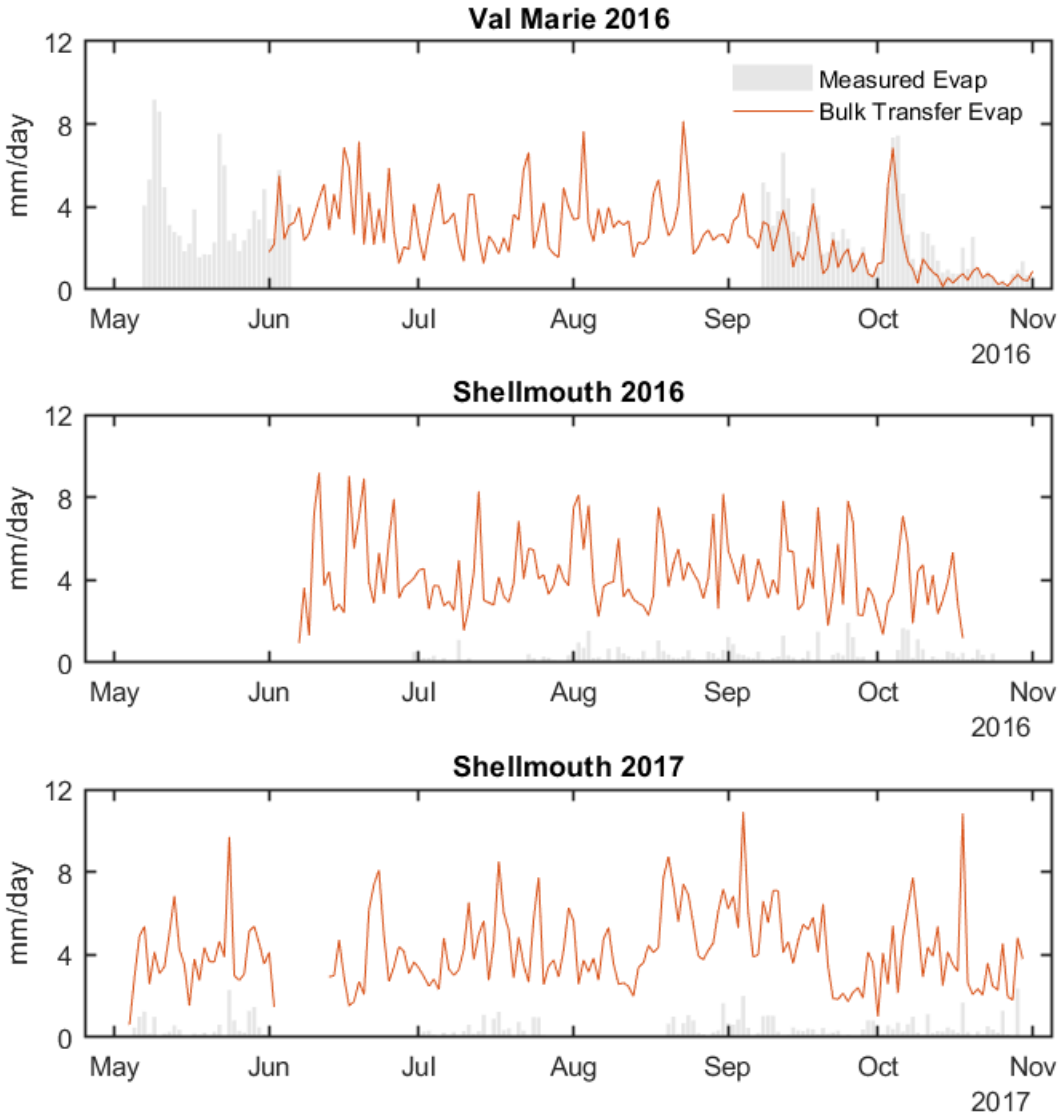

Figure 5.5 – Daily total evaporation (mm) measured using eddy covariance compared to daily Bulk Transfer estimates using the best available inputs to model gaps at Val Marie Reservoir in 2016 and Shellmouth Reservoir in 2016 and 2017.

5.3 Summary

Four estimation methods were applied to Val Marie 2017 with varying results. All four approaches slightly overestimated summer evaporation when land-based data limitations were assumed. Meyer estimates were improved when measured surface temperature replaced the modeled surface temperature. While improvements to Meyer could be made by adjusting the coefficients, doing so could limit the applicability of the resulting equation at other sites. Morton's Shallow Lake estimates for weekly and monthly evaporation were closer in magnitude to evaporation measurements but displayed a seasonal bias that might be addressed by using the heat storage routing model in Morton's Deep Lake estimates. Penman estimates were poor for daily time steps but improved at longer intervals, likely due to the characteristics of heat storage. Bulk Transfer estimates also performed better at longer time steps when restricted to land-based inputs and simple assumptions to model over-lake conditions.

Using over-lake inputs did not improve Penman estimates but produced strong Bulk Transfer estimates at daily, weekly and monthly timescales. Using time-matched mean inputs as opposed to hourly or daily aggregates generally resulted in slightly lower estimates that were most pronounced for the Penman over-lake model. Considering stability vs assuming neutral conditions for the Bulk Transfer estimates resulted in minimal change to the results.

Bulk Transfer estimates using hourly over-lake inputs and stability factor performed the best of all versions of the four methods considered and should be used as gap filling and/or modelling of lake evaporation moving forward. While challenges remain with obtaining over-lake measurements or appropriate models for over-lake wind, temperature and humidity, reasonable estimates are possible with further work in this area using a combination of land-based measurements, models or alternative techniques (i.e. satellite surface temperature measurements). It is proposed that Bulk Transfer estimates for the summertime gap at Val Marie 2016 and the full 2016 and 2017 open-water seasons at Shellmouth Reservoir be considered.

6 Conclusion

This study presents the first eddy covariance measurements for open water evaporation in the southern Prairie Provinces. Evaporation measurements at Val Marie Reservoir varied widely throughout the season, averaging 3.0 mm/day during spring and fall 2016 (summertime data unavailable) and 4.0 mm/day from May to October 2017. Evaporation measurements at Shellmouth Reservoir were much lower than anticipated (<1 mm/day on average). Surface energy balance modelling, comparison with previous studies, and concerns with data processing equipment at the buoy suggest that these evaporation measurements are not reflective of the true evaporation loss from the reservoir. Regardless, the meteorological data collected from the Shellmouth buoy is still extremely valuable to future research.

Evaporation at Val Marie Reservoir is aerodynamically driven: hourly, daily and weekly fluxes are most strongly correlated with the product of over-lake windspeed and the vapour pressure difference between the water surface and the overlying air. Land-based measurements of windspeed and surface temperature are not representative of these conditions. Seasonal heat storage is minimal, but still decouples seasonal peak evaporation from seasonal peak net radiation by a few weeks.

Two main recommendations came from the preliminary evaluation of four practical estimation approaches. First, since the Bulk Transfer approach performed very well at all timescales using input data from Val Marie Reservoir 2017, it can and should be used to estimate evaporation and gap-fill if over-lake data are available or can be reliably modelled. Second, pursuing methods to measure or model over-lake conditions is important to improve practical evaporation estimates.

It is hoped that the findings presented here encourage future research using the data collected at Val Marie and Shellmouth Reservoirs. More work is required to determine the best course of action for modelling evaporation when over-lake data is not available. Continued efforts to measure and/or model over-lake data would be beneficial to this work.

References

Abdelrady, A., Timmermans, J., Vekerdy, Z., & Salama, M. S. (2016). Surface energy balance of fresh and saline waters: AquaSEBS. *Remote Sensing*, *8*(7). https://doi.org/10.3390/rs8070583

Allen, R. G., Trezza, R., & Tasumi, M. (2006). Analytical integrated functions for daily solar radiation on slopes. *Handbook of Environmental Chemistry, Volume 5: Water Pollution*, *139*(1–2), 55–73. https://doi.org/10.1016/j.agrformet.2006.05.012

Anderson, D. E., Striegl, R. G., Stannard, D. I., Michmerhuizen, C. M., Mcconnaughey, T. A., & Labaugh, J. W. (1999). Estimating lake–atmosphere CO2 exchange. *Limnology and Oceanography*, *44*(4), 988–1001.

Andrade, C., Alcântara, E., Bernardo, N., & Kampel, M. (2019). An assessment of semi-analytical models based on the absorption coefficient in retrieving the chlorophyll-a concentration from a reservoir. *Advances in Space Research*, *63*(7), 2175–2188. https://doi.org/10.1016/j.asr.2018.12.023

Andreasen, M., Rosenberry, D. O., & Stannard, D. I. (2017). Estimating daily lake evaporation from biweekly energy-budget data. *Hydrological Processes*, *31*(25), 4530–4539. https://doi.org/10.1002/hyp.11375

Apergis, N., Chang, T., Gupta, R., & Ziramba, E. (2016). Hydroelectricity consumption and economic growth nexus: Evidence from a panel of ten largest hydroelectricity consumers. *Renewable and Sustainable Energy Reviews*, *62*, 318–325. https://doi.org/10.1016/j.rser.2016.04.075

Assouline, S., & Mahrer, Y. (1993). Evaporation from Lake Kinneret: 1. Eddy correlation system measurements and energy budget estimates. *Water Resources Research*, *29*(4), 901–910. https://doi.org/10.1029/92WR02432

Assouline, S., Parlange, M. B., & Katul, G. G. (2008). Evaporation from three water bodies of different sizes and climates : Measurements and scaling analysis. *WATER RESOURCES*, *31*, 160–172. https://doi.org/10.1016/j.advwatres.2007.07.003

Assouline, S., Narkis, K., & Or, D. (2011). Evaporation suppression from water reservoirs: Efficiency considerations of partial covers. *Water Resources Research*, *47*(7), 1–8. https://doi.org/10.1029/2010WR009889

Assouline, S., Li, D., Tyler, S., Tanny, J., Cohen, S., Bou-Zeid, E., et al. (2016). On the variability of the Priestley-Taylor coefficient over water bodies. *Water Resources Research*, *52*(1). https://doi.org/10.1002/2015WR017504

Bailey, W. G., Oke, T. R., & Rouse, W. R. (Eds.). (1997). *The Surface Climates of Canada*. Montreal: McGill-Queen's University Press.

Beyrich, F., Leps, J. P., Mauder, M., Bange, J., Foken, T., Huneke, S., et al. (2006). Area-averaged surface fluxes over the litfass region based on eddy-covariance measurements. *Boundary-Layer Meteorology*, *121*(1), 33–65. https://doi.org/10.1007/s10546-006-9052-x

Blanken, P. D., Rouse, W. R., Culf, A. D., Spence, C., Boudreau, L. D., Jasper, J. N., et al. (2000). Eddy covariance measurements of evaporation from Great Slave Lake, Northwest Territories, Canada, *36*(4), 1069–1077.

Blanken, P. D., Rouse, W. R., & Schertzer, W. M. (2003). Enhancement of evaporation from a large Northern Lake by the entrainment of warm, dry air. *Journal of Hydrometeorology*, *4*, 680–693.

Blanken, P. D., Spence, C., Hedstrom, N., & Lenters, J. D. (2011). Evaporation from Lake Superior: 1. Physical controls and processes. *Journal of Great Lakes Research*, *37*, 707–716. https://doi.org/10.1016/j.jglr.2011.08.009

Bouchet, R. (1963). Evapotranspiration reelle et potentielle signification climatique. *IAHS Publication 62. Wallingford: International Association of Hydrological Sciences*, 134–142.

Bouin, M. N., Caniaux, G., Traullé, O., Legain, D., & Le Moigne, P. (2012). Long-term heat exchanges over a Mediterranean lagoon. *Journal of Geophysical Research Atmospheres*, *117*, 1–18. https://doi.org/10.1029/2012JD017857

De Bruin, H. A. R., & Keijman, J. Q. (1979). The Priestley-Taylor Evaporation Model Applied to a Large, Shallow Lake in the Netherlands. *Journal of Applied Meteorology*. https://doi.org/10.1175/1520-0450(1979)018<0898:TPTEMA>2.0.CO;2

Buckler, S. J., & Quine, J. F. (1971). *A Further Report on Evaporation Studies on a Small Reservoir at Weyburn, Saskatchewan*. Regina, Saskatchewan, CANADA.

Burba, G. (2013). *Eddy Covariance Method for Scientific, Industrial, Agricultural, and Regulatory Applications: A Field Book on Measuring Ecosystem Gas Exchange and Areal Emission Rates*. Lincoln, NE: LI-COR Biosciences.

Cork, H. F. (1976). *Prairie Hydrometeoroloigcal Centre Report No. 16: Evaporation from Val*

Marie Reservoir - 1975. Regina, Canada.

Dalton, J. (1802). Experimental essays on the constitution of mixed gases: on the force of steam or vapour from water or other liquids in different temperatures, both in a Torricelli vacuum and in air; on evaporation; and on expansion of gases by heat. *Memoirs and Proceedings of the Manchester Literary & Philosophical Society*, *5*, 536–602.

Duan, Z., & Bastiaanssen, W. G. M. (2015). A new empirical procedure for estimating intra-annual heat storage changes in lakes and reservoirs: Review and analysis of 22 lakes. *Remote Sensing of Environment*, *156*, 143–156. https://doi.org/10.1016/j.rse.2014.09.009

Duan, Z., & Bastiaanssen, W. G. M. (2017). Evaluation of three energy balance-based evaporation models for estimating monthly evaporation for five lakes using derived heat storage changes from a hysteresis model. *Environmental Research Letters*, *12*(2), 024005. https://doi.org/10.1088/1748-9326/aa568e

Edson, J. B., Hinton, A. A., Prada, K. E., Hare, J. E., & Fairall, C. W. (1998). Direct covariance flux estimates from mobile platforms at sea. *Journal of Atmospheric and Oceanic Technology*, *15*(2), 547–562. https://doi.org/10.1175/1520-0426(1998)015<0547:DCFEFM>2.0.CO;2

Ehsani, N., Vörösmarty, C. J., Fekete, B. M., & Stakhiv, E. Z. (2017). Reservoir Operations Under Climate Change: Storage Capacity Options to Mitigate Risk. *Journal of Hydrology*. https://doi.org/10.1016/j.jhydrol.2017.09.008

Eichinger, W. E., Nichols, J., Prueger, J. H., Hipps, L. E., Neale, C. M. U., Cooper, D. I., & Bawazir, A. S. (2003). *Lake Evaporation Estimation in Arid Environments*. Iowa City IA.

Environment and Climate Change Canada. (2017). Val Marie Reservoir Migratory Bird Sanctuary. Retrieved from https://www.canada.ca/en/environment-climate-change/services/migratory-bird-sanctuaries/locations/val-marie-reservoir.html

Eugster, W., Kling, G., Jonas, T., McFadden, J. P., Wüest, A., MacIntyre, S., & Chapin, F. S. (2003). CO2 exchange between air and water in an Arctic Alaskan and midlatitude Swiss lake: Importance of convective mixing. *Journal of Geophysical Research Atmospheres*, *108*(D12). https://doi.org/10.1029/2002jd002653

Flugge, M., Mostafa, B. P., Rueder, J., Edson, J. B., & Plueddemann, A. J. (2016). Comparison of Direct Covariance Flux Measurements from an Offshore Tower and a Buoy. *Journal of Atmospheric and Oceanic Technology*, *33*(May), 873–890. https://doi.org/10.1175/JTECH-

D-15-0109.1

Gibson, J. J., Birks, S. J., Yi, Y., Moncur, M. C., & McEachern, P. M. (2016). Stable isotope mass balance of fifty lakes in central Alberta: Assessing the role of water balance parameters in determining trophic status and lake level. *Journal of Hydrology: Regional Studies*, *6*, 13–25. https://doi.org/10.1016/j.ejrh.2016.01.034

Granger, R. J., & Hedstrom, N. (2010). Controls on open water evaporation. *Hydrology and Earth System Sciences Discussions*, *7*(3), 2709–2726. https://doi.org/10.5194/hessd-7-2709-2010

Granger, R. J., & Hedstrom, N. (2011). Modelling hourly rates of evaporation from small lakes. *Hydrology and Earth System Sciences*, *15*, 267–277. https://doi.org/10.5194/hess-15-267-2011

Grubert, E. A. (2016). Water consumption from hydroelectricity in the United States. *Advances in Water Resources*, *96*, 88–94. https://doi.org/10.1016/j.advwatres.2016.07.004

Han, K. W., Shi, K. Bin, Yan, X. J., & Cheng, Y. Y. (2019). Water Savings Efficiency of Counterweighted Spheres Covering a Plain Reservoir in an Arid Area. *Water Resources Management*, *33*(5), 1867–1880. https://doi.org/10.1007/s11269-019-02214-x

Heikinheimo, M., Kangas, M., Tourula, T., Venäläinen, A., & Tattari, S. (1999). Momentum and heat fluxes over lakes Tamnaren and Raksjo determined by the bulk-aerodynamic and eddy-correlation methods. *Agricultural and Forest Meteorology*, *98–99*, 521–534. https://doi.org/10.1016/S0168-1923(99)00121-5

Heiskanen, J. J., Mammarella, I., Ojala, A., Stepanenko, V., Erkkilä, K. M., Miettinen, H., et al. (2015). Effects of water clarity of lake stratification an dlake-atmosphere heat exchange. *Journal of Geophysical Research: Atmospheres*, *120*, 7412–7428. https://doi.org/10.1002/2013JD021290.Received

Helfer, F., Lemckert, C., & Zhang, H. (2012). Impacts of climate change on temperature and evaporation from a large reservoir in Australia. *Journal of Hydrology*, *475*, 365–378. https://doi.org/10.1016/j.jhydrol.2012.10.008

Hood, J. L., Roy, J. W., & Hayashi, M. (2006). Importance of groundwater in the water balance of an alpine headwater lake, *33*(July), 1–5. https://doi.org/10.1029/2006GL026611

Ikebuchi, S., Seki, M., & Ohtoh, A. (1988). Evaporation from Lake Biwa. *Journal of Hydrology*, *102*(1–4), 427–449. https://doi.org/10.1016/0022-1694(88)90110-2

Jiang, H., Tang, K., & He, X. (2015). Experimental Studies on Reduction of Evaporation from Plain Reservoirs in Drought Areas by Benzene Board Covering Technology. *Journal of Coastal Research*, (73), 177–182. https://doi.org/10.2112/1551-5036-SI.54.fmi

Jonsson, A., Åberg, J., Lindroth, A., & Jansson, M. (2008). Gas transfer rate and CO2 flux between an unproductive lake and the atmosphere in northern Sweden. *Journal of Geophysical Research: Biogeosciences*, *113*(4), 1–13. https://doi.org/10.1029/2008JG000688

Kohler, M. A., Nordenson, T. J., & Fox, W. E. (1955). *Evaporation from Pans and Lakes*.

Lensky, N. G., Lensky, I. M., Peretz, A., Gertman, I., Tanny, J., & Assouline, S. (2018). Diurnal Course of Evaporation From the Dead Sea in Summer: A Distinct Double Peak Induced by Solar Radiation and Night Sea Breeze. *Water Resources Research*, *54*(1), 150–160. https://doi.org/10.1002/2017WR021536

Lenters, J. D., Kratz, T. K., & Bowser, C. J. (2005). Effects of climate variability on lake evaporation: Results from a long-term energy budget study of Sparkling Lake, northern Wisconsin (USA). *Journal of Hydrology*, *308*(1–4), 168–195. https://doi.org/10.1016/j.jhydrol.2004.10.028

LI-COR Inc. (2018). Eddy Covariance Processing Software. Retrieved from https://www.licor.com/env/products/eddy_covariance/eddypro.html

Li, X.-Y., Ma, Y.-J., Huang, Y.-M., Hu, X., Wu, X.-C., Wang, P., et al. (2016). Evaporation and surface energy budget over the largest high-altitude saline lake on the Qinghai-Tibet Plateau. *Journal of Geophysical Research : Atmospheres*, *121*, 10,470-10,485. https://doi.org/10.1002/2015JC010796

Li, Z., Lyu, S., Zhao, L., Wen, L., Ao, Y., & Wang, S. (2016). Turbulent transfer coefficient and roughness length in a high-altitude lake, Tibetan Plateau. *Theoretical and Applied Climatology*, *124*(3–4), 723–735. https://doi.org/10.1007/s00704-015-1440-z

Liu, A., Taylor, N., Kiyani, A., & Mooney, C. (2014). *Prairie Provinces Water Board Report #171: Evaluation of Lake Evaporation in the North Saskatchewan River Basin Technical Report to the PPWB Committee on Hydrology*.

Liu, Heping., Zhang, Y., Liu, S., Jiang, H., Sheng, L., & Williams, Q. L. (2009). Eddy covariance measurements of surface energy budget and evaporation in a cool season over southern open water in Mississippi. *Journal of Geophysical Research*, *114*, 1–13.

https://doi.org/10.1029/

Liu, Heping., Zhang, Q., & Dowler, G. (2012). Environmental Controls on the Surface Energy Budget over a Large Southern Inland Water in the United States: An Analysis of One-Year Eddy Covariance Flux Data. *Journal of Hydrometeorology*, *13*(6), 1893–1910. https://doi.org/10.1175/JHM-D-12-020.1

Liu, HuiZhi., Feng, J., Sun, J., Wang, L., & Xu, A. (2015). Eddy covariance measurements of water vapor and CO2 fluxes above the Erhai Lake. *Science China: Earth Sciences*, *58*(3), 317–328. https://doi.org/10.1007/s11430-014-4828-1

Liu, X., Yu, J., Wang, P., Zhang, Y., & Du, C. (2016). Lake evaporation in a hyper-arid environment, northwest of China-measurement and estimation. *Water (Switzerland)*. https://doi.org/10.3390/w8110527

Majidi, M., Alizadeh, A., Farid, A., & Vazifedoust, M. (2015). Estimating evaporation from lakes and reservoirs under limited data condition in a semi-arid region. *Water Resources Management*, *29*(10). https://doi.org/10.1007/s11269-015-1025-8

Mammarella, I., Nordbo, A., Rannik, Ü., Haapanala, S., Levula, J., Laakso, H., et al. (2015). Carbon dioxide and energy fluxes over a northern boreal lake in Southern Finland. *Journal of Geophysical Research: Biogeosciences*, *120*, 1296–1314. https://doi.org/10.1002/2014JG002873

Martin, F. (1988). *Prairie Farm Rehabilitation Administration Hydrology Report #113: Determination of gross evaporation for small to moderate-sized water bodies in the canadian prairies using the Meyer formula*.

Martínez Alvarez, V., González-Real, M. M., Baille, A., Maestre Valero, J. F., & Gallego Elvira, B. (2008). Regional assessment of evaporation from agricultural irrigation reservoirs in a semiarid climate. *Agricultural Water Management*, *95*(9), 1056–1066. https://doi.org/10.1016/j.agwat.2008.04.003

Martínez Alvarez, V., Leyva, J. C., Maestre Valero, J. F., & Górriz, B. M. (2009). Economic assessment of shade-cloth covers for agricultural irrigation reservoirs in a semi-arid climate. *Agricultural Water Management*, *96*(9), 1351–1359. https://doi.org/10.1016/j.agwat.2009.04.008

McGloin, R., McGowan, H., McJannet, D., & Burn, S. (2014a). Modelling sub-daily latent heat fluxes from a small reservoir. *Journal of Hydrology*, *519*, 2301–2311.

https://doi.org/10.1016/j.jhydrol.2014.10.032

McGloin, R., McGowan, H., McJannet, D., Cook, F., Sogachev, A., & Burn, S. (2014b). Quantification of surface energy fluxes from a small water body using scintillometry and eddy covariance. *Water Resources Research*, *50*, 494–513. https://doi.org/10.1002/2013WR013899

McGloin, R., McGowan, H., & McJannet, D. (2015). Effects of diurnal, intra-seasonal and seasonal climate variability on the energy balance of a small subtropical reservoir. *International Journal of Climatology*, *35*(9), 2308–2325. https://doi.org/10.1002/joc.4147

McJannet, D. L., Cook, F. J., McGloin, R. P., McGowan, H. A., & Burn, S. (2011). Estimation of evaporation and sensible heat flux from open water using a large-aperture scintillometer. *Water Resources Research*, *47*(1), 14. https://doi.org/10.1029/2010WR010155

McMahon, T. A., Peel, M. C., Lowe, L., Srikanthan, R., & McVicar, T. R. (2013). Estimating actual, potential, reference crop and pan evaporation using standard meteorological data: a pragmatic synthesis. *Hydrology and Earth System Sciences*, *17*, 1331–1363. https://doi.org/10.5194/hess-17-1331-2013

Metzger, J., Nied, M., Corsmeier, U., Kleffmann, J., & Kottmeier, C. (2018). Dead Sea evaporation by eddy covariance measurements versus aerodynamic, energy budget, Priestley-Taylor, and Penman estimates. *Hydrology and Earth System Sciences*, *22*, 1135–1155. https://doi.org/10.5194/hess-2017-187

Meyer, A. (1915). Computing runoff from rainfall and other physical data. *Transactions of the American Society of Civil Engineers*, *79*, 1055–1155.

Meyer, A. (1942). *Evaporation from Lakes and Reservoirs*.

Miller, S. D., Hristov, T. S., Edson, J. B., & Friehe, C. A. (2008). Platform motion effects on measurements of turbulence and air-sea exchange over the open ocean. *Journal of Atmospheric and Oceanic Technology*, *25*(9), 1683–1694. https://doi.org/10.1175/2008JTECHO547.1

Morton, F. I. (1983a). Operational Estimates Of Areal Evapotranspiration and Their Significance to the Science and Practice of Hydrology. *Journal of Hydrology*, *66*, 1–76.

Morton, F. I. (1983b). Operational estimates of lake evaporation. *Journal of Hydrology*, *66*(1–4), 77–100. https://doi.org/10.1016/0022-1694(83)90178-6

Morton, F. I. (1986). Practical Estimates of Lake Evaporation. *Journal of Climate and Applied*

Meteorology, *25*, 371–387.

Nordbo, A., Launiainen, S., Mammarella, I., Leppäranta, M., Huotari, J., Ojala, A., & Vesala, T. (2011). Long-term energy flux measurements and energy balance over a small boreal lake using eddy covariance technique. *Journal of Geophysical Research Atmospheres*, *116*(2), 1–17. https://doi.org/10.1029/2010JD014542

North, R. L., Davies, J. M., Doig, L. E., Lindenschmidt, K. E., & Hudson, J. J. (2015). Lake Diefenbaker: The prairie jewel. *Journal of Great Lakes Research*, *41*, 1–7. https://doi.org/10.1016/j.jglr.2015.10.003

Panin, G. N., Nasonov, A. E., Foken, T., & Lohse, H. (2006). On the parameterisation of evaporation and sensible heat exchange for shallow lakes. *Theoretical and Applied Climatology*, *85*, 123–129. https://doi.org/10.1007/s00704-005-0185-5

Penman, H. (1948). Natural evaporation from open water, hare soil and grass. *Proceedings of the Royal Society of London. Series A, Mathematical and Physical Sciences*, *193*(1032), 120–145.

Piccolroaz, S., Healey, N. C., Lenters, J. D., Schladow, S. G., Hook, S. J., Sahoo, G. B., & Toffolon, M. (2018). On the predictability of lake surface temperature using air temperature in a changing climate: A case study for Lake Tahoe (U.S.A.). *Limnology and Oceanography*, *63*(1), 243–261. https://doi.org/10.1002/lno.10626

Potes, M., Salgado, R., Costa, M. J., Morais, M., Bortoli, D., Kostadinov, I., & Mammarella, I. (2017). Lake-atmosphere interactions at Alqueva reservoir: A case study in the summer of 2014. *Tellus, Series A: Dynamic Meteorology and Oceanography*, *69*(1), 1272787. https://doi.org/10.1080/16000870.2016.1272787

Province of Manitoba. (2017). Shellmouth Dam. Retrieved from https://www.gov.mb.ca/legal/copyright.html

Ramírez, J. A., Hobbins, M. T., & Brown, T. C. (2005). Observational evidence of the complementary relationship in regional evaporation lends strong support for Bouchet's hypothesis. *Geophysical Research Letters*, *32*, L15401. https://doi.org/10.1029/2005GL023549

Riveros-Iregui, D. A., Lenters, J. D., Peake, C. S., Ong, J. B., Healey, N. C., & Zlotnik, V. A. (2017). Evaporation from a shallow, saline lake in the Nebraska Sandhills: Energy balance drivers of seasonal and interannual variability. *Journal of Hydrology*, *553*, 172–187.

https://doi.org/10.1016/j.jhydrol.2017.08.002

Rosenberry, D. O., Winter, T. C., Buso, D. C., & Likens, G. E. (2007). Comparison of 15 evaporation methods applied to a small mountain lake in the northeastern USA. *Journal of Hydrology*, *340*(3–4), 149–166. https://doi.org/10.1016/j.jhydrol.2007.03.018

Rouse, W. R., Oswald, C. M., Binyamin, J., Blanken, P. D., Schertzer, W. M., & Spence, C. (2003). Interannual and seasonal variability of the surface energy balance and temperature of central Great Slave Lake. *Journal of Hydrometeorology*, *4*, 720–730. https://doi.org/10.1175/1525-7541(2003)004<0720:IASVOT>2.0.CO;2

Rouse, W. R., Blanken, P. D., Bussières, N., Oswald, C. J., Schertzer, W. M., Spence, C., & Walker, A. E. (2008). An Investigation of the Thermal and Energy Balance Regimes of Great Slave and Great Bear Lakes. *Journal of Hydrometeorology*, *9*, 1318–1334. https://doi.org/10.1175/2008JHM977.1

Salgado, R., & Le Moigne, P. (2010). Coupling of the FLake model to the Surfex externalized surface model. *Boreal Environment Research*, *15*(2), 231–244.

Scherer, L., & Pfister, S. (2016). Global water footprint assessment of hydropower. *Renewable Energy*, *99*, 711–720. https://doi.org/10.1016/j.renene.2016.07.021

Scott, R. L. (2010). Using watershed water balance to evaluate the accuracy of eddy covariance evaporation measurements for three semiarid ecosystems. *Agricultural and Forest Meteorology*. https://doi.org/10.1016/j.agrformet.2009.11.002

Shao, C., Chen, J., Stepien, C. A., Chu, H., Ouyang, Z., Bridgeman, T. B., et al. (2015). Diurnal to annual changes in latent, sensible heat, and CO 2 fluxes over a Laurentian Great Lake: A case study in Western Lake Erie. *Journal of Geophysical Research: Biogeosciences*, *120*, 1587–1604. https://doi.org/10.1002/2015JG003025

Slota, P. M. A. (2013). *Evaluation of Operational Lake Evaporation Methods in a Canadian Shield Landscape*. University of Manitoba.

Spence, C., Blanken, P. D., Lenters, J. D., & Hedstrom, N. (2013). The importance of spring and autumn atmospheric conditions for the evaporation regime of lake superior. *Journal of Hydrometeorology*, *14*(5), 1647–1658. https://doi.org/10.1175/JHM-D-12-0170.1

Spence, C., & Hedstrom, N. (2015). Attributes of Lake Okanagan evaporation and development of a mass transfer model for water management purposes. *Canadian Water Resources Journal*, *40*(3), 250–261. https://doi.org/10.1080/07011784.2015.1046140

Stannard, D. I., & Rosenberry, D. O. (1991). A Comparison of Short-Term Measurements of Lake Evaporation Using Eddy Correlation and Energy Budget Methods. *Journal of Hydrology*, *122*, 15–22.

Strachan, I. B., Tremblay, A., Pelletier, L., Tardif, S., Turpin, C., & Nugent, K. A. (2016). Does the creation of a boreal hydroelectric reservoir result in a net change in evaporation? *Journal of Hydrology*. https://doi.org/10.1016/j.jhydrol.2016.06.067

Sun, J., Hu, W., Wang, N., Zhao, L., An, R., Ning, K., & Zhang, X. (2018). Eddy covariance measurements of water vapor and energy flux over a lake in the Badain Jaran Desert, China. *Journal of Arid Land*, *10*(4), 517–533. https://doi.org/10.1007/s40333-018-0057-3

Swinbank, W. C. (1951). The Measurement of Vertical Transfer of Heat and Water Vapor By Eddies in the Lower Atmosphere. *Journal of Meteorology*. https://doi.org/10.1175/1520-0469(1951)008<0135:TMOVTO>2.0.CO;2

Tanny, J., Cohen, S., Assouline, S., Lange, F., Grava, A., Berger, D., et al. (2008). Evaporation from a small water reservoir: Direct measurements and estimates. *Journal of Hydrology*, *351*(1–2), 218–229. https://doi.org/10.1016/j.jhydrol.2007.12.012

Tanny, J., Cohen, S., Berger, D., Teltch, B., Mekhmandarov, Y., Bahar, M., et al. (2011). Evaporation from a reservoir with fluctuating water level : Correcting for limited fetch. *Journal of Hydrology*, *404*(3–4), 146–156. https://doi.org/10.1016/j.jhydrol.2011.04.025

Taylor, C. J., Pedregal, D. J., Young, P. C., & Tych, W. (2007). Environmental Time Series Analysis and Forecasting with the Captain Toolbox. *Environmental Modelling and Software*, *22*, 797–814. https://doi.org/http://dx.doi.org/doi:10.1016/j.envsoft.2006.03.002

Vardavas, I. M., & Fountoulakis, A. (1996). Estimation of lake evaporation from standard meteorological measurements: Application to four Australian lakes in different climatic regions. *Ecological Modelling*, *84*, 139–150. https://doi.org/10.1016/0304-3800(94)00126-x

Vercauteren, N., Bou-Zeid, E., Huwald, H., Parlange, M. B., & Brutsaert, W. (2009). Estimation of wet surface evaporation from sensible heat flux measurements. *Water Resources Research*, *45*(6), 1–7. https://doi.org/10.1029/2008WR007544

Vesala, T., Huotari, J., Rannik, Ü., Suni, T., Smolander, S., Sogachev, A., et al. (2006). Eddy covariance measurements of carbon exchange and latent and sensible heat fluxes over a boreal lake for a full open-water period. *Journal of Geophysical Research*, *111*, 1–12. https://doi.org/10.1029/2005JD006365

Wang, B., Ma, Y., Ma, W., & Su, Z. (2017). Physical controls on half-hourly, daily, and monthly turbulent flux and energy budget over a high-altitude small lake on the Tibetan Plateau. *Journal of Geophysical Research*, *122*(4), 2289–2303. https://doi.org/10.1002/2016JD026109

Wang, B., Ma, Y., Ma, W., Su, B., & Dong, X. (2019). Evaluation of ten methods for estimating evaporation in a small high-elevation lake on the Tibetan Plateau. *Theoretical and Applied Climatology*, *136*, 1033–1045. https://doi.org/10.1007/s00704-018-2539-9

Wang, W., Xiao, W., Cao, C., Gao, Z., Hu, Z., Liu, S., et al. (2014). Temporal and spatial variations in radiation and energy balance across a large freshwater lake in China. *Journal of Hydrology*, *511*, 811–824. https://doi.org/10.1016/j.jhydrol.2014.02.012

Wiens, L. H., & Godwin, R. B. (1978). *Prairie Farm Rehabilitation Administration Hydrology Report #90: The Adaptation of Two Components of the Meyer Formula to Canadian Prairie Conditions*. Regina, Canada. https://doi.org/10.1192/bjp.112.483.211-a

Winter, T. C., Rosenberry, D. O., & Sturrock, A. M. (1995). Evaluation of 11 equations for determining evaporation for a small lake in the north central United States. *Water Resources Research*, *31*(4), 983–993.

Winter, T. C., Buso, D. C., Rosenberry, D. O., Likens, G. E., Sturrock Jr, A. M., & Mau, D. P. (2003). Evaporation determined by the energy budget method for Mirror Lake, New Hampshire. *Limnol. Oceanogr.*, *48*(3), 995–1009. https://doi.org/10.4319/lo.2003.48.3.0995

Woodvine, R. J. (1995). *Prairie Farm Rehabilitation Administration Hydrology Report # 139: Determination of coefficients for use in the Meyer formula*. Regina, Canada.

Woolway, R. I., Verburg, P., Lenters, J. D., Merchant, C. J., Hamilton, D. P., Brookes, J., et al. (2018). Geographic and temporal variations in turbulent heat loss from lakes: A global analysis across 45 lakes. *Limnology and Oceanography*, *63*, 2436–2449. https://doi.org/10.1002/lno.10950

Wurbs, R. A., & Ayala, R. A. (2014). Reservoir evaporation in Texas, USA. *Journal of Hydrology*, *510*, 1–9. https://doi.org/10.1016/j.jhydrol.2013.12.011

Xiao, K., Griffis, T. J., Baker, J. M., Bolstad, P. V., Erickson, M. D., Lee, X., et al. (2018). Evaporation from a temperate closed-basin lake and its impact on present, past, and future water level. *Journal of Hydrology*, *561*, 59–75. https://doi.org/10.1016/j.jhydrol.2018.03.059

Xiao, W., Liu, S., Wang, W., Yang, D., Xu, J., Cao, C., et al. (2013). Transfer Coefficients of Momentum, Heat and Water Vapour in the Atmospheric Surface Layer of a Large Freshwater Lake. *Boundary-Layer Meteorology*, *148*, 479–494. https://doi.org/10.1007/s10546-013-9827-9

Youssef, Y. W., & Khodzinskaya, A. (2019). A Review of Evaporation Reduction Methods from Water Surfaces. *E3S Web of Conferences*, *97*, 1–10. https://doi.org/10.1051/e3sconf/20199705044

Zhao, D., & Liu, J. (2015). A new approach to assessing the water footprint of hydroelectric power based on allocation of water footprints among reservoir ecosystem services. *Physics and Chemistry of the Earth*, *79–82*, 40–46. https://doi.org/10.1016/j.pce.2015.03.005

Zhao, X., & Liu, Y. (2018). Variability of Surface Heat Fluxes and Its Driving Forces at Different Time Scales Over a Large Ephemeral Lake in China. *Journal of Geophysical Research: Atmospheres*, *123*, 4939–4957. https://doi.org/10.1029/2017JD027437

Zolá, R. P., Bengtsson, L., Berndtsson, R., Martí-Cardona, B., Satgé, F., Timouk, F., et al. (2019). Modelling Lake Titicaca's daily and monthly evaporation. *Hydrology and Earth System Sciences*, *23*, 657–668. https://doi.org/10.5194/hess-23-657-2019

Appendix A: Field study timelines

Table A.1 – Timeline of important dates at Val Marie Reservoir

Date	Description
May 6, 2016	- buoy deployed
June 1, 2016	- site visit (data download, routine maintenance)
June 6, 2016	- buoy is damaged by vandalism and is left in inverted position
June 29, 2016	- site visit (discovery of overturned buoy)
July 7, 2016	- recovery of overturned buoy
Aug 10, 2016	- new buoy deployed
Aug 16, 2016	- site visit (replace damaged memory card)
Aug 30, 2016	- site visit (data download, routine maintenance)
Sept 7, 2016	- site visit (replace defective sonic anemometer)
Sept 14, 2016	- site visit (data download, routine maintenance)
Oct 11, 2016	- site visit (data download, routine maintenance)
Nov 1, 2016	- buoy and thermistor string removed
May 5, 2017	- buoy deployed and land station installed
May 6, 2017	- thermistor string deployed
May 15, 2017	- site visit (data download, new modem and antennae installed on buoy)
June 21, 2017	- site visit (data download, routine maintenance)
July 11, 2017	- site visit (data download, routine maintenance)
Aug 4, 2017	- site visit (data download, replace poor battery at buoy)
Sept 21, 2017	- site visit (data download, routine maintenance)
Nov 1, 2017	- land station removed
Nov 2, 2017	- buoy and thermistor string removed

Table A.2 – Timeline of important dates at Shellmouth Reservoir

Date	Description
June 7, 2016	- buoy deployed
June 17, 2016	- site visit (too windy to access buoy)
June 30, 2016	- site visit (replace defective hygrometer)
July 21, 2016	- site visit (data download, routine maintenance)
Aug 15, 2016	- site visit (data download, routine maintenance)
Sept 5, 2016	- site visit (data download, routine maintenance)
Sept 28, 2016	- site visit (data download, routine maintenance)
Oct 25, 2016	- remove buoy for season
May 3, 2017	- buoy deployed
May 4, 2017	- thermistor string deployed
June 1, 2017	- site visit (data download, routine maintenance)
June 29, 2017	- site visit (data download, routine maintenance)
July 28, 2017	- site visit (data download, routine maintenance)
Aug 17, 2017	- site visit (no data on card, routine maintenance)
Aug 25, 2017	- buoy detached from anchor
Aug 25, 2017	- site visit (located buoy and secured to shore)
Aug 29, 2017	- site visit (data download, re-anchored buoy in original location)
Sept 5, 2017	- lost remote connection
Sept 14, 2017	- site visit (data download, routine maintenance)
Oct 5, 2017	- site visit (data download, routine maintenance)
Oct 31, 2017	- buoy and thermistor string removed

Appendix B: Thermistor water temperature measurements

Table B.1 - Val Marie Reservoir depth temperature measurements from field visits
Note: Temperatures are in degrees Celsius; second temperatures were measured on the way back up

Depth (m)	Aug 30, 2016	Sept 14, 2016	May 6, 2017	June 21, 2017
Air		22.3	18.8	22.9
0.25	17.7	14.0 / 13.9	12.9 / 12.8	18.5
0.5	17.9 / 17.7	13.6 / 13.5	12.8 / 12.7	18.4
0.75			12.6 / 12.7	18.4
1.0	17.8 / 17.7	13.0 / 12.9	12.6 / 12.7	18.4
1.25			------ / 12.6	18.4
1.5	17.6 / 17.5	12.7 / 12.7	12.3 / 12.3	18.4
1.75			------ / 12.1	18.4
2.0	17.3 / 17.4	12.6 / 12.6	12.0 / 12.1	18.4
2.25			------ / 11.9	
2.5	17.1 / 17.1	12.6 / 12.6	11.9 / 11.9	18.4
2.75			------ / 11.8	
3.0	17.0 / 17.0	12.6 / 12.6	11.4 / 11.4	18.3
3.25			------ / 11.0	
3.5		12.6 / 12.6	11.0 / 11.0	
4.0			10.7	
Hit bottom	3.4 m	3.9 m	4.0 m	3.0 m

Table B.2 – Shellmouth Reservoir depth temperature measurements from field visits
Note: Temperatures are in degrees Celsius; second temperatures were measured on the way back up

Depth (m)	Sept 5, 2016	June 1, 2017	June 29, 2017	Aug 18, 2017
Air				19
0.25	19.1	14.9	18.1	22.4
0.5	19.2	14.9	18.0	22.4
0.75				22.4
1.0	19.2	14.8	17.9	22.4
1.25			17.9	
1.5	19.2	14.8	17.9	22.4
1.75			17.8	
2.0	19.2	14.7	17.8	22.4
2.5	19.2	14.7	17.8	
3.0	19.2	14.6	17.8	22.4
3.5	19.2	14.6	17.8	
4.0	19.2	14.6	17.8	22.4
4.5	19.2	14.5	17.8	
5.0	19.2	----- / 13.4	17.7	22.3
5.5			17.6	
6.0	19.2	13.6	17.4	21.9
6.5			17.3	
7.0	19.2	13.4	17.0	21.6
7.5			16.8	
8.0	19.2	13.1	16.6	21.5
8.5	19.2	13.4	16.5	
9.0			16.5	
9.5			16.5	
10.0			16.4	
10.5			16.3	
11.0			16.2	
11.5			16.2	
12.0			16.2	
Hit bottom	8.6 m	8.75 m	12.3 m	8.75 m

Appendix C: EddyPro station settings

Table C.1 – Buoy station settings for EddyPro flux corrections
Note: Val Marie 1.0 is pre-tip 2016, Val Marie 2.0 is post-tip 2016 and all 2017 open-water season

Buoy	**Val Marie 1.0**	**Val Marie 2.0**	**Shellmouth**
Canopy Height (m)	0.01	0.01	0.01
Station Altitude (m)	803	803	427
Station Latitude (N)	49º18’28.44”	49º18’28.44”	51º06’20.16”
Station Longitude (W)	107º48’46.08”	107º48’46.08”	101º25’58.08”
CSAT Height (m)	1.9	2.3	2.2
KH20 longitudinal path length (cm)	1.25	1.25	1.25
KH20 transversal path length (cm)	1.00	1.00	1.00
kw ($m^3\ g^{-1}cm^{-1}$)	0.152	0.152	0.152
ko ($m^3\ g^{-1}cm^{-1}$)	0.0045	0.0045	0.0045

Appendix D: Correlation of over-lake meteorology at Val Marie Reservoir

Table D.1 – Correlation of hourly, daily and weekly variables, differences and cross-products measured at the Val Marie Reservoir buoy
Note: R^2 values are insignificant (p-values > 0.05)

Variables	Hourly R^2	Daily R^2	Weekly R^2
U (windspeed)	0.22	0.30	(0.03)
T (air temperature)	0.03	0.03	0.33
T_s (surface temperature)	0.07	0.12	0.54
T_w (mean depth-weighted water temperature)	0.02	0.02	0.20
T_s-T (temperature difference)	0.04	0.05	0.38
RH (relative humidity)	0.00	(0.00)	(0.01)
e_a (actual vapour pressure of the air)	0.00	0.02	0.28
e_s (saturated vapour pressure of the air)	0.03	0.02	0.30
e_w (vapour pressure of the water surface)	0.07	0.11	0.53
e_w-e_a (vapour pressure difference)	0.07	0.19	0.58
e_s-e_a (vapour pressure deficit)	(0.00)	(0.00)	0.16
p (atmospheric pressure)	(0.00)	0.06	(0.05)
R_n (net radiation)	0.01	0.05	0.15
Q_x (reservoir heat storage flux)	0.10	0.17	0.60
H (sensible heat flux)	0.03	0.02	0.25
R_n-Q_x	0.02	0.02	0.11
U(e_w-e_a)	0.33	0.52	0.80
U(e_w-e_a)(R_n-Q_x)	0.08	0.18	0.46

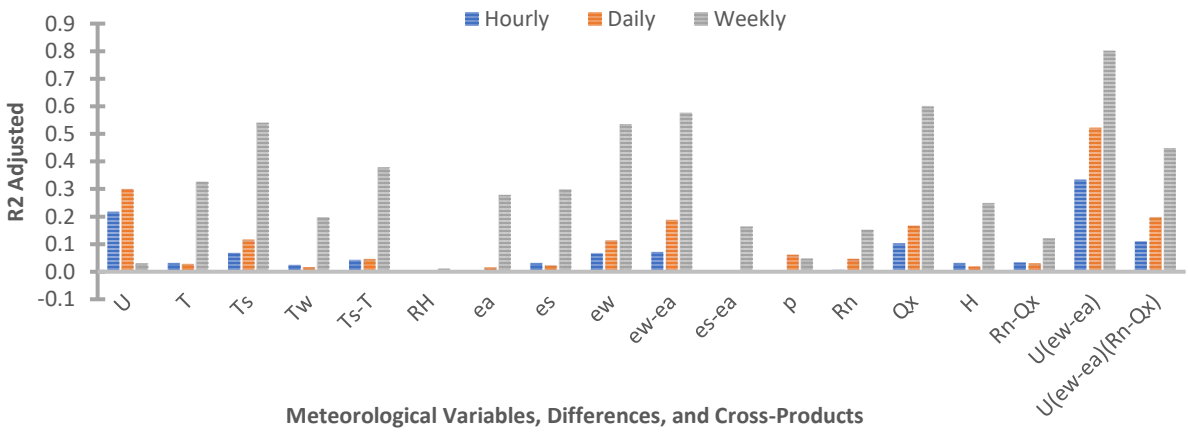

Figure D.1 – Correlation of hourly, daily and weekly variables, differences and cross-products at Val Marie Reservoir buoy

Appendix E: Radiation model validation plots

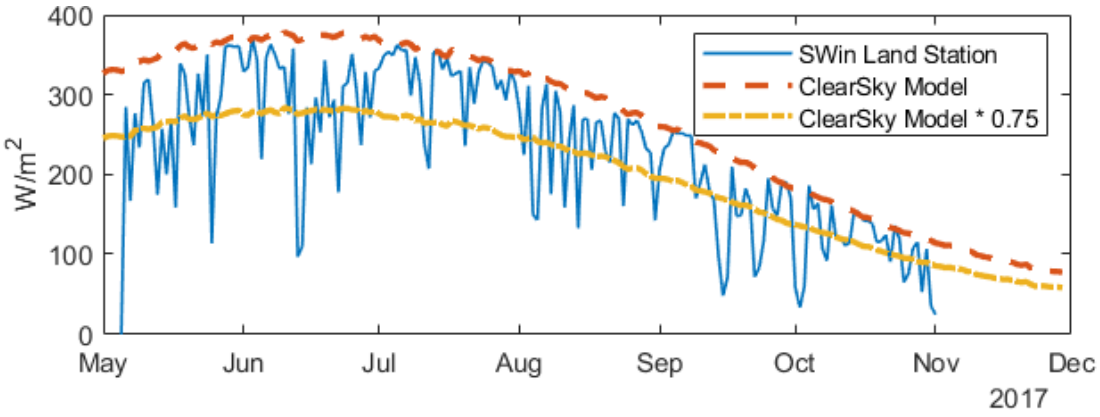

Figure E.1 – ClearSky model with and without cloud cover factor compared to shortwave incoming radiation measured at the Val Marie Land Station 2017

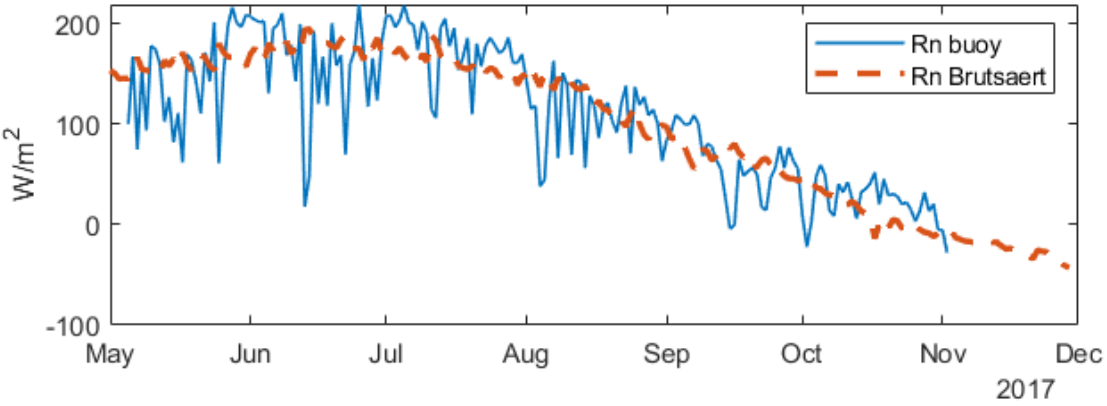

Figure E.2 – Net radiation model compared to measurements at the Val Marie buoy 2017

Appendix F: Comparison of CSAT and KH20 outputs with other meteorological variables measured at the Shellmouth buoy

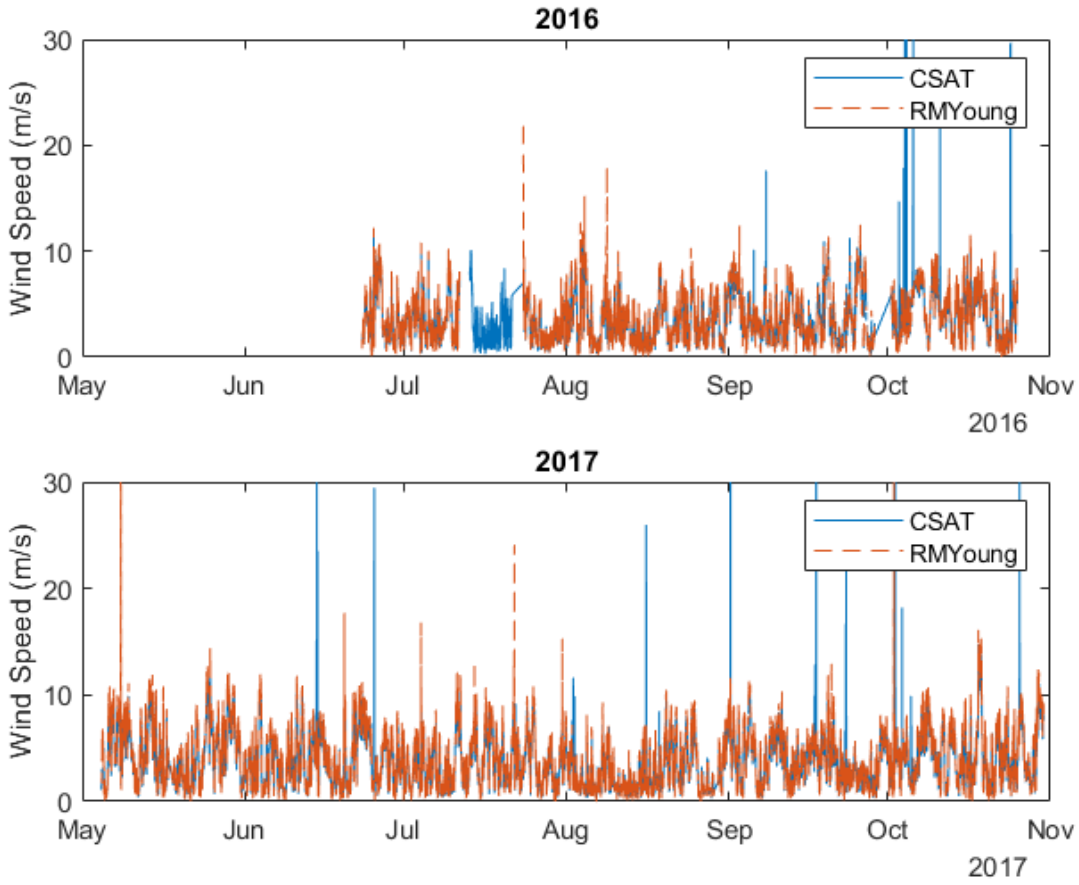

Figure F.1 – Plots comparing windspeeds measured by the sonic anemometer (CSAT) and the main temperature recorder (HMP) at the Shellmouth Buoy in 2016 and 2017

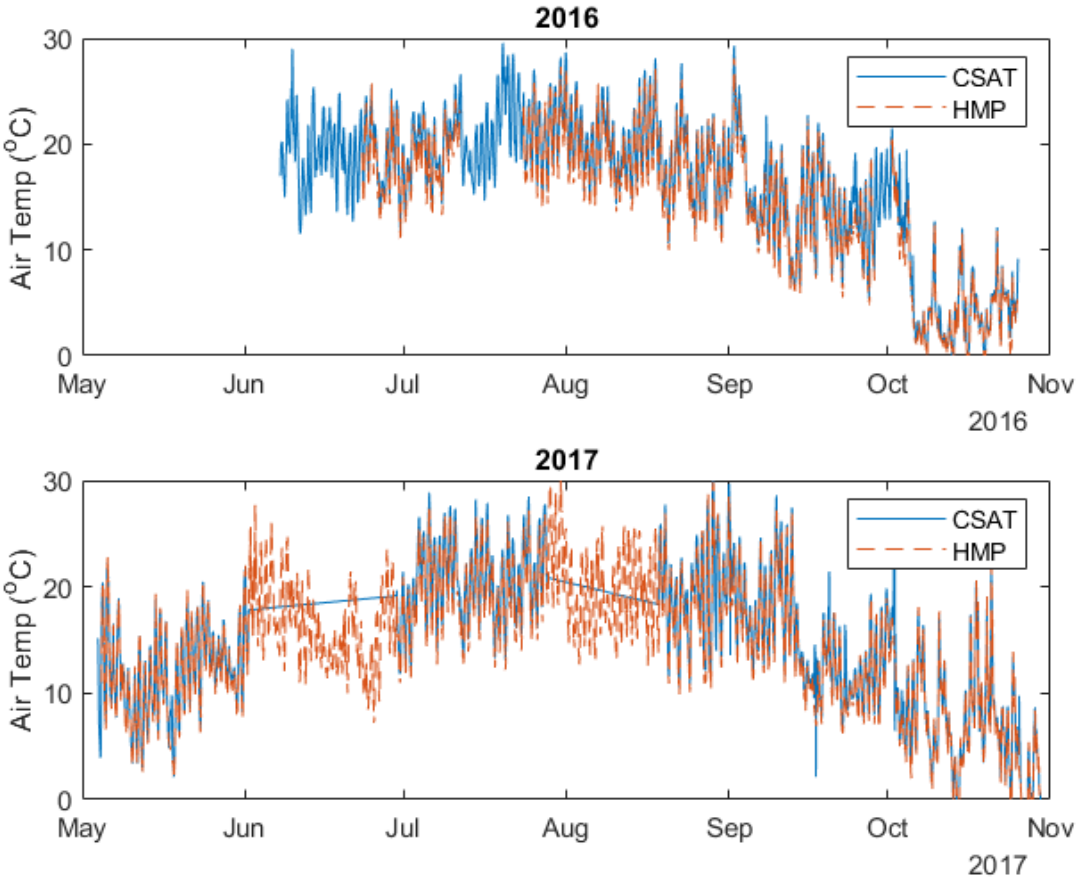

Figure F.2 – Plots comparing air temperatures measured by the sonic anemometer (CSAT) and the main temperature recorder (HMP) at the Shellmouth Buoy in 2016 and 2017

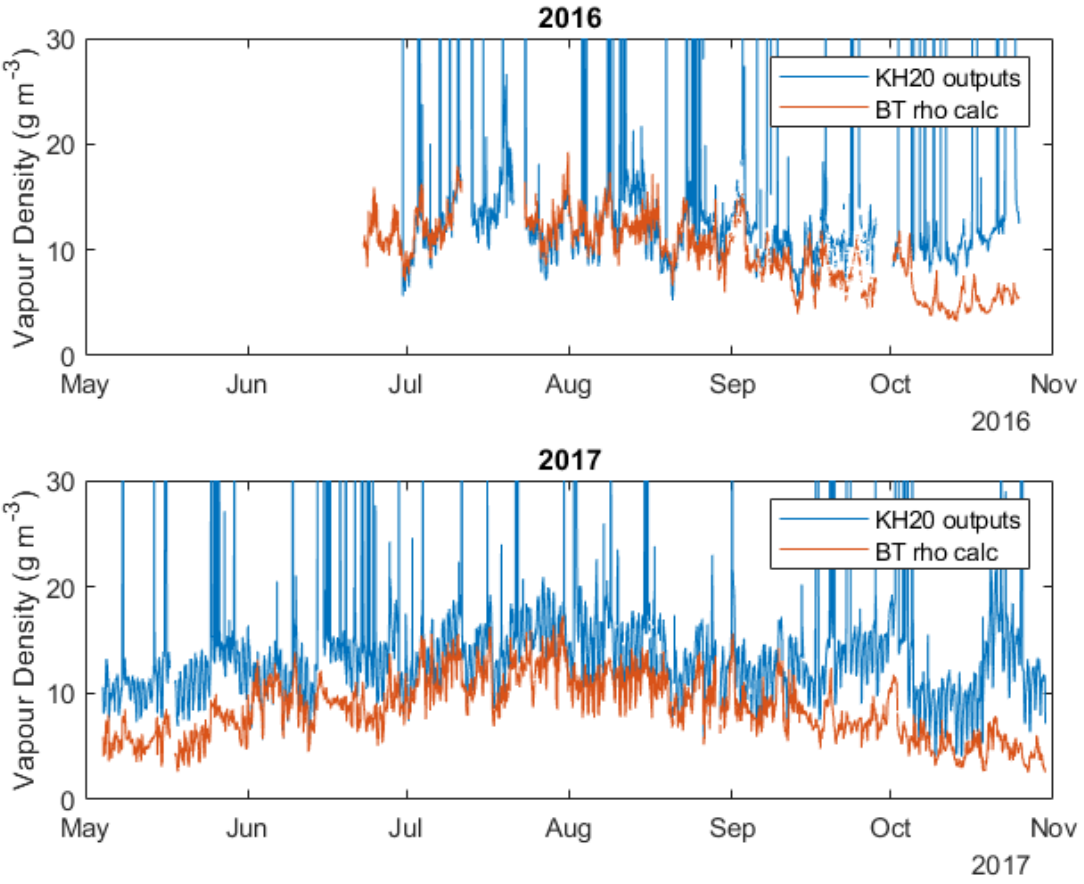

Figure F.3 – Plots comparing vapour densities measured by the gas analyzer (KH20) and calculated from the other sensors (BT rho calc) at the Shellmouth Buoy in 2016 and 2017

Appendix G: Monthly means of data collected at field sites

Table G.1 – Monthly mean measurements at Val Marie Reservoir buoy 2016

Month	N (days)	E (mm/d)	U (m/s)	T (ºC)	Ts (ºC)	Tw (ºC)	RH (%)	Rn (W/m^2)	p (kPa)
May	25	3.8	4.6	11.3	12.4	n/a	69	116	92.1
June	6	2.9	4.0	16.2	15.4	18.6	61	184	92.4
July	0	n/a	n/a	n/a	n/a	21.4	n/a	n/a	n/a
August	16	n/a	4.2	17.4	17.1	19.7	61	112	92.3
September	30	2.9	3.8	12.9	13.2	14.4	67	59	92.2
October	31	1.9	4.1	4.8	5.5	6.3	80	16	92.0
November	1	0.0	5.5	4.9	4.7	5.7	84	-9	91.3

Table G.2 – Monthly mean measurements at Val Marie Reservoir buoy 2017

Month	N (days)	E (mm/d)	U (m/s)	T (ºC)	Ts (ºC)	Tw (ºC)	RH (%)	Rn (W/m^2)	p (kPa)
May	26	4.0	4.9	12.9	12.4	13.9	57	147	92.0
June	30	4.9	4.9	16.9	15.4	17.9	56	161	91.9
July	31	5.2	3.9	22.4	n/a	22.4	51	178	92.2
August	31	3.9	3.4	18.9	17.1	19.4	53	109	92.3
September	30	3.0	3.4	13.3	13.2	14.3	58	64	92.2
October	31	2.3	5.6	5.5	5.5	6.0	64	25	92.0
November	2	1.0	4.9	-1.6	4.7	1.8	87	-11	91.3

Table G.3 – Monthly mean measurements at Val Marie Reservoir land station 2017

Month	N (days)	U (m/s)	T (ºC)	Ts (ºC)	RH (%)	Rn (W/m^2)	LWin (W/m^2)	SWin (W/m^2)	Total P (mm)
May	26	3.6	12.7	12.3	54	127	378	274	9.4
June	30	3.3	16.8	18.2	54	127	401	291	8.6
July	31	2.9	22.3	24.5	49	139	434	323	9.1
August	31	2.5	18.3	19.4	51	90	410	238	8.1
September	30	2.4	12.6	12.6	56	57	377	175	6.1
October	31	3.8	5.2	4.1	60	222	338	112	18.0
November	1	4.6	0.3	-0.3	85	-1	313	23	0.3

Table G.4 – Monthly mean measurements at Shellmouth Reservoir buoy 2016

Month	N (days)	E (mm/d)	U (m/s)	T (ºC)	Ts (ºC)	Tw (ºC)	RH (%)	Rn (W/m^2)	p (kPa)
May	0	n/a	n/a	n/a	n/a	n/a	n/a	n/a	n/a
June	1	0.53	3.9	18.2	20.1	18.7	73	n/a	n/a
July	20	0.24	3.3	19.6	21.8	21.5	75	n/a	n/a
August	31	0.44	3.5	18.3	21.3	21.4	74	n/a	n/a
September	28	0.51	3.9	13.6	16.8	16.8	71	n/a	n/a
October	25	0.43	4.4	5.0	5.8	9.9	81	n/a	n/a
November	0	n/a	n/a	n/a	n/a	n/a	n/a	n/a	n/a

Table G.5 – Monthly mean measurements at Shellmouth Reservoir buoy 2017

Month	N (days)	E (mm/d)	U (m/s)	T (ºC)	Ts (ºC)	Tw (ºC)	RH (%)	Rn (W/m^2)	p (kPa)
May	27	0.52	5.0	11.9	n/a	114	59	n/a	n/a
June	30	0.03	4.2	16.3	20.1	16.8	67	n/a	n/a
July	31	0.34	3.9	20.2	21.8	20.7	68	n/a	n/a
August	31	0.23	2.9	18.9	21.3	21.9	67	n/a	n/a
September	30	0.47	4.0	14.2	16.8	17.4	67	n/a	n/a
October	30	0.49	4.7	6.7	5.8	10.3	68	n/a	n/a
November	0	n/a	n/a	n/a	n/a	n/a	n/a	n/a	n/a